Modeling the Medium Access Control Layer Performance of Cellular Vehicle-to-Everything Mode 4 and IEEE 802.11p

Wijesiri Narayana Badal Arachchige Geeth Priyankara

(188008U)

Thesis submitted in partial fulfillment of the requirements for the degree
Doctor of Philosophy

Department of Electronic and Telecommunication Engineering

University of Moratuwa
Sri Lanka

December 2021

Declaration

I declare that this is my own work, and this thesis does not incorporate without acknowledgement any material previously submitted for a degree or diploma in any other university or institute of higher learning, and to the best of my knowledge and belief it does not contain any material previously published or written by another person except where the acknowledgement is made in the text.

Also, I hereby grant to University of Moratuwa the non-exclusive right to reproduce and distribute my thesis, in whole or in part, in print, electronic, or any other medium. I retain the right to use this content in whole or part in future works (such as articles or books).

UOM Verified Signature

Signature: W. N. B. A. G. Priyankara (188008u) Date: 15th February 2023

The candidate, whose signature appears above, carried out research for the Ph.D. dissertation under my supervision.

UOM Verified Signature

Signature: Dr. Tharaka Samarasinghe Date: 16th February 2023

Abstract

The capability of vehicle-to-everything (V2X) communication to wirelessly exchange information on speed and location of vehicles over an ad hoc network envisions promise substantially reducing vehicle collisions, congestion, fuel usage and pollution. V2X communication plays a pivotal role in intelligent transport systems (ITS), with IEEE 802.11p and cellular V2X (C-V2X) being the two competing enabling technologies. This thesis focuses on discrete-time Markov chain (DTMC) based modeling of the medium access control (MAC)-layer performance of the two enabling technologies for evaluation, comparison and enhancement. Firstly, DTMC-based models for the MAC layer operations of IEEE 802.11p and C-V2X Mode 4 are developed, considering periodic and event-driven messages. The results show that IEEE 802.11p is superior in average delay, whereas C-V2X Mode 4 excels in collision resolution, which leads to its higher throughput. Then, the models are extended to support the parallel operation of four multi-priority data streams, which are crucial for quality of service (QoS). Results show that IEEE 802.11p is superior in maintaining fairness among multi-priority data streams. It is also shown that the higher delay values in C-V2X lead to unfavorable packet delays in the low priority streams. The thesis studies the allocation of multiple candidate single-subframe resources (CSRs) per vehicle as a solution. It proposes a methodology to determine the number of CSRs for each vehicle based on the number of total vehicles, and to assign the multiple data streams for simultaneous transmission. The numerical results highlight the achievable delay gains of the proposed approach and its negligible impact on packet collisions.

Index terms— C-V2X Mode 4, discrete-time Markov chain, IEEE 802.11p, medium access control, multi-priority data streams.

Acknowledgements

First and foremost, I would like to thank my supervisor, Dr. Tharaka Samarasinghe, for offering me an opportunity to pursue my Ph.D. in the Department of Electronic and Telecommunication Engineering, University of Moratuwa (UoM). I am deeply grateful to him for the guidance, immense support, confidence, and invaluable encouragement during my Ph.D. research. He has always emphasized the importance of quality in research, which has helped me in my achievements in the past years. I am also grateful to my co-supervisor, Adjunct Professor Dr. Jussi Haapola from the Centre for Wireless Communication (CWC), University of Oulu, Finland, for the guidance provided to me during my doctoral studies. His comments and the opportunity provided to me to visit CWC contributed immensely to the scientific quality of my research. I wish to express my sincere gratitude to Professor Premanandana Rajatheva at the University of Oulu, Finland, and Professor Dileeka Dias at the UoM, Sri Lanka, for the guidance, support, inspiration, encouragement they have provided, and the confidence shown in me throughout my research career.

I want to thank the UoM, Sri Lanka, for providing me with excellent facilities, and a good work environment to conduct my research. My gratitude also goes to the CWC, University of Oulu, Finland, who provided me financial support and offered me an opportunity to pursue my Ph.D. at a top-notch research unit. I would also like to thank my university, the University of Ruhuna (UoR), Sri Lanka, where I am currently working as a lecturer and did my undergraduate degree, for providing me financial support during my Ph.D., and a sound technical foundation to carry out post-graduate studies and research.

In addition to my supervisors, it is a pleasure to also thank the following members of my Ph.D. progress review panel for their advice and support - Prof. Ruwan Udayanga, Prof. Frank Yong Li, and Dr. Prathapasinghe Dharmawansa. Special thanks go to Professor Frank Yong Li, University of Agder, Norway, who was my master thesis supervisor, for providing me encouragement and guidance throughout my Ph.D. I would also like to thank the Faculty of Graduate Studies,

Postgraduate Studies Division, and the administrative staff at the department of Electronic and Telecommunication Engineering of the UoM, who helped me in various administrative activities related to my Ph.D.

I also wish to extend my gratitude to all the academic and non-academic staff of the Faculty of Engineering, UoR. Special thanks go to Dr. Keerthi Gunawickrama, Dr. Rajitha Udawalpola, Dr, Anuradha Indika and Mr. Eranda Jayathunge at the Faculty of Engineering, UoR.

I want to express my unreserved gratitude to my mother Mallika De Silva and father Rathnasiri Wijesiri for their love, kindness, support, and encouragement provided throughout my life. The dedications you have made during my life are priceless. I am also grateful to my parents-in-law for their blessings. I also wish to extend my thanks to my cousin, Mr. Aruna Buddika, and brother-in-law Dr. Lalindra Ranaweera, for their continuous support. Then, to my sweet little three sons Kuvindu, Jeniru, and Yumeth thank you for bringing happiness to my life and that crucial motivation required to get things done. Finally, I would like to express my deepest gratitude to my loving wife, Isuru. Without your love, concern, understanding, encouragement, and support, none of this would have been possible.

Contents

List of Figures

List of Tables

List of Abbreviations

Abbreviation	Description
3GPP	Third generation partnership project
AC	Access category
AIFS	Arbitrary inter-frame space
C-V2X	Cellular vehicle-to-everything
CAM	Cooperative awareness messages
CCH	Control channel
CSMA/CA	Carrier sense multiple access with collision avoidance
CSR	Candidate single-subframe resources
CTMC	Continuous time Markov chains
CTS	Clear to send
CW	Contention window
D2D	Device-to-device
DCC	Decentralized congestion control
DENM	Decentralized environmental notification messages
DSRC	Dedicated short-range communication
DTMC	Discrete-time Markov chain
ETSI	European telecommunications standards institute
GPS	Global positioning system
HPD	High priority DENM
ICT	Information communication technology
ITS	Intelligent transport systems
LTE	Long-term evolution
MAC	Medium access control
MHD	Multi-hop DENM
OSI	Open system interconnection
PHY	Physical
QoS	Quality of service
RC	Reselection counter
RTS	Request to send
SC-FDMA	Single-carrier frequency-division multiple access
SCI	Sidelink control information
SPS	Semi-persistent scheduling
TB	Transport block
TRC	Transmit rate control
TTI	Transmission time interval
URLLC	Ultra-reliable low-latency communication
WHO	World health organization

Chapter 1

INTRODUCTION

1.1 Background

According to the figures of the World Health Organization (WHO), road accidents cause nearly 1.35 million deaths and between twenty to fifty million injuries worldwide annually. This scenario is proof that prompt action should be taken to enhance the safety of vehicle users. Vehicular communication is identified as a measure to enhance the safety of vehicle users. The main objective of vehicular communication is to increase safety and reduce the high cost of traffic collisions. Apart from these main advantages, vehicular communication has several other advantages such as reducing traffic congestion, finding the best path by evaluating the real-time traffic data, analyzing traffic and pedestrian flow rates, and increasing effective road utilization

Vehicular communication helps to increase the intelligence of a vehicle by giving broader visibility about the road network; a concept known as the intelligent transportation system (ITS). A vehicle has to communicate with different elements in the road network, such as other vehicles, the infrastructure, the pedestrians, and the network to enhance its visibility. All of these communication types are commonly termed as the vehicle to everything (V2X) communication [2–8]. The precise position and velocity data can be generated using the global positioning system (GPS) and dead-reckoning data, combined with an accurate and detailed map. The reliability of positioning further improves with precise maps for automated driving and sensing well-mapped fixed infrastructure objects along the road. Each vehicle's position and velocity data to generate and maintain the dynamic map of its surroundings enable situational awareness and predict potential hazards. The existing sensors will be complementary to the communication and adding redundancy. Proper safety-related V2X communication has low latency, can cope with the high relative speeds between vehicles, high dynamics of the collection of nearby vehicles involved, and can bridge a substantial distance

and work under non-line-of-sight (NLOS) conditions.

Under V2X communication, two key enabling technologies had been introduced. The first commercial V2X communication technology is the IEEE 802.11p / dedicated short-range communication (DSRC) [9–17]. The initial version of this standard was approved under IEEE 802.11p in 2010 [18], then included in IEEE 802.11-2012 [19], and currently superseded by IEEE 802.11-2016 [20]. The third generation partnership project (3GPP) initializes the support for V2X communications using long-term evolution (LTE) sidelink communications and also known as LTE-V, LTE-V2X, LTE-V2V, or cellular-V2X (C-V2X) [21–29] in Release 14 (2017) [30, 31].

The medium access control (MAC) layer performance directly affects the latency and reliability of V2X communication. Similarly, managing the information exchange over the V2X communication is critical when different priority data streams are exchanged. Therefore, studying the MAC-layer performance, the priority management among multi-priority data streams and enhancing the MAC later performance of V2X communication technologies are of importance.

1.2 Motivation for the Thesis

- **Importance of the MAC Layer Performance Modeling:** The broadcast nature and the strict latency and reliability constraints of the packets in V2X communication make modeling of the MAC layer performance of IEEE 802.11p and C-V2X Mode 4 crucial. These models help to understand how the MAC layer operation affects the performance, that includes latency, reliability and throughput of both enabling technologies. The knowledge gained can be utilized for comparison and further enhancement of the V2X communication technologies.

- **Importance of Managing Multi-priority Data Streams:** Supporting multi-priority data streams plays a pivotal role in satisfying the stringent QoS requirements set for V2X communications. To address this problem, the European Telecommunications Standards Institute's intelligent transport systems operating in the 5 GHz frequency band (ETSI ITS G5) [32] has defined four traffic classes that utilize different broadcast packets, namely, decentralized environmental notification messages (DENM), high priority DENM (HPD), cooperative awareness messages (CAM), and multi-hop DENM (MHD), for V2X communication. Each packet type has its own frequency of generation, number of repetitions, latency constraints, and a

priority level. Studying the effects of multi-priority data streams is again crucial for the V2X networks that support a multitude of services such as safety-related messages, sensor information, and Internet sharing, creating the necessity of maintaining different priority levels among the data streams.

- **Importance of Enhancing the V2X Enabling Technologies:**

  The different delay and reliability constraints of the multi-priority data streams require further enhancing the V2X enabling technologies. For example, under ultra-reliable low-latency communication (URLLC) [33–41], which is a target usage scenario of 5G, the most stringent reliability requirement being standardized is 99.999 % with a latency bound of 1 ms. Enhancing V2X enabling technologies according to URLLC guidelines will be highly beneficial to V2X communications, particularly in future releases and the evolution of V2X in 5G and beyond.

1.3 The Focus of the Thesis

This thesis focuses on the MAC layer performance of the two enabling technologies of V2X communications, which are IEEE 802.11p and C-V2X Mode 4. Both these technologies enable the vehicles to autonomously select and manage their resources and communicate without infrastructure support. We utilize a discrete-time Markov chain (DTMC) [42–50] based approach to model the packet generators, queue models, and the MAC layer operations of the two technologies, and compare their performance by evaluating performance metrics such as the average delay, the collision probability, the channel utilization, and the throughput.

Subsequently, we focus on the operation of multi-priority data streams in the V2X communication. To this end, we extend the aforementioned DTMC models created for the packet generation, queues, and the MAC layer operations to support concurrent multi-priority data streams, according to the standards. This enables us to carry out a new performance comparison of the two technologies.

From these studies, it is shown that in the presence of multi-priority data streams, the IEEE 802.11p outperforms C-V2X Mode 4 in terms of delay and priority management, thanks to its enhanced distributed channel access (EDCA) [43, 51–56] mechanism. Thus, providing a delay-wise enhancement for C-V2X Mode 4 is vital, specifically in avoiding stale packets in the lower priority data streams. Therefore, we focus on a mechanism to enhance the MAC layer performance C-V2X Mode 4 in the presence of multi-priority data streams. To this

end, we study the possibility of enhancing the MAC-layer performance of C-V2X Mode 4 by allowing vehicles to use multiple candidate single-subframe resources (CSRs). For this, we modify the DTMC models to support multiple CSRs at each vehicle, and carryout a performance comparison.

1.4 Contributions and the Outline of the Thesis

Firstly, we discuss the fundamentals and background information in Chapter 2. This chapter presents V2X communication for ITS by explaining the ITS protocol stack and V2X communications applications based on the two enabling technologies. The MAC layer operation of each technology is presented, and then we briefly discuss the theory behind DTMCs. We conclude the chapter by presenting the related works for this thesis. The main contributions of this thesis are presented in Chapters 3, 4, and 5, respectively.

Firstly, Chapter 3 presents a comparison of the MAC-layer performance of the two enabling technologies by utilizing DTMC-based analytical models. The complete Markov model presented in this chapter consists of a DTMC each for the MAC layer operations of the two competing technologies, two DTMCs to model the generation of CAM and DENM packets, and a queuing model to represent a device-level packet queue. We obtain closed-form expressions for the steady-state probabilities of the DTMCs, which are then used to derive expressions for key performance metrics such as the average delay, the collision probability, and the channel utilization of a vehicular network. We present an application of the models to provide further insights and comparisons of the derived performance indicators through numerical evaluations. In particular, we show that C-V2X Mode 4 exhibits a lower collision probability compared to IEEE 802.11p, but IEEE 802.11p maintains a lower average delay compared to C-V2X Mode 4. Finally, the design insights on how the MAC layer performance of both technologies can be improved are presented. These insights can be utilized for future releases and evolution of the new radio V2X (NR-V2X) and IEEE 802.11bd [57, 58].

Chapter 4 presents the effect of four parallel multi-priority data streams, namely HPD, DENM, CAM, and MHD, on the MAC layer performance of the two enabling technologies. Firstly, we model the generation of the four multi-priority data packets by utilizing four DTMCs. The separate DTMCs provide us the flexibility of altering the traffic arrival patterns of the individual packet types, and create a more realistic V2X communication scenario compared to the simpler models with predefined traffic rates found in the literature [59], [60]. We

use four more DTMCs to model the device-level packet queues of the generated packet types, and each generator model is appropriately coupled with its queue model. We then model the MAC layer operations of each V2X enabling technology using DTMCs. These models are appropriately coupled with the generator and queue models while taking priority levels among data streams into consideration. The priority management makes this approach significantly different from Chapter 3, in terms of the overall models, the results, and the drawn insights. Since Chapter 3 neglects the priority levels of the packets, the generated packets are transmitted in the order of generation. We then present an application of the models. We first highlight the importance of considering all four parallel data streams when studying the MAC layer performance of the two technologies, by comparing them with a scenario where only one subset of the packet types is utilized for communication. We compare the two technologies using the derived performance measures while providing insights on the synchronous operation of multi-priority data streams. In particular, IEEE 802.11p is superior in terms of average delay but exhibits a higher number of collisions than C-V2X Mode 4. Also, it can be seen that IEEE 802.11p treats multi-priority data streams more fairly than its counterpart, thanks to its inbuilt EDCA mechanism. Finally, the numerical evaluations are used to draw insights on how the performance of each technology can be enhanced in the presence of parallel multi-priority data streams. We also present comparisons with similar results obtained according to the models in Chapter 3 to highlight the significance of priority management in the MAC layer performance.

Chapter 5 presents the proposed modifications for the MAC layer operations of C-V2X Mode 4. We use the DTMC-based overall model in Chapter 4 consisting of multi-priority data streams for this analysis. Since there is no special mechanism for priority management, C-V2X Mode 4 faces the risk of encountering stale packets in the low priority queues. We propose allowing a vehicle to use multiple radio resources to address this problem. In this approach, we identify two fundamental problems; *i.e.,* how many radio resources should be allocated to each vehicle based on the number of vehicles in the system and how to distribute the multi-priority data streams among those radio resources. We propose an algorithm for performance enhancement by answering those two questions. From the results, we can observe that using multiple radio resources can significantly reduce the average delay of the low priority data streams, alleviating the issue of stale packets. Chapter 6 presents conclusions and potential future work.

1.5 Publications List

1.5.1 Journal Papers

1. G. P. Wijesiri, J. Haapola, and T. Samarasinghe, "A discrete-time Markov chain based comparison of the MAC layer performance of C-V2X Mode4 and IEEE 802.11p," *IEEE Transactions on Communications,* vol. 69, no. 4, pp. 2505–2517, Apr. 2021. - Presented in Chapter 3.

2. G. P. Wijesiri, J. Haapola, and T. Samarasinghe, "The Effect of Concurrent Multi-priority Data Streams on the MAC Layer Performance of IEEE 802.11p and C-V2X Mode 4," *IEEE Transactions on Communications*, vol. 70, no. 1, pp. 592-605, Jan. 2022. - Presented in Chapter 4.

3. G. P. Wijesiri, T. Samarasinghe, and J. Haapola, "Performance Enhancement of C-V2X Mode 4 Utilizing Multiple Candidate Single-subframe Resources," *Submitted to IEEE Transactions on Intelligent Transportation Systems*, Dec. 2021. (Revised 12-Apr-2022, Revised 02-Nov-2022) - Presented in Chapter 5.

1.5.2 Conference Papers

1. G. P. Wijesiri, J. Haapola, and T. Samarasinghe, "A Markov Perspective on C-V2X Mode 4," in *Proc. IEEE 90th Vehicular Technology Conference*, pp. 1-6, Honolulu, HI, USA, Sep. 2019. - Presented in Chapter 3.

2. G. P. Wijesiri, J. Haapola, and T. Samarasinghe, "The Effect of Multiple Access Categories on the MAC Layer Performance of IEEE 802.11p," in *Proc. IEEE Global Communications Conference,* pp. 1-6, Taipei, Taiwan, Dec. 2020. - Presented in Chapter 4.

Chapter 2

BACKGROUND AND RELATED WORKS

2.1 V2X Communications for ITS

ITS can be considered a combination of the transportation systems and information communication technology (ICT). They integrate advanced sensors, computers, electronics, communication technologies, and management strategies to achieve safety and efficiency in vehicular networks. The reference protocol stack of an ITS station (Figure 2.1) specified in [61] follows the international organization of standardization – open system interconnection (ISO-OSI) reference model and defines four horizontal and two vertical protocol layers. The four horizontal layers from the bottom to the top of the reference model are the access layer, the network and transport layer, the facilities layer, and the application layer.

ITS access technologies cover various communication media and related protocols for physical and MAC layers. The access technologies are used in two ways, *i.e.,* within the ITS station communication (among ITS station's internal components) and between the ITS stations' communications. The network and transport layer contains data communication protocols among ITS stations and ITS station to the core network (for example, the internet). The network protocols carry information related to routing data between the communicating nodes. ITS transport layer protocols are responsible for the end-to-end data delivery. The additional services, *i.e.,* reliable data transfer, flow control, and congestion avoidance are operated by the transport layer protocols based on the application requirement and facilities of the ITS station. The IPv6 portion of the network and transport layer provide the transmission of IPv6 packets over ITS network protocols, dynamic selection of ITS access technologies, and handover and interoperability between IPv6 and IPv4. The ITS facilities layer protocols provide its services to ITS applications. The facilities layer services include data structuring, aggregation, maintaining the data of different sources, addressing, and message handling. The application layer is responsible for handling the ITS application

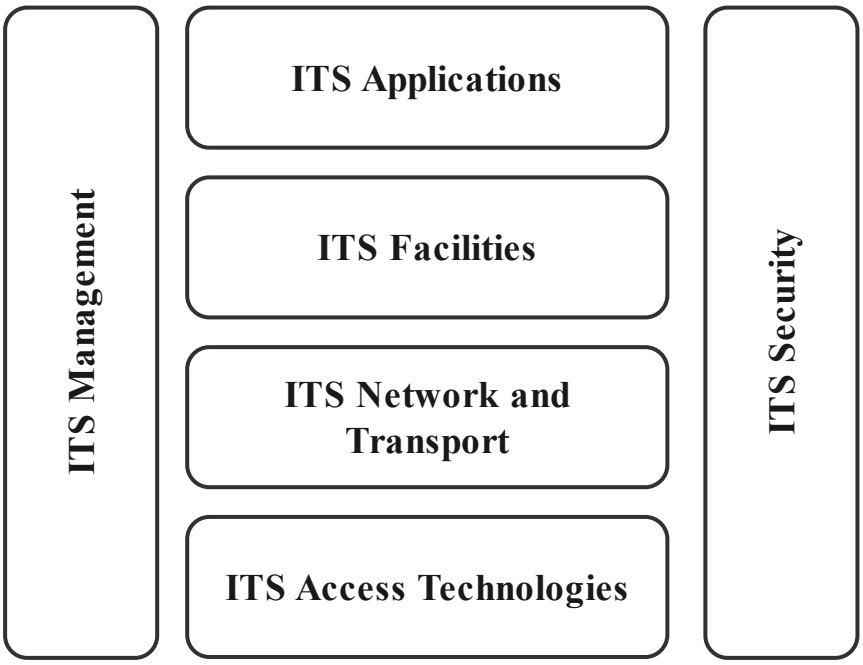

Figure 2.1: ITS protocol stack of an ITS station.

as similar to the OSI model.

The ITS management and security are the two vertical protocol entities. ITS management entity handles the configuration of an ITS station and the communication between different layers (cross-layer communication). ITS security entity protocols manage the security and privacy between the ITS stations communication. It provides secure messaging between the communication stack layers, manages identities and credentials within ITS stations, and handles secure platforms such as security gateways and firewalls.

Next, we introduce applications of V2X communications [62–66] and the two key enabling technologies of V2X communication together with their protocol stacks and operations.

2.2 V2X Communication Applications

A significant improvement in the wireless communication for ITS applications for road transportation can be observed in the last decade. Vehicle to vehicle (V2V), vehicle to infrastructure (V2I), vehicle to pedestrian (V2P), vehicle to the network (V2N) are expected to bring important benefits in terms of safety, granular traffic management, reduced congestion, and fuel savings. These communication modes are compiled in the term V2X communication, as illustrated in Figure 2.2.

The V2X communication requirements are drafted by considering large sets of ITS use case scenarios [67]. The difference between the safety and non-safety ap-

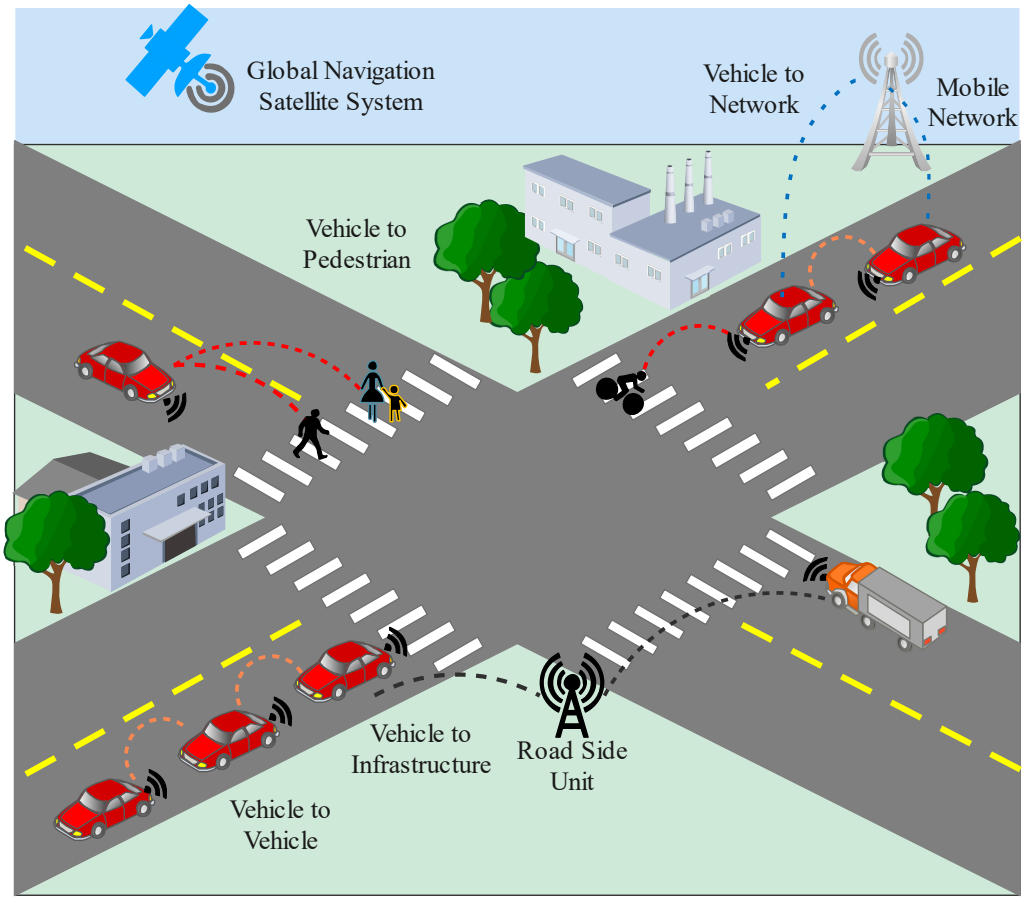

Figure 2.2: V2X communication network.

plications are clearly defined. The communication requirement benchmark is set by focusing on safety applications in terms of maximum latency, reliability, and information exchange frequency. Many safety-related use cases aim to avoid collisions between vehicles and vulnerable road users such as cyclists and pedestrians. Safety applications aim to minimize the collision between vehicles and vulnerable road users such as cyclists and pedestrians. Some examples include a vehicle reaching a junction or a blind bend, weakened visibility under foggy conditions, and cyclist or pedestrian crossings. Information gathered from sensors such as radar, camera, and lidar can be utilized to identify specific hazardous scenarios. However, continuous and event-triggered information exchanging and processing can significantly increase the visibility of vehicles in all kinds of weather conditions and visible range. Next, we present the two key enabaling technologies for V2X communications.

2.3 Communication Technologies for V2X

2.3.1 IEEE 802.11p

IEEE 802.11p is a reformation of the IEEE 802.11 standard to include wireless access in vehicular environments (WAVE). IEEE 802.11p is the IEEE standard used by V2X applications in the 5.9 GHz (5.85-5.925 GHz) band. The United States department of transportation's DSRC and the European standard for vehicular communication known as ETSI ITS-G5 are also based on the IEEE 802.11p standard.

Since we are constantly moving towards intelligent vehicles, providing for fast and reliable communication is vital in V2X, not only for increased services, but also for the safety concerns. Failure to communicate important information can be fatal in high-speed vehicle movements. IEEE 802.11p mainly aims to provide such information and has become an international standard communication protocol for WAVE.

V2X communication requires a reliable connection with low latency since the communication link between vehicles, pedestrians, and roadside infrastructure will mainly exist for short intervals, which means there will not be sufficient time to perform the usual authentication procedures. The principal modification in IEEE 802.11p compared to IEEE 802.11 is the reduction of MAC layer overhead for establishing communications between vehicles. A beacon is used to distribute the required information and offered services to establish a connection between vehicles, which excludes the authentication process.

The protocol stack for the IEEE 802.11p standard is shown in Figure 2.3. This follows the reference protocol stack of the ITS station. The application layer supports for both safety and non-safety protocols. Messages/facilities and network and transport layers provide protocols to support the same purposes described in the ITS protocol stack. Security is handled by the family of IEEE 1609 standard. The access layer contains the IEEE 802.11p MAC and PHY sub-layer protocols and services.

2.3.2 Cellular-Vehicle to Everything

The 3GPP introduced its initial version of V2X enabling technology in Release 14 in 2017 as a competitor to IEEE 802.11p. This standard is commonly referred to as LTE-V, LTE-V2X, or C-V2X.

Through ETSI and IEEE, the automotive industry has conducted considerable work defining the applications, the message or facilities, security services, and

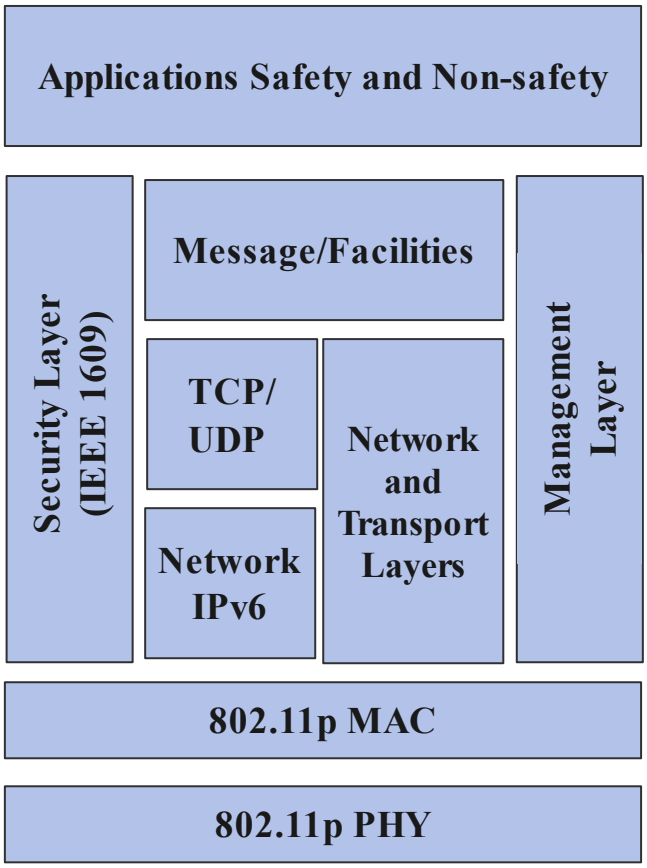

Figure 2.3: IEEE 802.11p protocol stack.

the network and transport layers. C-V2X reuses all of the existing standards in these layers and only replaces the PHY and the MAC (commonly called the access layers) from 3GPP to provide the end-to-end solution. The C-V2X station protocol stack is shown in Figure 2.4.

The physical layer of C-V2X deploys the single-carrier frequency-division multiple access (SC-FDMA) as the access technology with 10 and 20 MHz channels. The channel is partitioned into subframes in the time domain and subchannels in the frequency domain. A subframe represents the transmission time interval (TTI) of 1 ms. The smallest unit of channel resources assigned to a node is named a resource block (RB). An RB represents 180 kHz in the frequency domain and a slot time (half of a subframe) in the time domain. The subchannel in C-V2X represents a group of RBs within a subframe, and the RB count in a subchannel can vary. Data and signaling information are transmitted in the transmit blocks (TBs) and sidelink control information (SCI), respectively. A whole packet *e.g.*, a CAM is transmitted over the TB with its associated SCI, which includes information such as the RBs it utilizes, modulation and coding scheme, and resource reservation interval related to the semi-persistent scheduling algorithm (SPS) in

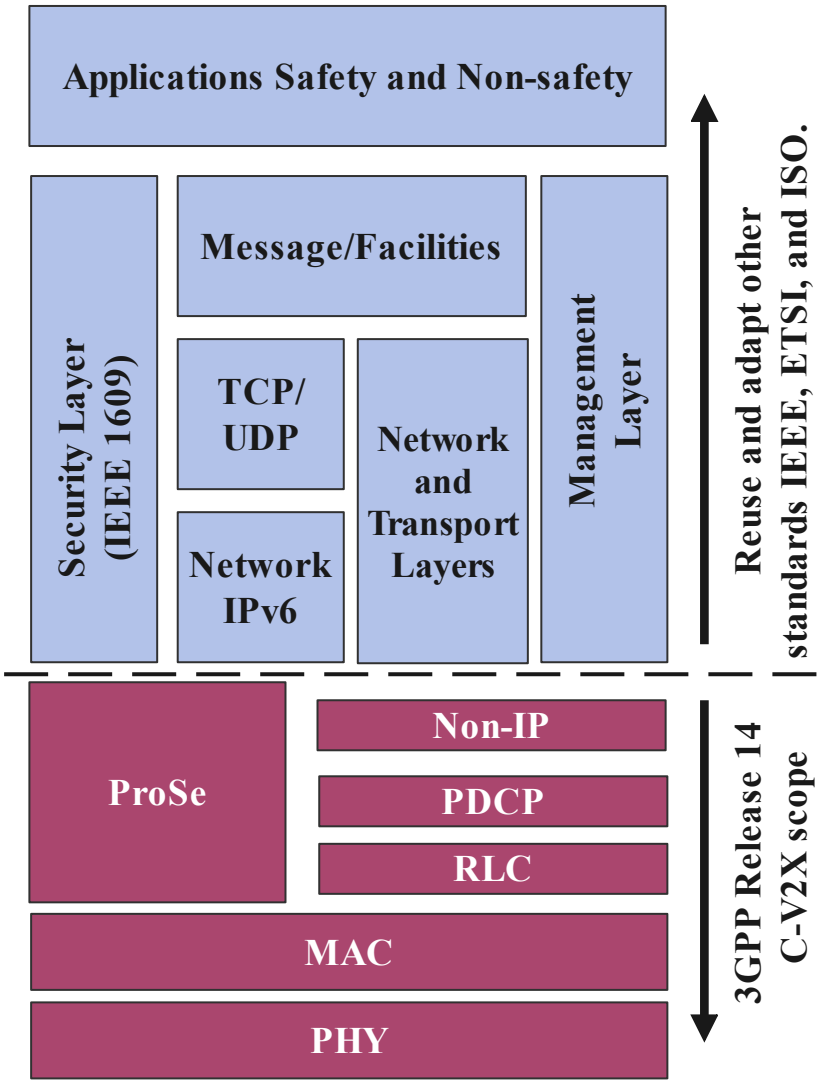

Figure 2.4: C-V2X protocol stack.

the MAC layer. The accuracy of the SCI information is crucial to decode the TB accurately by neighboring vehicles.

C-V2X includes two radio-interfaces, namely PC5, and the cellular interface (Uu) that support vehicle-to-infrastructure and V2V communications, respectively. In 3GPP Release 12, device-to-device (D2D) communication was introduced for public safety applications, including two modes: Mode 1 and Mode 2 [68]. The main aim of these modes was to extend the battery life of a node by sacrificing the latency. Since V2X communication demands high reliability and low-latency, Mode 1 and 2 were not deemed suitable for handling V2X communication.

In 3GPP Release 14, two novel communication modes namely Modes 3 and 4 are introduced explicitly for V2V communications, as shown in Figure 2.5. In

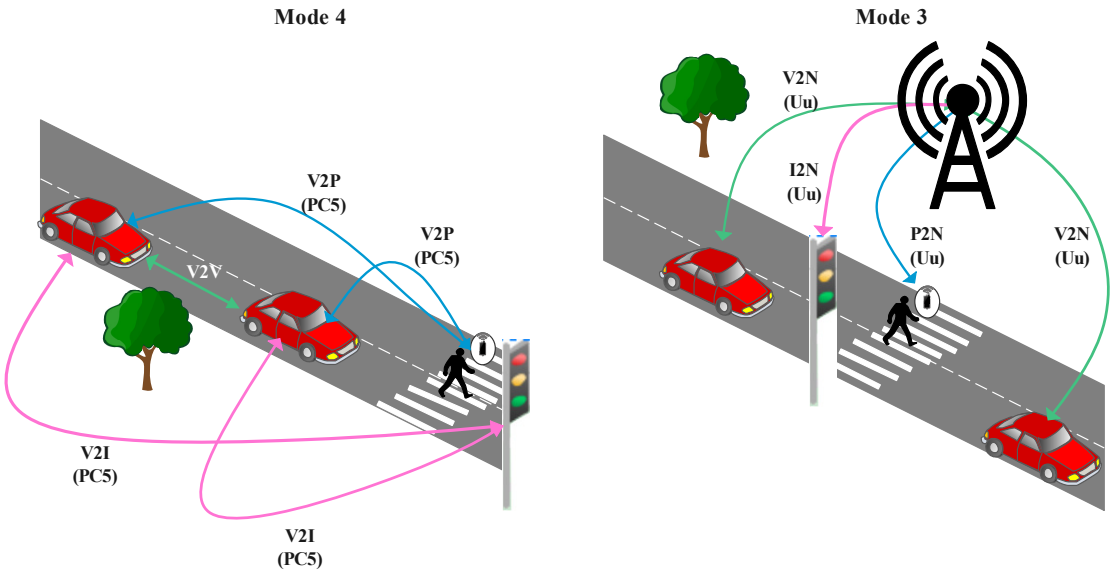

Figure 2.5: C-V2X Mode 4 vs Mode 3.

C-V2X Mode 3, V2V communication radio resource allocation and management are handled by the base station. Conversely, in C-V2X Mode 4, vehicles by themselves select the radio resources thanks to the SPS algorithm. In other words, C-V2X Mode 4 can operate without cellular coverage. Therefore, C-V2X Mode 4 is considered the baseline V2V communication mode since the safety applications cannot depend on cellular coverage availability. C-V2X Mode 4 provides a non-centralized/distributed scheduling scheme by allowing vehicles to select radio resources. Figure 2.6 illustrates how the emergency electronic brake light (EEBL) warning is transmitted from the initiated vehicle to another vehicle and network infrastructure through the protocol stack and the air interface.

2.4 MAC Layer Operation of V2X Communication Technologies

In this section, the MAC layer operation of each V2X enabling technology is descried in detail. The MAC layer operation of IEEE 802.11p uses a contention based mechanism called carrier sense multiple access/ collision avoidance mechanism (CSMA/CA). In this thesis, we focus on the C-V2X Mode 4 MAC layer operation as it shows similar connectivity to IEEE 802.11p, as they can directly connect between vehicles without the help of network infrastructure. The MAC layer operation of C-V2X Mode 4 is based on the SPS algorithm which uses a distributed scheduling mechanism to select radio resources for communication. We start by explaining the MAC layer operation of IEEE 802.11p.

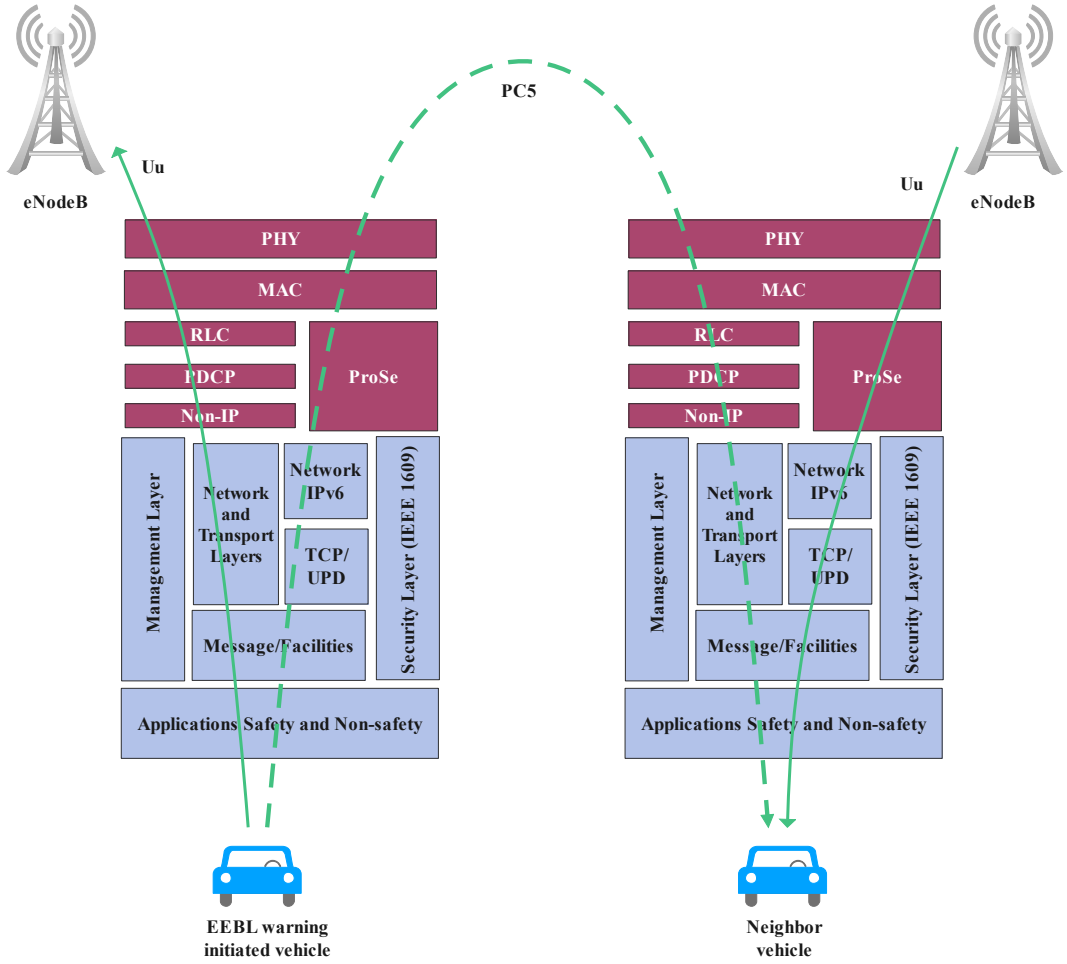

Figure 2.6: An illustration of the communication for a V2X application.

2.4.1 MAC Layer Operation of IEEE 802.11p

The primary medium access control mechanisms used in IEEE 802.11p are CSMA /CA, backoff (BO), and the EDCA mechanism. A node using the well-known CSMA/CA mechanism senses the medium before it transmits a packet, and if the channel is idle, it transmits the whole packet. However, if the channel is not idle, the node initiates a random backoff counter and tries to sense the channel at the end of the backoff time duration. The CA is utilized to enhance the performance of the CSMA method by attempting to share the channel equally among the competitors within the collision domain. In CSMA/CA mechanism, one common problem is the hidden node problem, in which the target node does not detect another nodes' transmission. Different factors can be the cause of this problem; receiver sensitivity, transmit power, and distance between nodes are a few of them. The request to send/clear to send (RTS/CTS) mechanism is one solution for the hidden terminal problem. However, IEEE 802.11p does

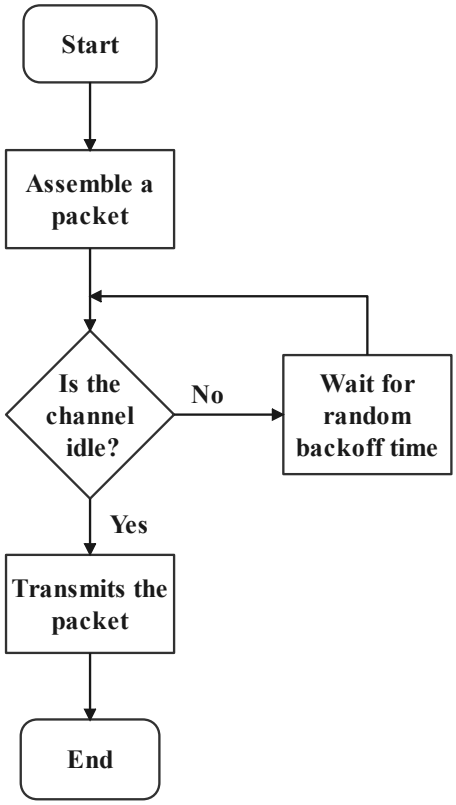

Figure 2.7: Simplified algorithm of CSMA/CA.

not use that option since the RTS/CTS mechanism adds more overhead to V2X communication. A simplified algorithm of the CSMA/CA mechanism is shown in Figure 2.7.

IEEE 802.11p MAC layer enhances its ability to support the quality of service (QoS) by deploying the EDCA mechanism. Different priority packets are assigned to different access category (AC) queues in the MAC layer based on their priority level. In this thesis, we consider the four ACs namely, voice (AC_{vo}), video (AC_{vi}), best-effort (AC_{be}), and background (AC_{bk}). The different types of packets with various QoS requirements are assigned to those ACs. The packet has to wait an arbitrary inter-frame space ($AIFS$) time before entering into the backoff process. Each backoff stage packet has to wait a random amount of time, depending on the contention window (CW) size and the channel state before it transmits. The $AIFS$ values in each AC are set based on the standard [1]. The logic behind allocating time for $AIFS$ is allocating longer $AIFS$ duration for the lower priority packets and vice-versa. Similarly, smaller CW sizes are assigned for the higher priority ACs, and large CW sizes are allocated for the lower priority ACs. The assignment of $AIFS$ and CW values with ACs are shown in Table. 2.1.

Table 2.1: Parameter values for different ACs [1]

AC	CW	$AIFS$ (ms)
AC_{vo}	3	58
AC_{vi}	7	71
AC_{be}	15	110
AC_{bk}	15	149

2.4.2 The MAC layer Operation of C-V2X Mode 4

The MAC layer process of C-V2X Mode 4 is significantly different from the IEEE 802.11p, and it uses a distributed scheduling mechanism called a sensing-based SPS algorithm. In this algorithm, the target vehicle learns the radio resource usage of neighboring vehicles in its vicinity and randomly selects a radio resource from the most feasible radio resource list in the selection window. The selection window is the time window that initiates at the time of the generation of a packet. The target vehicle identifies all possible radio resources that can be reserved for the transmission from the selection window as shown in Figure 2.8.

In the sensing process, the target vehicle looks back for the previous 1000 ms period, and it studies the usage of radio resources of the neighboring vehicles in its vicinity using the SCI. When the vehicle is going to select the radio resource for transmitting its next available packet, it makes sure that it avoids the radio resources that may be used by neighboring vehicles that creates packet collisions. Parallelly, during the scanning period of 1000 ms, the target vehicle transmits using the radio resources. The vehicle cannot listen to this resource due to half-duplex transmission in the wireless medium. Therefore, the target vehicle excludes all the radio resources it uses during the previous 1000 ms period. After excluding all these radio resources, which might cause collisions, the target vehicle randomly selects the radio resource from the rest of the radio resources in the selection window.

After selecting a radio resource, a vehicle reuses it for resource counter (RC) times. The resource counter is a parameter uniform and randomly selected from a window set by the standard [31], which varies on the selection window size. At each transmission opportunity, the RC is reduced by one, and when it reaches one, a new radio resource is selected with $1-p$ probability and keeps the old radio resource with the p probability as shown in Figure 2.8. The main objective of this MAC layer operation is to empower the vehicle to select the radio resource to transmit its data with minimum collision probability, being independent from the

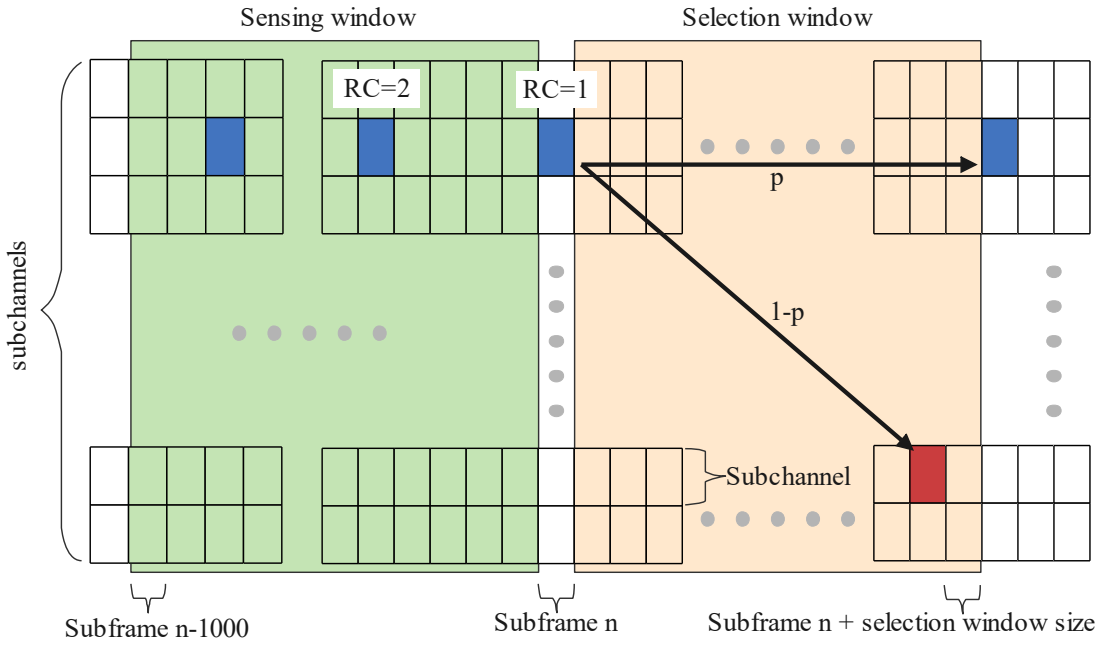

Figure 2.8: Reselection process in the SPS algorithm.

cellular network. The detailed description of the MAC layer operation of C-V2X Mode 4 is presented in Chapter 3.

2.5 Markov Modeling

Markov chain [69] models consist of two types which are DTMCs and continuous time Markov chains (CTMCs). A typical random process X where $\{X_t : t \in T\}$ of random variables index by elements of set T. When $T = \{0, 1, 2, \dots\}$, we consider the DTMC and, alternatively, for $T = [0, \infty)$ consider as the CTMC [70].

In this thesis, DTMCs are utilized for the modeling. DTMC-based modeling facilitates improved granularity in the models. This enables us to precisely model the MAC layer operations in discrete time. The memoryless property in DTMCs makes the analysis mathematically tractable. Next, we discuss some important properties of DTMCs.

Memorylessness: Let $\{X_0, X_1, \dots\}$ be a sequence of random variables which take values in some countable set S, called the state space. We assume that each X_n is a discrete random variable which takes one of N possible values, where $N = |S|$. The process X is a discrete time Markov chain if it satisfies the memoryless property:

$$P[X_{n+1} = x_{n+1} | X_0 = x_0, ..., X_n = x_n] = P[X_{n+1} = x_{n+1} | X_n = x_n],$$

for all $n \geq 1$ and all $x_0, x_1, ..., x_{n+1} \in S$.

Interpreting n as the 'present' and $n+1$ as a 'future' moment of time, we can rephrase the memoryless property as "given the present value of a Markov chain, its future behaviour does not depend on the past" [70].

Irreducible: Two states communicate ($i \leftrightarrow j$) if they can access each other. If two states communicate, they are in the same class. A Markov chain is irreducible if it has only one class.

Recurrence/Transience: A state i is said to be transient if, given that Markov chain starts in state i, there is a non-zero probability that it will never return to i. Let $f_{ii}^{(n)}$ be the probability that we return to state i for the first time after n steps. State i is transient if $\sum_{n=1}^{\infty} f_{ii}^{(n)} < 1$. State i is recurrent if it is not transient. Recurrent states are guaranteed to have a finite re-visit time. The mean recurrence time at state i is given by $M_i = \sum_{n=1}^{\infty} n.f_{ii}^{(n)}$. State i is positive recurrent if $M_i < \infty$; otherwise, state i is null recurrent. A finite state-space irreducible Markov chain is positive recurrent [70].

Periodic/Aperiodic: State i is periodic with period $k > 1$ if k is the smallest number such that all paths leading from state i back to state i have a length which is a multiple of k. If the returning to a recurrent state happens at irregular times, it is called aperiodic. A Markov chain is ergodic if it is positive recurrent and aperiodic.

Homogeneous: A Markov chain X is named homogeneous [70] if

$$P(X_{n+1} = j | X_n = i) = P(X_1 = j | X_0 = i) \ \forall i, j, n$$

Let P_{ij}^n denote the transition probability from state i to state j at time n. One step transition probability can be expressed as

$$P_{ij} = P(X_{n+1} = j | X_n = i) = P(X_1 = j | X_0 = i),$$

and the k-step transition probability can be expressed as

$$P_{ij}^k = P(X_{n+k} = j | X_n = i) = P(X_k = j | X_0 = i).$$

A stationary distribution π is a (row) vector, whose entries are non-negative and sum to 1, and is unchanged by the operation of the transition matrix $\mathbf{P}$ on it. That is π P$= \pi$, where $\mathbf{P}$ denotes the transition matrix. An irreducible chain has a stationary distribution if and only if all of its states are positive recurrent. If a Markov chain is time homogeneous, irreducible, aperiodic, and it has a stationary distribution $\{\pi_i\}_{i \in S}$, then $\lim_{n \to \infty} P_{ij}^n = \pi_j, \forall j \in S$. It holds

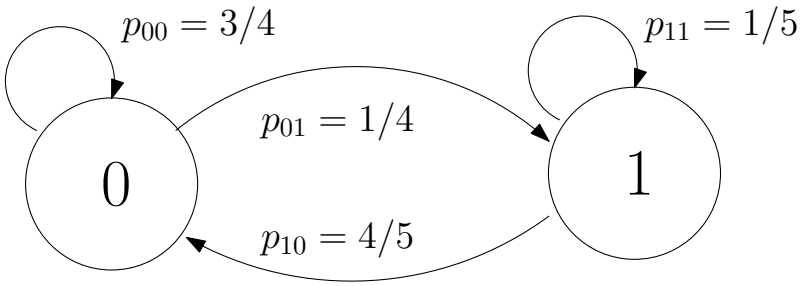

$$\text{State space } S = \{0, 1\}$$

$$\text{Transition matrix } \mathbf{P} = \begin{bmatrix} p_{00} & p_{01} \\ p_{10} & p_{11} \end{bmatrix} = \begin{bmatrix} 3/4 & 1/4 \\ 4/5 & 1/5 \end{bmatrix}$$

Figure 2.9: A DTMC example.

the property, $\sum_{j=0}^{\infty} \pi_j = 1$. For an example scenario, Figure 2.9 illustrates a two states DTMC. Therefore, by solving the (2.1) and (2.2) we can calculate the steady-state probabilities of the states π_0 and π_1.

$$[\pi_0, \pi_1] \begin{bmatrix} 3/4 & 1/4 \\ 4/5 & 1/5 \end{bmatrix} = [\pi_0, \pi_1] \tag{2.1}$$

$$\pi_0 + \pi_1 = 1 \tag{2.2}$$

$$\pi_0 = 0.762, \pi_1 = 0.238$$

2.6 Literature Review

Some of the literature associated with enabling technologies of V2X communication has already been introduced and discussed in Chapter 1 and the previous sections of this chapter. To summarize, the first commercial V2X communication technology is IEEE 802.11p/DSRC and the initial version of this standard was approved under IEEE 802.11p in 2010 [18], and was then included in IEEE 802.11p-2012 [19], which is currently superseded by IEEE.11-2016 [20]. As an alternative, 3GPP initiated C-V2X in Release 14 [30, 31] with two modes, *i.e.,* Mode 3 and Mode 4. In this research, we study the standards related to the IEEE 802.11p and C-V2X Mode 4.

Since IEEE 802.11p was introduced in 2010, a considerable number of research

works have been done to analyze its MAC layer performance. In [71], the authors investigate the performance of IEEE 802.11p by proposing a novel mathematical model based on queuing theory and stochastic geometry. The authors in [72] present a multidimensional Markov chain model that models the deferring period, allowing them to solve for the broadcast scheme of 802.11p systems accurately. In [73] the authors propose a Markov chain-based analytical model that depicts a representation of the IEEE 802.11p MAC layer and considers both saturated and unsaturated traffic conditions. Even though analytical models already exist [73], they do not have the modeling granularity of $aSlotTime$, which is the smallest unit in IEEE 802.11p standard.

Performance analysis of C-V2X Mode 4 has become an active research area recently. The related works can be mainly categorized as simulation [22, 74] and analytical modeling based [75–77] studies. The authors of [22] present the first open-source simulator for C-V2X Mode 4, utilizing the NS3 software, and study the performance of the technology. A similar study using the VEINS open-source framework is presented in [74]. The first analytical model for the MAC layer operations of C-V2X Mode 4 is proposed in [75]. They consider a PHY layer model to capture the effect of distance between the vehicles, and the MAC layer operation is handled by the SPS algorithm [31]. The authors then obtain analytical expressions for several performance measures at the MAC layer as a function of the distance between the communicating nodes. In [76], the authors compare the MAC layer performance of C-V2X Mode 4 with IEEE 802.11p for the transmission of periodic and aperiodic messages, having both fixed and variable sizes. The authors in [77] propose an enhancement to the SPS algorithm in order to reduce the wireless blind spot duration. The proposed method demonstrates the benefits against the legacy mode, both analytically in a simplified scenario and through simulations in a highway environment.

In the context of studying MAC layer performance, generating packets is another crucial aspect. To achieve this, the authors of [75] use a packet generator with a constant packet arrival rate, producing packets with similar traits to CAM. On the other hand, the authors of [73] use a straightforward Bernoulli process for their random packet generator to simulate event-driven packet generation like DENM. However, this generator overlooks periodic traffic like CAM and the repeated transmission of DENM packets for enhanced reliability, as mentioned in [78].

Then, we consider modeling the MAC layer performance of the two enabling technologies with multi-priority data streams in operation. Several research works

that focus on the MAC layer performance of IEEE 802.11p in the presence of parallel multi-priority data streams can be identified in the literature [59, 60, 79–81]. The initial work on the MAC layer performance modeling of the IEEE 802.11p EDCA mechanism has considered only a selective subset of the four ACs [79–81]. Subsequently, the authors of [59] and [60] considered the parallel operation of all four ACs in their DTMC-based modeling, and can be considered to be closely related to our work. Our model firstly improves the slight inconsistencies of [59] and [60] with the standard, in terms of broadcast traffic. The increased granularity makes our model more complex, but in turn, more accurate compared to [59] and [60]. We precisely model the waiting times of different ACs before resuming channel contention, enabling us to correctly capture the effects of prioritization among the ACs, which are not done in [59] and [60]. An AC bearing a higher priority can initiate transmission during the long waiting period of an AC with lower priority. Transmission delays are also calculated more accurately than in [59] and [60] by taking the payload size into account. However, there is no separate mechanism to handle the multi-priority data streams in C-V2X Mode 4 MAC layer operation, we use the same model we have initially developed. The priority management is achieved by giving preference to higher priority packets, upon a transmission opportunity implemented in the queue models.

Finally, we study the different approaches on enhancing the C-V2X Mode 4 MAC layer performance. In [82] the authors propose a nonlinear power averaging phase, where the most up–to–date measurements are assigned higher priority via weighting. This shows performance enhancement compared to the linear average of the perceived power intensities on each of the subchannels during a monitoring window, according to 3GPP. The study in [74] analyzes the optimum configuration of the parameters that mostly influence the operation and performance of C-V2X Mode 4. This study has shown the operating conditions for which increasing the probability of using the previous radio resource can improve the performance, while some enhancements can be obtained using an exponential sensing window sizes under high channel load levels. A comprehensive analysis of the impact of variations in the transmit power of the vehicle on the performance of sensing-based SPS for C-V2X Mode 4 in various traffic scenarios is presented in [83].

More related works have been discussed in Chapters 3, 4, and 5.

Chapter 3

DTMC BASED COMPARISON OF THE MAC LAYER PERFORMANCE OF C-V2X MODE 4 and IEEE 802.11P

V2V communication plays a pivotal role in intelligent transport systems (ITS) with C-V2X and IEEE 802.11p being the two competing enabling technologies. This chapter presents multi-dimensional discrete-time Markov chain (DTMC) based models to study the MAC layer performance of the IEEE 802.11p standard and C-V2X Mode 4, considering periodic CAM and event-driven DENMs. Closed-form solutions for the models' steady-state probabilities are obtained, which are then utilized to derive expressions for several key performance metrics. Numerical results are provided to draw insights on the performance. In particular, a performance comparison between IEEE 802.11p and C-V2X Mode 4 in terms of the average delay, the collision probability, and the channel utilization is presented. The results show that IEEE 802.11p is superior in terms of average delay, whereas C-V2X Mode 4 excels in collision resolution. The chapter also includes design insights on possible future MAC layer performance enhancements of both standards.

3.1 Introduction

3.1.1 Background and motivation

V2X communication is envisioned to be a major technological advancement that shapes our future mobility and quality of life. Vehicular networks primarily depend on V2X communications in enabling an active safety environment. To this end, IEEE 802.11p/DSRC is known to be the first commercial V2X communication technology. The first WiFi-based standard specifically designed for vehicular communications was approved under IEEE 802.11p in 2010 [18], later included in IEEE 802.11-2012 [19], and now superseded by IEEE 802.11-2016 [20]. The ETSI ITS-G5 [1, 32, 84, 85] subsequently has been approved as the European version of the IEEE 802.11p standard.

As an alternative to IEEE 802.11p, the 3GPP included support for V2X communications using LTE sidelink communications, *a.k.a.*, LTE-V, LTE-V2X, LTE-V2V, or Cellular-V2X (C-V2X). The LTE sidelink was introduced for public safety D2D communications in Release 12 as Mode 1 and Mode 2. Release 14 introduced Mode 3 and Mode 4, specifically designed for V2X communications [30, 86]. Mode 3 enables direct communication between two vehicles, but the selection and management of the radio resources are taken care by the cellular infrastructure. C-V2X Mode 4 on the other hand has many operational similarities with 802.11p. Both technologies facilitate the vehicles to autonomously select and manage their resources and communicate without any infrastructure support. In this chapter, we focus on ETSI ITS-G5 802.11p and C-V2X Mode 4.

Vehicular communication mainly consists of an exchange of small broadcast packets with critical latency and reliability constraints. To this end, CAM and DENM are two types of broadcast packets used by both IEEE 802.11p and C-V2X Mode 4 in enabling effective communication and ensuring safety. Information related to cooperative awareness, such as position, dynamics, and attributes, is packed in the periodically transmitted CAM packets [84]. On the other hand, DENM are event-driven messages, triggered by random events such as sudden human-initiated disturbances to the vehicle's pattern of motion, (*e.g.,* lane changing, signal violation, emergency braking, road-works), and events caused by weather or nature [85]. The broadcast nature, and the strict latency and reliability constraints of the packets make the MAC layer performance of these technologies crucial, which triggered our motivation for this study.

The MAC layer operations of the two competing technologies are significantly different from one another. The multiple access technique in IEEE 802.11p is a version of the well-known CSMA/CA. The contention-based protocol requires a vehicle to sense the medium and check if it is idle before transmitting. A mechanism based on random backoff is executed to reduce the probability of collisions. On the other hand, C-V2X Mode 4 utilizes a distributed sensing-based scheduling protocol called semi-persistent scheduling [31]. Vehicles sense and keep track of the previous transmissions of all neighboring vehicles to estimate free resources and pick a free resource for transmission to avoid packet collisions. This work primarily focuses on analytically modeling the MAC layer protocols of C-V2X Mode 4 and IEEE 802.11p by utilizing DTMCs.

3.1.2 Related works

Several works have recently discussed the two technologies from various perspectives, mainly focusing on the physical (PHY) layer, with some providing performance comparisons as well [68, 87–94]. The MAC layer performance has been studied in [73, 75, 95, 96]. The first analytical model for the MAC layer performance of C-V2X Mode 4 is proposed in [75]. The chapter considers a PHY layer model to capture the effect of the distance between a transmitting node and a receiving node, and the SPS algorithm for resource allocation. The authors then obtain analytical expressions for key MAC layer performance metrics as a function of the distance between the transmitter and the receiver. The first DTMC based analytical model for C-V2X Mode 4 is presented by the authors in [96].

In addition to the model for C-V2X Mode 4 presented in [96], this chapter also presents a DTMC based analytical model for the MAC layer operations of IEEE 802.11p, which facilitates a comparison of these two technologies. The proposed model in this work improves the DTMC for IEEE 802.11p presented in [73] along multiple facets. The main novelty is the higher modeling granularity (resolution). The improved modeling granularity allows us to study the whole protocol operation at the $aSlotTime$ level, which is the smallest time unit of 13 μs defined in the standard. The representation also in turn leads to a fair comparison with our model for C-V2X Mode 4, that can be studied at the smallest time unit in its standard, called the subframe (1 ms). Additionally, the model in our chapter, captures the effect of the arbitration inter-frame spacing (AIFS) duration, which is an important parameter used in IEEE 802.11p when dealing with multi-priority data streams. Thus, the model in this chapter is significantly different from the one in [73].

Modeling the packet generation is another important aspect of a study on MAC layer performance. To this end, [75] utilizes a packet generator with a fixed inter-arrival rate, generating packets with similar characteristics to CAM. The authors of [73] utilize a simple Bernoulli process for the random packet generator to model event-driven packet generation such as DENM. However, such a generator omits periodic traffic such as CAM, and also the periodic re-transmission of DENM packets, which is done for added reliability [78]. Another novel aspect of our work is implementing separate DTMC models for CAM (synchronous) and DENM (asynchronous) packet generation, intending to create a more realistic V2X communication environment. With these novel traffic generators, the system can be modeled for more complex and realistic traffic arrival patterns than

the packet generators found in the literature.

3.1.3 Contributions

The main contributions of this work can be summarized as follows:

- **Analytical modeling:** We provide detailed modeling of the MAC layer protocols of C-V2X Mode 4 and ETSI ITS-G5 IEEE 802.11p by utilizing DTMCs. The complete Markov model consists of a DTMC each for the MAC layer operations of the two competing technologies, two DTMCs to model the generation of CAM and DENM packets, and a queue model to represent a device level packet queue.

- **Derivation of performance metrics:** We obtain closed-form expressions for the steady-state probabilities of the DTMCs, which are then used to derive expressions for key performance metrics such as the average delay, the collision probability, and the channel utilization of a vehicular network.

- **Numerical comparison of performance:** We present an application of the models to provide further insights and comparisons on the derived performance indicators through numerical evaluations. In particular, we show that C-V2X Mode 4 exhibits a lower collision probability compared to IEEE 802.11p, but IEEE 802.11p maintains a lower average delay compared to C-V2X Mode 4.

- **Design insights for performance enhancement:** Design insights on how the MAC layer performance of both technologies can be improved are presented. These insights can be utilized for future releases and evolution into new radio V2X (NR-V2X) and IEEE 802.11bd [57, 58].

The remainder of the chapter is organized as follows. The analytical models and the steady-state solutions are presented in Sections 3.2 and 3.3, respectively. Section 3.4 consists of the performance analysis. The numerical results and discussion follow in Section 3.5, and Section 3.6 concludes this chapter.

3.2 Analytical Models

This section presents five DTMCs that are dependent on each other. Firstly, we use two DTMCs to model the generation of CAM and DENM packets. We refer to them as packet generators. The third DTMC models the device level packet queue of a vehicle that consists of the generated CAM and DENM packets. The

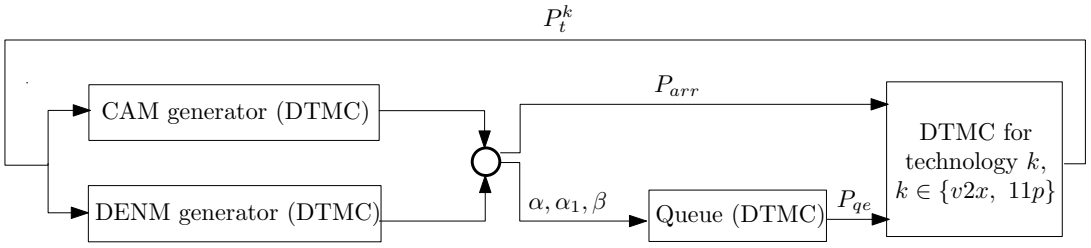

Figure 3.1: Flowchart illustrating the total model and the dependence among the individual DTMCs.

remaining two DTMCs model the MAC layer operations of C-V2X Mode 4 and ETSI ITS-G5 IEEE 802.11p, respectively. A holistic view of the overall model that consists of these DTMCs is illustrated in Figure 3.1, while also showing how they are interrelated. The parameters that lead to the dependence among the DTMCs will be formally introduced later in the section, while presenting the individual DTMCs.

All DTMCs ensure that there is a sequence of transitions of non-zero probability from any state to another (irreducible), and that the states are not partitioned into sets such that all state transitions occur cyclically from one set to another (aperiodic). Thus, the DTMCs are ergodic, and hence, a steady-state distribution exists [97]. The models are based on non-saturation conditions with regards to transmission, *i.e.*, they consider situations when there are no packets to transmit as well, making them more realistic compared to models that assume continuous transmission of packets (saturation conditions). However, the models do not account for a real received power based sensing mechanism. Thus the impact of relative distance, exposed and hidden terminals, are omitted in this study.

3.2.1 Packet generator and queue models

The generator models of CAM and DENM share significant similarities. Therefore, we use a single figure (Figure 3.2) to illustrate the DTMCs of the two generator models. The solid lines (black) are used to represent the states and transitions common to the state spaces of both models, and the states and transitions unique to the generation of a particular type of packet are differentiated using line styles and colors. The periodic CAM packet generation is modeled using a fixed inter-arrival time model, where the inter-arrival time T_C is set between 100 ms and 1000 ms according to the standard [84]. DENM, on the other hand, are random event-driven messages that are not periodic. Thus, an additional idle state ($Idle$) is included in the DENM generator to capture the periods with no DENM packet generation. Furthermore, DENM are generated on the observation of random

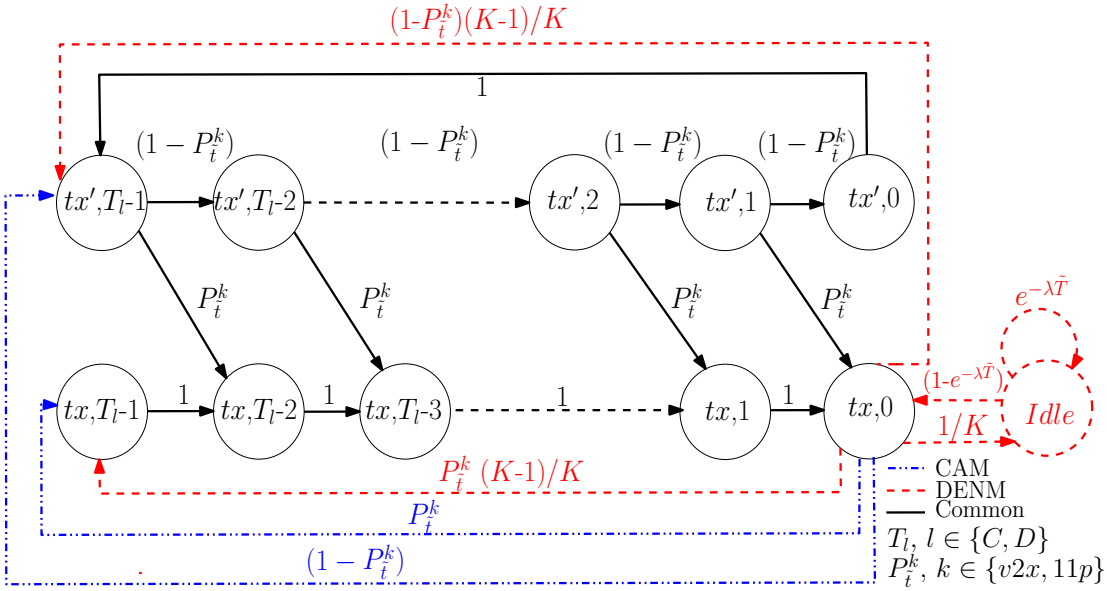

Figure 3.2: DTMC models for CAM and DENM packet generation, where the line styles are used to differentiate the two models.

events, thus the packet generation is random. Using a Poisson arrival process for such random packet generation is common in the literature on queuing theory (*e.g.*, the arrival of calls at an exchange), and the same has been implemented in [98] for DENM packets. Therefore, we model the triggered arrivals of DENM packets using a Poisson process of intensity λ packet/s, by assuming that the triggering events are independent of each other and do not occur simultaneously. Thus, the probability of at least one DENM packet trigger during $\tilde{T}$ s is given by $1 - e^{-\lambda\tilde{T}}$. Due to its critical nature, a DENM packet is repeated K times at a fixed period of T_D, for added reliability [78]. This means, the DENM generator captures two distinct packet types: a Poisson based triggered generation referred to as *trigger* and subsequent fixed-period repeat packet generations referred to as *repetition*. The trigger occurs only once per DENM event, and the repetition occurs $K - 1$ times following a trigger, periodically, similar to CAM. Due to this reason, the CAM generation and the DENM repetition are modeled using the common states. Moreover, according to the standard [85], the originator vehicle has the liberty of setting T_D.

The packet generation is represented using states $(i, 0)$, $i \in \{tx, tx'\}$. tx and tx' is used to differentiate between the transmit status of the previously generated packet, *i.e.*, whether it has been transmitted, or not, respectively. A packet generation is followed by a wait of T_l ms, $l \in \{C, D\}$, until the next packet generation. The waiting time is represented by states (i, j), $i \in \{tx, tx'\}$ and $j \in [0, T_l - 1]$, with a modeling granularity of 1 ms for C-V2X Mode 4, referred

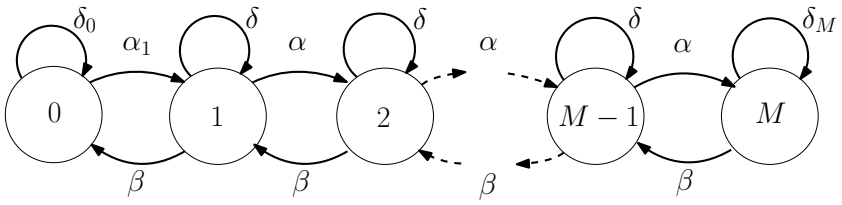

Figure 3.3: DTMC model for the common packet queue of length M consisting of the generated CAM and DENM packets.

to as a subframe, and 13 μs for IEEE 802.11p, referred to as $aSlotTime$. If a transmission opportunity is not available upon generation, it waits for an opportunity, represented by states (tx', j), $j \in [1, T_l - 1]$. A successful transmission results in a state transition from (tx', j) to $(tx, j-1)$, $j \in [1, T_l - 1]$. P_t^{v2x} and P_t^{11p} denote the probability of transmitting a packet in C-V2X Mode 4 and IEEE 802.11p, respectively, and these probability values link the generators with the DTMCs modeling the MAC layer operations as illustrated in Figure 3.1.

Figure 3.3 illustrates the DTMC that models the device level packet queue per vehicle, consisting of the generated CAM and DENM packets. State (i), $i \in [0, M]$, represents a queue length of i, where M is the maximum length of the queue. It is not hard to see that the state transitions of this DTMC depend on the packet generation and transmission. Thus, the transition probabilities of the queue model are directly related to the packet generators, as shown in Figure 3.1. A transmission of a packet may either lead to maintaining the current state (i) or a state transition from (i) to $(i-1)$, for $i \in [1, M]$, depending on whether a new packet has been generated concurrently, or not, respectively. Similarly, not being able to transmit a generated packet (*i.e.*, traversing through states (tx', j), $j \in [0, T_l - 1]$, in Figure 3.2 without a transmission opportunity), leads to a state transition from (i) to $(i+1)$, for $i \in [0, M-1]$. Let P_{qe} denote the probability of the queue being empty, $P_{qne} = 1 - P_{qe}$, and P_{arr} denote the conditional probability of a new packet arrival given the queue is empty. P_{qe} and P_{arr} link the queue model and the packet generators with the DTMCs modeling the MAC layer operation, respectively, as illustrated in Figure 3.1.

3.2.2 DTMC model for C-V2X Mode 4

We begin this subsection by presenting the sensing-based SPS algorithm, which is used for radio resource allocation in C-V2X Mode 4. We follow it up with the respective DTMC model.

Semi-persistent scheduling algorithm

The SPS algorithm enables a vehicle to select radio resources without the assistance of an eNodeB, and each vehicle follows the following three steps for resource reservation.

Step 1: Within the selection window, which is the time window that initiates with a generation of a packet, vehicle v identifies all possible candidate single-subframe resources (CSRs) that can be reserved. CSRs are groups of adjacent sub-channels within the given 1 ms subframe that are large enough to fit in the SCI and the TB to be transmitted. The length of the selection window, which is denoted by Γ, is defined in the standard as the maximum latency in ms [30], and a CSR should be selected within this duration.

Step 2: Based on the information received in the previous 1000 subframes (sensing window), vehicle v creates list L_1 that consists of CSRs that it can reserve. L_1 includes all the CSRs in the selection window except the ones that satisfy the following conditions.

1. CSRs used by vehicle v during the sensing window. This is done as a precautionary measure due to vehicle v not being able to sense these CSRs during its half-duplex transmissions.

2. CSRs that are being used by other vehicles at the time vehicle v tries to utilize them (which are known thanks to the information contained in the SCI), and have a received signal strength indicator (RSSI) value above a threshold level l_{th}.

If L_1 contains more than 20% of the total CSRs identified in *Step 1*, the system moves to *Step 3*. Otherwise, l_{th} is increased by 3 dB and *Step 2* is repeated.

Step 3: From L_1, vehicle v filters out the CSRs that experience the lowest average RSSI values, where the averaging is done over the previous 10 subframes. These CSRs are added to a new list L_2 such that the size of L_2 amounts to 20% of the total CSRs in the selection window. Vehicle v randomly and uniformly selects a CSR in L_2 and reserves it for the next RC transmissions, where RC denotes the value of the resource counter. Let $RC_F \in [R_l, R_h]$ denote the starting value of the resource counter, where R_h and R_l are upper and lower limits of RC_F, respectively. RC is decremented by 1 for each transmission of a packet, which happens periodically every Γ ms until RC reaches 1. When $RC = 1$, new CSRs should be selected and reserved with probability $(1 - P_{rk})$, where $P_{rk} \in [0, 0.8]$. This can be done by generating a number randomly and uniformly in $(0, 1)$, and

then comparing it with the predefined value of P_{rk}. Vehicle v continues using the same CSR if the generated random number is less than P_{rk}, and it continues using the subframes encountered in intervals of Γ ms for the subsequent transmissions. Else, vehicle v selects a new CSR for the next transmission from L_2. Upon new CSR selection, the vehicle randomly and uniformly selects a subframe that falls within the next Γ ms for the next transmission. Please refer to [95] for a pseudo-code of this algorithm.

DTMC model

Figure 3.4 illustrates the DTMC model for C-V2X Mode 4 operation. The state-space of the model is denoted by S^{v2x}. Let P_{sch} denote the probability of allocating a suitable CSR for a vehicle through *Steps 1-3*. State ($Idle$) represents the state with no packets to transmit, or no CSRs to transmit. According to the standard [86], there are three selection window sizes with respective ranges for RC_F. To this end, the standard includes $\Gamma = 100$ ms with $RC_F \in [5, 15]$, $\Gamma = 50$ ms with $RC_F \in [10, 30]$ and $\Gamma = 20$ ms with $RC_F \in [25, 75]$.

Consider the arrival of a new packet while vehicle v is idle. This necessitates the allocation of a CSR utilizing the SPS algorithm. As Γ ms is the maximum allowable latency, the transmission should happen within the next Γ subframes. Upon allocation of the CSR, vehicle v selects (randomly and uniformly) a subframe for transmission. Thus, the waiting time before the transmission is modeled by assuming $\Gamma - 1$ equiprobable states $(w,\ j)$, where $j \in [0, \Gamma - 2]$. As the waiting time elapses, vehicle v selects a value for RC randomly and uniformly from the set of $(1 + R_h - R_l)$ values. At every state $(i, 0)$, where $i \in [1, R_h]$, there is a transmission opportunity, and i represents the current RC value. The device utilizes this opportunity to transmit the control information related to its persistent scheduling. If the queue is not empty, the transmission opportunity is also utilized for data transmission, i is decremented, and the vehicle waits for the next transmission opportunity that arises in Γ ms. This waiting time is represented by states $(i - 1, j)$, where $j \in [1, \Gamma - 1]$. On the other hand, if the queue is empty, the vehicle similarly waits Γ ms for the next transmission opportunity. We consider that the vehicle maintains the same RC value i during this waiting period[1]. This process repeats until the system reaches state $(1, 0)$.

[1] As found often in standardization, the standard does not specifically describe what needs to happen to the RC value in such a scenario. Any realization that fulfills the requirements of the standard is deemed to be correct. Note that both decrementing the RC value or maintaining the same RC value during this waiting period satisfy the standard. We have used the latter for our model.

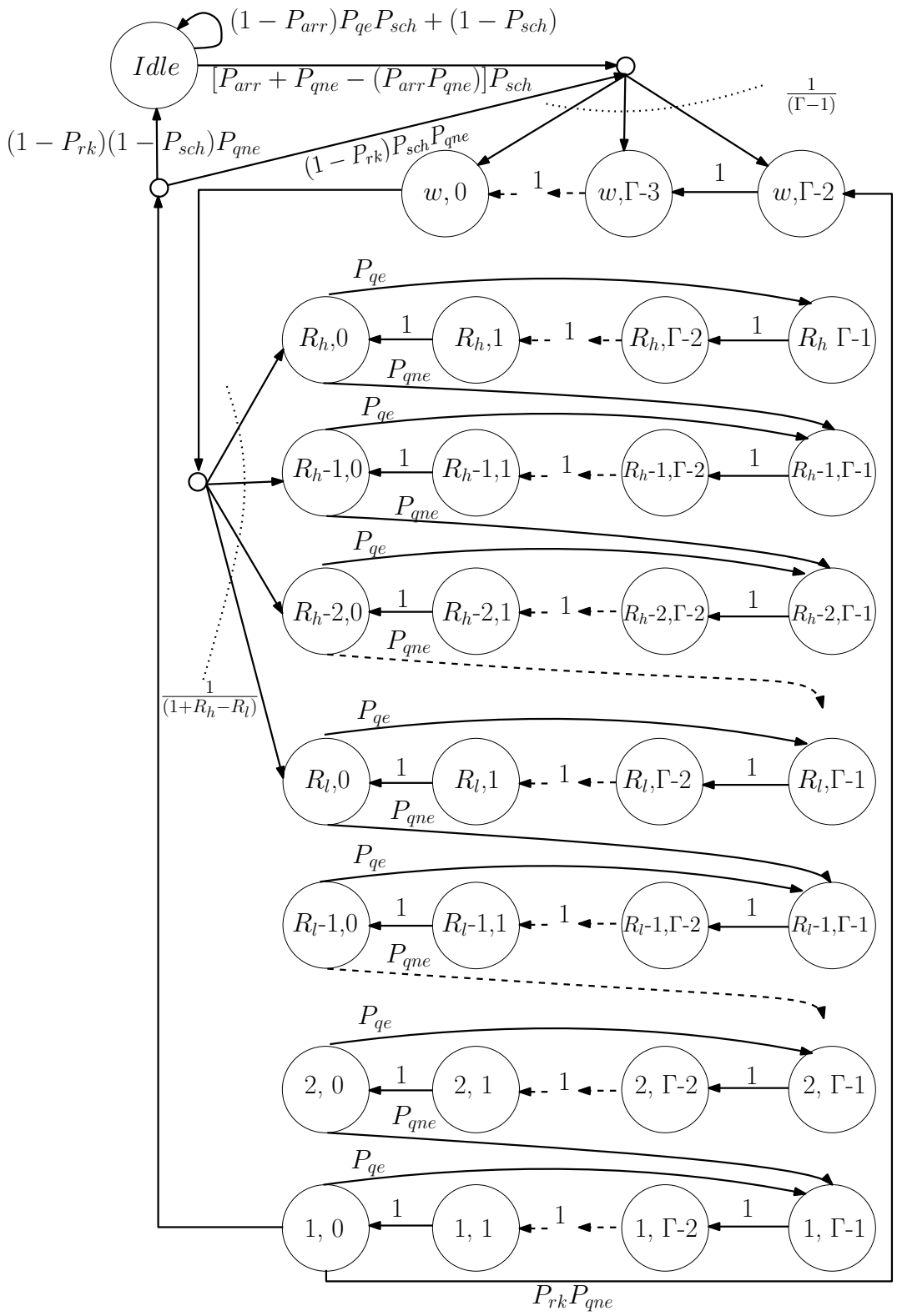

Figure 3.4: The DTMC modeling the MAC layer operations of C-V2X Mode 4.

If the queue is still not empty at state $(1, 0)$, the vehicle has the option of using the same CSR (with probability P_{rk}), or choose a new CSR. If the same CSR is used, the vehicle waits for the maximum waiting time of $\Gamma - 1$ ms before choosing a RC value and transmitting. The state transitions for selecting a new radio resource are similar to the transitions described for packet arrival while vehicle v is idle. It is not hard to see that selecting a new radio resource may lead to a lower delay due to the possibility of a lower waiting time.

3.2.3 DTMC model for IEEE 802.11p

The state space of the model is denoted by S^{11p} and the DTMC model is presented in Figure 3.5. $\check{C}$ denotes the minimum contention window size. State $(Idle)$ represents the state where there are no packet arrivals, thus the queue is empty. If a packet arrives while being idle, the MAC protocol listens for an $AIFS$ duration before transmitting. The $AIFS$ duration is calculated according to $AIFS = aSIFSTime + AIFSN \times aSlotTime$, where $aSIFSTime$ is 32 μs, and the $AIFSN$ value is selected according to the access category (AC). ETSI specifications do provide four ACs: background, best effort, video, and voice. In this chapter, we assume that both CAM and DENM packets utilize the best effort AC. We thus have $AIFSN = 6$ and $\check{C} = 15$ according to the standard [1].

States (A_i) for $i \in \{1, \ldots, \Omega\}$, represent the $AIFS$ waiting time, and Ω denotes the maximum number of $aSlotTime$ intervals per $AIFS$ duration. θ represents the probability of the channel being busy (channel busy ratio). If the channel is found idle for an $AIFS$ duration, the vehicle is allowed to transmit. Data transmission is represented by states (Tx, i), where $i \in \{1, \ldots, \vartheta\}$, and ϑ denotes the number of $aSlotTime$ intervals required to transmit a packet of 134 bytes over a 6 Mbps control channel (CCH) [32].

If the channel becomes busy during the $AIFS$ duration, the vehicle waits for $\vartheta \times aSlotTime$, which is the time taken for data transmission, until the channel is free again. Waiting is represented by states (B, i), where $i \in \{1, \ldots, \vartheta\}$. The channel being busy at state A_1 depicts a scenario where the packet arrival of the vehicle of interest has occurred while the channel is busy, *i.e.*, another vehicle is transmitting. Thus, the time it has to wait before sensing a free channel is given by $\varrho \times aSlotTime$, where ϱ is a uniformly distributed random integer in $[1, \vartheta]$.

When the channel becomes free again, that is at state (B, ϑ), vehicle v initiates a backoff process. The backoff counter value is selected randomly (uniformly) in $\left[0, \check{C}\right]$, and the backoff stage is selected depending on the respective backoff counter value. According to the standard [1], backoff counter value 0 and 1

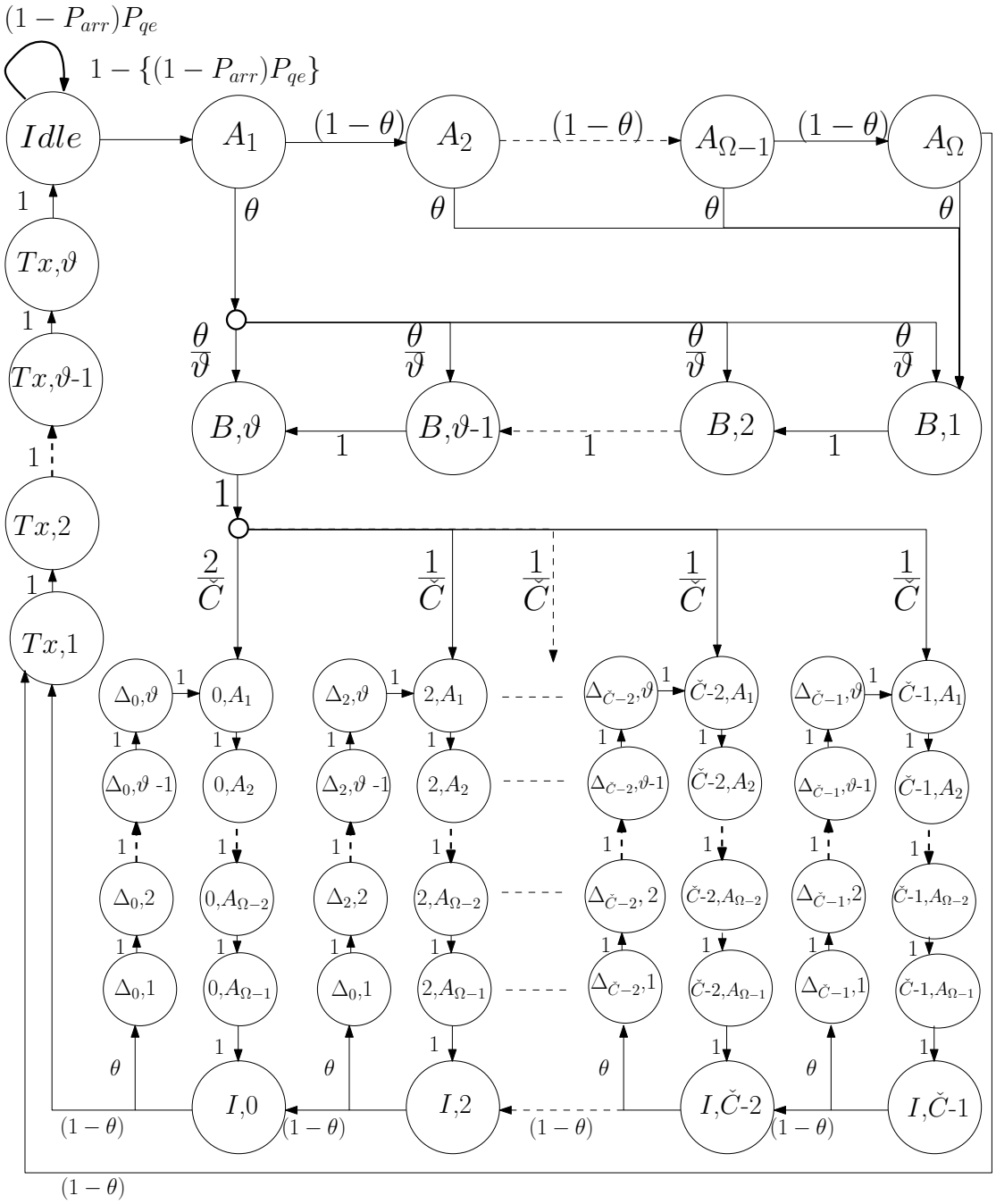

Figure 3.5: The DTMC modeling the MAC layer operations of IEEE 802.11p.

both lead to backoff stage 0. Thus, the probability of selecting backoff stage 0 is twice the probability of selecting any other backoff stage. Vehicle v waits for another $AIFS$ duration before sensing the channel again. For backoff counter value $i \in \{0, \ldots, (\check{C} - 1)\}$, states (i, A_j), where $j \in \{1, \ldots, (\Omega - 1)\}$, represent the waiting duration, and (I, i) represent the sensing states. If the channel is found busy at state (I, i), vehicle v waits for $\vartheta \times aSlotTime$, which is represented by states (Δ_i, j), where $j \in \{1, \ldots, \vartheta\}$, and another $AIFS$ duration at the same backoff stage i. This loop continues until the channel is found idle at state (I, i). The backoff counter is decremented when the channel is found idle, which takes us to state $(I, i-1)$. If vehicle v finds the channel to be free at state $(I, 0)$, it transmits data.

3.3 Steady-state Solutions

Steady-state solutions of the DTMCs are presented in this section for a system with N vehicles. Firstly, we focus on the CAM and DENM packet generators and the device level packet queue. By utilizing these results, we present the steady-state solutions of the DTMC models developed for C-V2X Mode 4 and IEEE 802.11p MAC layer operations.

3.3.1 Queue model

We have already discussed the importance of P_{qe}, as it links the DTMCs modeling the MAC layer operation with the DTMC modeling the device level packet queue. This value can be obtained through the steady-state probability of state (0) in the queue model. From Figure 3.3, the steady-sate probability of state (0) can be written as

$$\pi_0 = \left[1 + \alpha_1 \left(\frac{1 - \beta^{-M}\alpha^M}{\beta - \alpha}\right)\right]^{-1} = P_{qe}. \tag{3.1}$$

To obtain α, α_1, and β, we need the steady-state solutions of the CAM and DENM generators, as shown in Figure 3.1.

Let $\pi^C_{i,j}$ and $\pi^D_{i,j}$ denote the steady-state probabilities of state (i, j) of the CAM and the DENM generators, respectively. To this end, the steady-state

probabilities of the CAM generator are given by

$$\pi^C_{tx,0} = \left[1 - \left(1 - P_t^k\right)^{T_C-1}\right]\left[T_C\left[1 - P_t^k\left(1 - P_t^k\right)^{T_C-1}\right]\right]^{-1},$$
$$\pi^C_{tx,j} = P_t^k(\pi^C_{tx,0} + \sum_{l=j+1}^{T_C-1} \pi^C_{tx',l}) \text{ for } j \in [1, T_C - 2],$$
$$\pi^C_{tx,T_C-1} = \pi_{tx,0}P_t^k,$$
$$\pi^C_{tx',j} = \pi^C_{tx,0}\left[(1 - P_t^k)^{T_C-j}\right]\left[1 - (1 - P_t^k)^{T_C-1}\right]^{-1} \text{ for } j \in [0, T_C - 1].$$

Similarly, the steady-state probabilities of the DENM generator are given by

$$\pi^D_{tx,0} = \Big[\left(1-\frac{1}{K}\right)\frac{T_D\left[1 - P_t^k\left(1 - P_t^k\right)^{T_D-1}\right]}{1 - \left(1 - P_t^k\right)^{T_D-1}} + \frac{1}{K} + \frac{1}{K(1 - e^{-\lambda\tilde{T}})}\Big]^{-1},$$
$$\pi^D_{tx,j} = P_t^k\Big[(1 - \frac{1}{K})\pi^D_{tx,0} + \sum_{l=j+1}^{T_D-1} \pi^D_{tx',l}\Big] \text{ for } j \in [1, T_D - 2],$$
$$\pi^D_{tx,j} = \pi^D_{tx,0}\left(1 - \frac{1}{K}\right)P_t^k \text{ for } j = T_D - 1,$$
$$\pi^D_{tx',j} = \pi^D_{tx,0}(1 - \frac{1}{K})\left[(1 - P_t^k)^{T_D-j}\right]\left[1 - (1 - P_t^k)^{T_D-1}\right]^{-1} \text{ for } j \in [0, T_D - 1].$$

Since we are using a single queue for both CAM and DENM packets, the transition probabilities of the queue model in Figure 3.3 depend on both generator models that run simultaneously. For $x \in \{\alpha, \alpha_1, \beta\}$, let x^C and x^D denote the resulting transition probability if only the CAM generator or the DENM generator is in operation, respectively. For two events E_1 and E_2, $\Pr\{E_1 \cup E_2\} = \Pr\{E_1\} + \Pr\{E_2\} - \Pr\{E_1 \cap E_2\}$. Thus, $x = x^C + x^D - x^C x^D$ for $x \in \{\alpha, \alpha_1, \beta\}$. To this end,

$$\alpha^C = \pi^C_{tx',0},$$
$$\alpha_1^C = \pi^C_{tx,0}(1 - P_t^k),$$
$$\beta^C = \sum_{j=1}^{T_C-1} \pi^C_{tx',j}P_t^k,$$
$$\alpha^D = \pi^D_{tx',0},$$
$$\alpha_1^D = \pi^D_{tx,0}\left(1 - \frac{1}{K}\right)(1 - P_t^k),$$
$$\beta^D = \sum_{j=1}^{T_D-1} \pi^D_{tx',j}P_t^k, \text{ for } k \in \{v2x, 11p\}.$$

With similar reasoning,

$$P_{arr} = \pi^{C}_{tx,0} + 1 - e^{-\lambda\tilde{T}} - \pi^{C}_{tx,0}\left(1 - e^{-\lambda\tilde{T}}\right).$$

3.3.2 DTMC model for C-V2X

According to the 3GPP C-V2X standard [30], SC-FDMA is considered for the uplink, using a 10 MHz channel. 50 RB are allocated for this bandwidth per each slot (half subframe), and hence, one subframe contains 100 RBs. A CSR requires at least 4 RBs to transmit a 100 byte payload, using 64-QAM modulation. Therefore, each 1 ms subframe can hold up to 25 CSRs, and hence, the largest selection window of 100 ms can hold up to 2500 CSRs. 20% of this is 500, and l_{th} can be fine-tuned until we end up with the required number of CSRs. Thus, the standard itself makes it highly unlikely that a randomly selected vehicle ends up without an allocated CSR. Thus, we consider $P_{sch} = 1$ in our study without any loss of generality. Now that we have obtained P_{qe} and P_{qne}, the steady-state solutions of the DTMC model for C-V2X can be used to obtain P_t^{v2x} found in the packet generators.

The steady-state equations of the DTMC model in Figure 3.4 are used to derive expressions for its steady-state probabilities, which are presented next. To this end,

State *(Idle):*

$$\pi^{v2x}_{Idle} = b\pi_{w,0}, \text{ where } b = \frac{(1 - P_{rk})\left(\frac{1}{P_{sch}} - 1\right)}{P_{arr} + P_{qne}\,(1 - P_{arr})}.$$

States (w, j)***:*** for $j \in [0, \Gamma - 2]$

$$\pi_{w,j} = \left[1 - \frac{j}{(\Gamma - 1)}\right]\left[a\pi^{v2x}_{Idle} + (1 - P_{rk})P_{sch}\pi_{1,0}P_{qne}\right] + P_{rk}\pi_{1,0}P_{qne},$$

where $a = (P_{arr} + P_{qne} - P_{arr}P_{qne})\,P_{sch}$.

States (i, j)***:***

$$\pi_{i,j} = \begin{cases} \dfrac{\pi_{w,0}\,(R_h - i + 1)}{P^2_{qne}\,(1 + R_h - R_l)} & \text{for } i \in [R_l, R_h], j \in [1, \Gamma - 1] \\ \dfrac{\pi_{w,0}\,(R_h - i + 1)}{P_{qne}\,(1 + R_h - R_l)} & \text{for } i \in [R_l, R_h],\ j = 0 \\ \dfrac{\pi_{w,0}}{P_{qne}}, & \text{for } i \in [1, R_l - 1], j \in [0, \Gamma - 1] \end{cases}. \tag{3.2}$$

Since the sum of these steady-state probabilities is one, we get

$$\pi_{w,0} = \Big[1 - \Gamma + b + \left(\frac{\Gamma - 2}{2}\right)[ab + 2P_{rk} + (1 - P_{rk})P_{sch}] + \frac{\Gamma(R_h + R_l)}{2P_{qne}}\Big]^{-1}. \tag{3.3}$$

The probability of transmission opportunity can be written as $P_{txo} = \sum_{i=1}^{R_h} \pi_{i,0}$, for which an expression can be obtained by substituting (3.3) in (3.2). Finally, we find P_t^{v2x} through the product of P_{txo} and P_{qne}.

3.3.3 DTMC model for ETSI ITS-G5 based IEEE 802.11p

Next, we present the steady-state solutions for the DTMC model in Figure 3.5. To this end,

States (A_i)*:* for $i \in [1, \Omega]$

$$\pi_{A_i} = \pi_{Idle}^{11p}\left[1 - P_{qe}\left(1 - P_{arr}\right)\right](1 - \theta)^{(i-1)}.$$

States (B, j)*:* for $j \in [1, \vartheta]$

$$\pi_{B,j} = \pi_{Idle}^{11p}\left[1 - P_{qe}\left(1 - P_{arr}\right)\right]\left[\frac{\theta}{\vartheta}j - (1-\theta)^{\Omega} - \theta + 1\right].$$

States (Δ_i, j)*:* for $i \in \left[0, \left(\check{C} - 1\right)\right]$, $j \in [1, \vartheta]$

$$\pi_{\Delta_i,j} = \pi_{B,\vartheta}\frac{\left(\check{C} - i\right)\theta}{\check{C}\left(1 - \theta\right)}.$$

States (i, A_j)*:*

$$\pi_{i,A_j} = \begin{cases} \dfrac{\pi_{B,\vartheta}\left[1 + \left(\check{C} - i - 1\right)\theta\right]}{\check{C}\left(1 - \theta\right)} & \text{for } i \in \left[2, \left(\check{C} - 1\right)\right],\ j \in [1, (\Omega - 1)] \\ \dfrac{\pi_{B,\vartheta}\left(2 - 2\theta + \check{C}\theta\right)}{\check{C}\left(1 - \theta\right)} & \text{for } i = 0,\ j \in [1, (\Omega - 1)] \end{cases}.$$

States *(I, j):* for $j \in \left[0, \left(\check{C} - 1\right)\right]$ $\pi_{I,j} = \pi_{B,\vartheta}\dfrac{\left(\check{C} - j\right)}{\check{C}\left(1 - \theta\right)}$.

States *(Tx,j):* for $j \in [1, \vartheta]$ $\pi_{Tx,j} = \pi_{Idle}^{11p}\left[1 - P_{qe}\left(1 - P_{arr}\right)\right]$. (3.4)

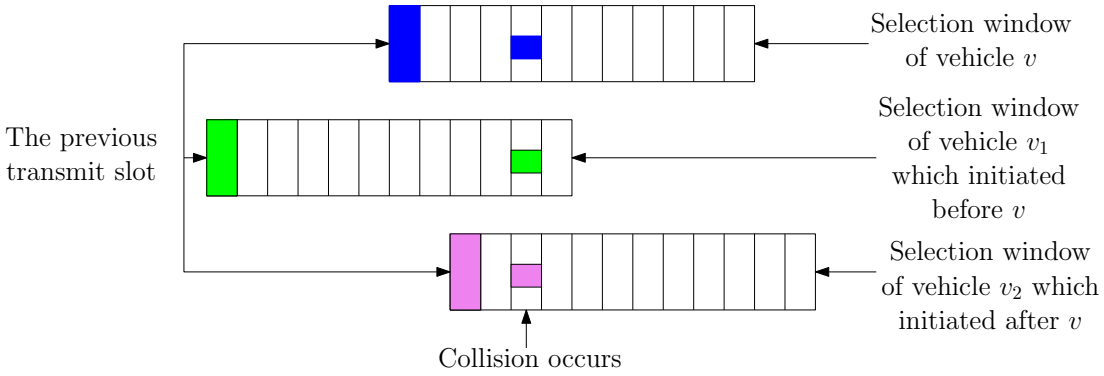

Figure 3.6: An illustration of a possible collision in C-V2X Mode 4.

Since the sum of these steady-state probabilities is one, we get

$$\pi_{Idle} = \Big[1 + [1-(1-P_{arr})P_{qe}]\Big[[1-(1-\theta)^{\Omega}]\Big[\frac{1}{\theta} + \frac{(\check{C}+1)\theta\vartheta}{2(1-\theta)} + \vartheta + (\Omega-1)\frac{[(\check{C}-2)[(\check{C}-3)\theta+2] + (4-4\theta+2\check{C}\theta)]}{2\check{C}(1-\theta)} + \frac{(\check{C}+1)}{2(1-\theta)}\Big] + \frac{\theta}{2}(1-\vartheta) + \vartheta\Big]\Big]^{-1}. \tag{3.5}$$

The obtained solution for π_{Idle}^{11p} is substituted in (3.4) to determine $P_t^{11p} = \sum_{j=1}^{\vartheta} \pi_{Tx,j}$ and $\theta = 1 - (1 - \sum_{j=1}^{\vartheta} \pi_{Tx,j})^{(N-1)}$.

3.4 Performance Analysis

This section focuses on deriving expressions for several useful performance parameters that can be used to compare the MAC layer performance of C-V2X Mode 4 and IEEE 802.11p.

3.4.1 Probability of collision P_{col}

Even though the SPS algorithm attempts to minimize packet collisions between vehicles at transmission by considering the radio resource utilization of vehicles during the 1000 ms sensing window, there still remains a possibility for collisions. To this end, a schedule collision can occur when a vehicle selects a new radio resource for transmission. In particular, a collision can occur when there is an overlap in the selection windows of neighboring vehicles, as illustrated in Figure 3.6. In such a scenario, the vehicles with overlap select a CSR independent of each other, and hence, there is a possibility of them selecting the same CSR that leads to collision. Let CSR_{tot} denote the total number of CSRs in the selection window. We start the analysis by obtaining an expression for the collision probability of C-V2X Mode 4.

Lemma 1. *The collision probability of C-V2X Mode 4 is given by*

$$P_{col}^{v2x} \approx 1 - \left[1 - \left[1 - \prod_{i=0}^{\Gamma-1} \left(1 - \frac{\pi_{i,0}}{1 - \pi_{i,0} i}\right)\right] \frac{(1 - P_{rk})}{(CSR_{tot} - N + 1)}\right]^{N-1}. \tag{3.6}$$

Proof. See Appendix 3.7.1. □

The collision probability of IEEE 802.11p is calculated according to $P_{col}^{11p} = 1 - P_{suc}$, where P_{suc} is the conditional probability that exactly one vehicle transmits on the channel, given that at least one vehicle transmits [11]. An expression for the collision probability of IEEE 802.11p is formally stated through the following lemma.

Lemma 2. *The collision probability of IEEE 802.11p is given by*

$$P_{col}^{11p} = 1 - \frac{N\left[(1-\theta)(\pi_{I,0} + \pi_{A_\Omega}) + \sum_{j=1}^{\vartheta} \pi_{Tx,j}\right]\left[1 - \left(\pi_{I,0} + \pi_{A_\Omega} + \sum_{j=1}^{\vartheta} \pi_{Tx,j}\right)\right]^{(N-1)}}{1 - \left[1 - \left(\pi_{I,0} + \pi_{A_\Omega} + \sum_{j=1}^{\vartheta} \pi_{Tx,j}\right)\right]^{N}}.$$

Proof. See Appendix 3.7.1. □

3.4.2 Average delay D_{ave}

Next, we focus on the average delay between the generation and the transmission of a packet. The delay value captures the queuing delay, which is the time a packet waits in the queue making way to the previously generated packets, and the access delay, which is the time a vehicle waits before being able to access the radio resources. Firstly, we present an expression for the average delay of C-V2X Mode 4 through the following lemma.

Lemma 3. *The average delay of C-V2X Mode 4 is given by*

$$d_{avg}^{v2x} = \frac{\sum_{i=1}^{M} \frac{2i-1}{2P_{txo}} \pi_i}{1 - P_{qe}}. \tag{3.7}$$

Proof. See Appendix 3.7.2. □

For IEEE 802.11p, the average delay is calculated by utilizing the delay of each state in the DTMC model, except the idle state. The normalized average delay of the system is calculated using the delay values of the individual states.

Let $D_{i,j}$ denote the delay at state (i,j). $aSlotTime$ is used as the unit delay, thus $D_{T,1} = \vartheta$ since the transmission of a packet of 134 bytes takes $\vartheta \times aSlotTimes$. We assume $D_I = 0$. To this end, the delay at each state of the system is calculated according to the following equations.

States (I,j)*:*

$$D_{I,j} = \begin{cases} \dfrac{1+\vartheta+\theta\left(\Omega-1\right)}{\left(1-\theta\right)} & \text{for } j=0 \\ \dfrac{j+\vartheta\left[1+\theta\left(j-1\right)\right]+j\theta\left(\Omega-1\right)}{\left(1-\theta\right)} & \text{for } j \in \left[2,\check{C}-1\right] \end{cases}.$$

States (i,A_j)*:* for $i \in \left\{0,2,\ldots,\check{C}-1\right\}$, $j \in [1,(\Omega-1)]$

$$D_{i,A_j} = (\Omega - j) + D_{I,j}.$$

State (Δ_i,j)*:* for $i \in \left\{0,2,\ldots,\check{C}-1\right\}$, $j \in [1,\vartheta]$

$$D_{\Delta_i,j} = (\vartheta - j + 1) + (\Omega - 1) + D_{I,j}.$$

States (B,j)*:*

$$D_{B,j}=\begin{cases} 1+\dfrac{2}{\check{C}}\left[(\Omega-1)+D_{I,0}\right]+\dfrac{\left(\check{C}-2\right)\left(\Omega-1\right)}{\check{C}}+\displaystyle\sum_{j=2}^{\check{C}-1} D_{I,j} & \\ & \text{for } j=\vartheta \\ 1+D_{B,(j+1)} & \text{for } j \in [1,(\vartheta-1)] \end{cases}.$$

States *(Tx, j):* for $j \in [1,\vartheta]$ $D_{Tx,j} = \vartheta - (j-1)$.

States (A_i)*:*

$$D_{A_i}=\begin{cases} 1+(1-\theta)\,D_{A_{i+1}}+\dfrac{\theta}{\vartheta}\displaystyle\sum_{j=1}^{\vartheta} D_{B,j} & \text{for } i=1 \\ 1+(1-\theta)\,D_{A_{i+1}}+\theta D_{B,1} & \text{for } i \in [2,(\Omega-1)] \\ 1+(1-\theta)\,D_{Tx,1}+\theta D_{B,1} & \text{for } i=\Omega \end{cases}.$$

By using these equations, the average delay of the system is obtained through the following lemma.

Lemma 4. *The average delay of IEEE 802.11p is given by*

$$d_{avg}^{11p} = \vartheta + 1 + \sum_{i=1}^{\Omega-1}(1-\theta)^i + \sum_{i\in\mathcal{S}} \frac{D_i \pi_i}{\left[1 - \left(\pi_{Idle}^{11p} + \sum_{j=1}^{\vartheta} \pi_{Tx,j} + \sum_{k=1}^{\Omega} \pi_{A_k}\right)\right]}, \quad (3.8)$$

where $\mathcal{S} = \left\{S^{11p} - \left\{Idle, \bigcup_{j=1}^{\vartheta}(Tx,j), \bigcup_{k=1}^{\Omega} A_k\right\}\right\}$.

Proof. See Appendix 3.7.2. □

3.4.3 Average channel utilization

The average channel utilization depicts the average number of users successfully accessing the channel simultaneously. Thus, the average channel utilization of C-V2X Mode 4 and IEEE 802.11p is given by

$$CU_{avg}^{v2x} = \frac{P_t^{v2x} N (1 - P_{col}^{v2x})}{CSRs\ per\ subframe} \quad (3.9)$$

and

$$CU_{avg}^{11p} = P_t^{11p} N (1 - P_{col}^{11p}), \quad (3.10)$$

respectively. Note that since we are interested in finding the average channel utilization within a single subframe in C-V2X Mode 4, we normalize the channel utilization value by the total number of CSRs within a single subframe, which is given by CSR_{tot}/Γ.

3.5 Numerical Results and Discussion

In this section, we present an application of the models to provide insights and comparisons on key performance indicators through numerical evaluations. We were unable to find or generate similar data from a real vehicular network testbed for validation.

3.5.1 Instantiation of CAM, DENM and the DTMC models in a highway

We consider a highway with four parallel lanes in each direction, with an average inter-vehicle gap of 50 m. Note that we have not done any location modeling, mobility modeling, or PHY-layer signal modeling. Thus, the highway scenario is only used as an illustrative setting such that it provides a feasible range for N within the coverage region of vehicle v. We also assume that only CAM

and DENM are utilized for V2V communication [99, 100], while their reference packet formats are specified according to ETSI [84, 85]. We consider T_C to be between 100 ms and 1 s [84], and T_D to be 100, 200 and 300 ms [85]. K is set at three arbitrary values 2, 5, and 9 to study scenarios with low, medium, and high repetitions, respectively. The standard allows the vehicle to select T_D and K based on the severity of the event. Two candidate values for λ are selected to study low and high packet generation rates, and the values are set by taking the use case scenarios in [67] into consideration. M is set at 10 in the queue model. In IEEE 802.11p, T_C is regulated under the transmit rate control (TRC) technique of ETSI ITS-G5 decentralized congestion control (DCC) algorithm, where during periods of high/low utilization, T_C is increased/decreased to manage congestion. This is termed as an adaptive CAM rate in the numerical results. The steady-state probabilities of the DTMCs are calculated in parallel, which are then used to calculate the probability values that link the DTMCs, as shown in Figure 3.1. The probability values are iteratively recomputed until they converge.

Average delay

Average delay is calculated according to (3.7) and (3.8) for C-V2X Mode 4 and IEEE 802.11p, respectively. Figure 3.7a illustrates the variation of the average delay with N. Firstly, we can observe that IEEE 802.11p is superior to C-V2X Mode 4 in terms of the average delay. The lower delay in IEEE 802.11p is mainly due to the maximum $AIFS$ duration being 149 μs [1]. This is approximately equal to 12 $aSlotTimes$, thus to transmit a 134 byte packet, it takes 14 $aSlotTimes$ over the CCH. Therefore, even after adding the average backoff delay to the above-calculated delay, it is unlikely that the total average delay is greater than a few milliseconds. This is much smaller compared 20 ms, which is the smallest selection window size in C-V2X Mode 4, and where it does the best in terms of average delay as shown in Figure 3.7a. The observation implies that IEEE 802.11p is a better choice for delay-critical use case scenarios such as emergency electronic brake lights, emergency vehicle warning, vulnerable road user warning, and pre-crash sensing warning.

According to Figure 3.7a, we can also observe that the average delay increases further with Γ in C-V2X Mode 4. Thus, Γ should be set small for low-latency applications. However, reducing Γ in turn reduces the number of CSR values, and hence, it reduces the number of vehicles that can be supported simultaneously, introducing a tradeoff. Thus, reducing Γ is more suited for a sparsely-populated vehicular network. For a given value of Γ, a higher average delay can be observed

when the CAM inter-arrival time is reduced from 200 to 100 ms. This is mainly due to the increased congestion in the network.

It is interesting to note from Figure 3.7a that the average delay is not sensitive to the number of vehicles in C-V2X Mode 4 compared to IEEE 802.11p, where the average delay increases with N. C-V2X Mode 4 uses a scheduling based resource allocation method, and in this setting and the range considered for N, there exist ample radio resources for all users to transmit. This is the main reason for the flat behavior of the average delay with respect to N. On the other hand, IEEE 802.11p resorts to a contention-based access mechanism. Therefore, the delay increases monotonically with N. The explanation is consistent with Figure 3.7b that depicts the channel-busy ratio θ, which is a metric used to capture the busyness of the channel in IEEE 802.11p. The channel is considered to be busy if a vehicle other than the target vehicle is transmitting. Due to the significant variation in the average delay of IEEE 802.11p with N, there may be scenarios where C-V2X Mode 4 may be the better choice for delay critical applications in densely-populated vehicular networks. It can also be seen from Figure 3.7b that the adaptive CAM rate affects the channel-busy ratio favorably, and thus helps in reducing the average delay associated with IEEE 802.11p further, as can be observed in Figure 3.7a. This implies that adaptive CAM facilitates a higher number of vehicles in a network that utilizes IEEE 802.11p for communication without violating the stringent delay constraints.

The average delay variation of both technologies with T_C is shown in Figure 3.8a. Intuitively, the behavior with T_D should be similar as the modeling of CAM generation and DENM repetition is identical. Firstly, we can see the average delay reducing with T_C as observed and explained in Figure 3.7a. Secondly, with regards to C-V2X, we can see that Γ has a higher impact on the average delay than T_C. The value of Γ dominates the delay, *i.e.*, we cannot negate the adverse effect on the delay caused by an increase in Γ by simultaneously increasing T_C. We note that there is a tradeoff in reducing Γ as well. While reducing the average delay, it simultaneously reduces the number of CSR values, and hence, it reduces the number of vehicles that can be supported simultaneously. The average delay associated with IEEE 802.11p reduces monotonically with T_C. The corresponding behavior associated with C-V2X is more interesting as it first decreases and then increases with regards to T_C (the variation is negligibly small for $\Gamma = 20$ ms). Thus, we further elaborate on the variation of the average delay of C-V2X Mode 4 with T_C, P_{rk}, and different parameter combinations of the DENM generator model such as T_D and K in Figure 3.8b.

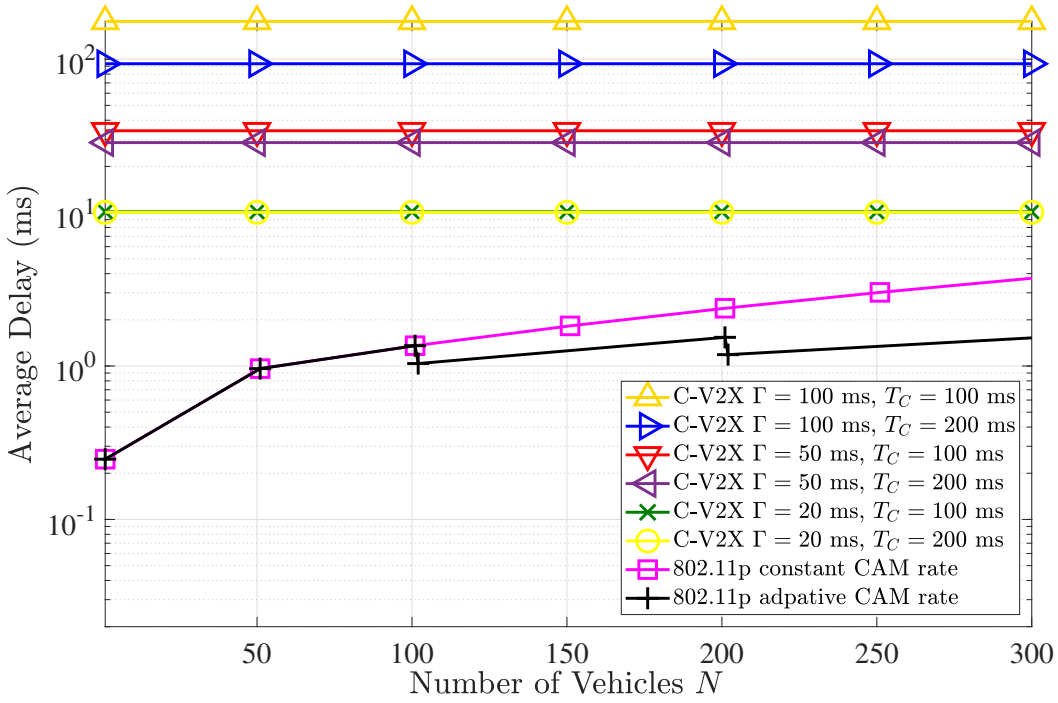

(a) The average delay vs N, where $P_{rk} = 0.4$.

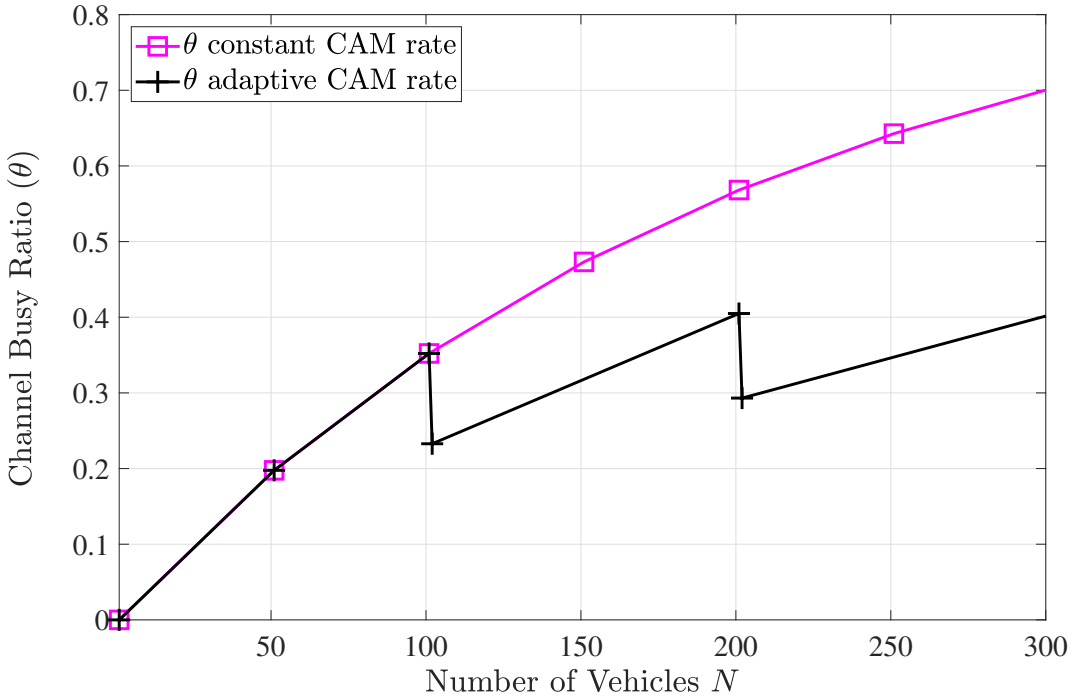

(b) The channel busy ratio vs N, where $T_C = 100$ ms.

Figure 3.7: The behavior of the average delay and the channel busy ratio with N, where $\lambda = 1$, $T_D = 100$ ms, and $K = 5$.

According to Figure 3.8b, we can observe that the average delay increases when T_D decreases or when the DENM packet arrival rate increases. Both of these observations are due to the congestion caused by more transmissions per unit time. When $T_D = 100$ ms, the average delay increases with K. However, when $T_D = 200$ ms, the average delay decreases with K. This phenomenon can be justified as follows. When $T_D = 100$ ms, the service rate is nearly equal to the packet repetition frequency. This results in more CAM and DENM packets in the queue, leading to higher queuing delays. However, when $T_D = 200$ ms, the service rate is higher than the repetition interval of DENM packets. In such a scenario, increasing the average number of repetitions results in the target vehicle encountering the random waiting time, which has a maximum average delay of 50 ms (when $\Gamma = 100$ ms), more frequently compared to waiting through the whole resource reservation interval (RRI), which is of 100 ms. This leads to a reduction in the average delay. Similar behavior can be observed for $T_D = 300$ ms as well.

An interesting observation in the behavior of the average delay is the existence of a locally optimal point. For example, when $T_D = 100$ ms, $K = 9$ and $\lambda = 0.2$ packets/s, the lowest average delay can be observed at $T_C = 300$ ms. This implies that the average delay can be reduced further by dynamically changing the CAM packet generation rate based on the generation rate of DENM packets. The DENM packet generation rate is based on the occurrence of an event and its severity. It can be concluded that the vehicle can reduce the overall average delay further in C-V2X Mode 4 communication if it can change the CAM packet generation rate based on λ, to achieve the local optimal point of the delay curve shown in Figure 3.8b.

We can also observe the average delay increasing with P_{rk} in Figure 3.8b. High values of P_{rk} curtails the vehicle from choosing new radio resources for transmission. When P_{rk} is low, a vehicle again receives more opportunities to encounter the waiting interval (average duration of $\Gamma/2$ ms), compared to the longer RRI intervals (duration of Γ ms). Thus, the variable P_{rk}, which is a parameter in the SPS algorithm, can be varied to adjust the average delay in a network that utilizes C-V2X Mode 4 for communication. The high P_{rk} values lead to higher average delays, but a reduction in jitter as the RRI intervals stay more homogeneous.

Further practical insights can be drawn by referring to the delay requirements stated for ETSI ITS use cases in [67]. For example, a vehicle's emergency electronic brake warning or a stationary vehicle warning requires a minimum of 10 Hz frequency and a maximum delay of 100 ms. On the other hand, a less safety-

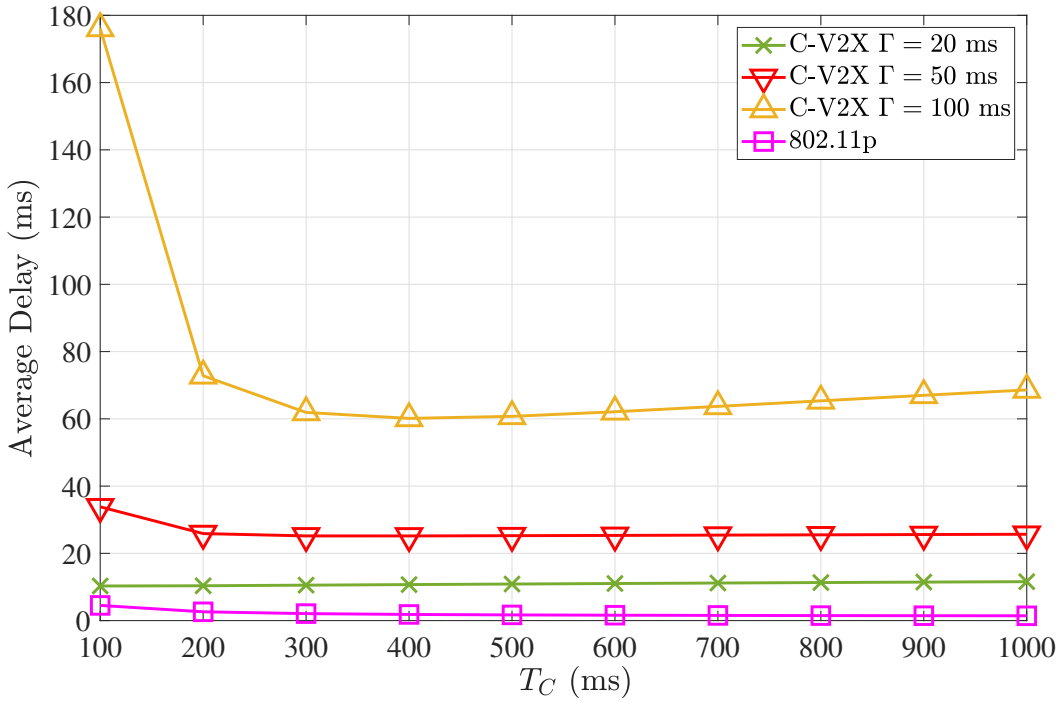

(a) Average delay vs T_C, $N = 300$, $\lambda = 1$, $T_D = 100$ ms, $P_{rk} = 0.4$, and $K = 5$.

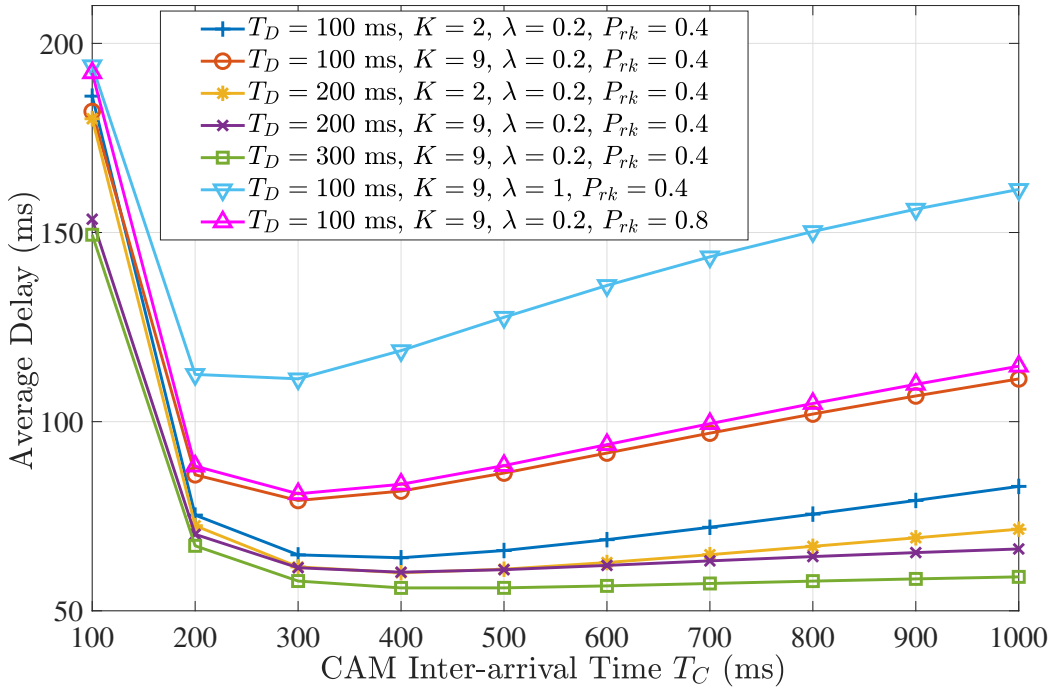

(b) Average delay of C-V2X Mode 4 vs T_C for different combinations of T_D, K, λ and P_{rk}, where $N = 50$, and $\Gamma = 100$ ms.

Figure 3.8: The behavior of the average delay with the inter-arrival time of CAM packets T_C.

critical scenario such as road works requires a minimum frequency of 2 Hz and a maximum delay of 100 ms. When considering all scenarios, we can conclude that a maximum delay of less than 100 ms is desirable for safety. Based on our results for C-V2X Mode 4, it can be seen that $\Gamma = 20$ ms and $\Gamma = 50$ ms can both satisfy this delay constraint on the average, at the highest CAM frequency of 10 Hz. However, as illustrated in Figure 3.8a, $\Gamma = 100$ ms fails to satisfy this delay requirement on the average, at the highest CAM rate of 10 Hz. On the other hand, as shown in Figure 3.7a, we can observe that the delay constraint is satisfied on the average for almost all parameter settings in IEEE 802.11p. Although the average delay increases with N, it can be observed that a system employing IEEE 802.11p for communication can support approximately 1000 vehicles without violating the 100 ms delay constraint on the average. The network can be made further dense by utilizing adaptive CAM.

Collision probability

As shown in Figure 3.9a, it is not surprising that the collision probability increases with N in both C-V2X Mode 4 and IEEE 802.11p. However, a vehicle that utilizes C-V2X Mode 4 has a lower collision probability than a vehicle that utilizes IEEE 802.11p. Thus, the SPS algorithm performs better in terms of collision resolution compared to the contention-based method in IEEE 802.11p. Therefore, C-V2X Mode 4 is a better choice for use cases that insist on ultra-reliable communications. We can observe that the collision probability in C-V2X Mode 4 increases with Γ. Higher values of Γ lead to longer selection windows, which increases the chances of two or more selection windows overlapping, as explained with regards to Figure 3.6. It can be observed that the adaptive CAM rate alleviates the collision probability of IEEE 802.11p marginally, but the collision rate is high when $N > 50$. The behavior of the collision probability with T_C is similar to what was observed for the average delay in Figure 3.8a. That is, it decreases monotonically with T_C for IEEE 802.11p, and it decreases first and then increases with a local optimum point for C-V2X. However, although the behavior for C-V2X is similar, the variation with T_C in terms of magnitude is negligibly small.

Average channel utilization

As illustrated in Figure 3.9b, the average channel utilization of C-V2X Mode 4 increases almost linearly with N. The rate at which the average channel utilization increases, decreases with the value of Γ. The system also exhibits lower average channel utilization for longer selection window sizes. In IEEE 802.11p, the av-

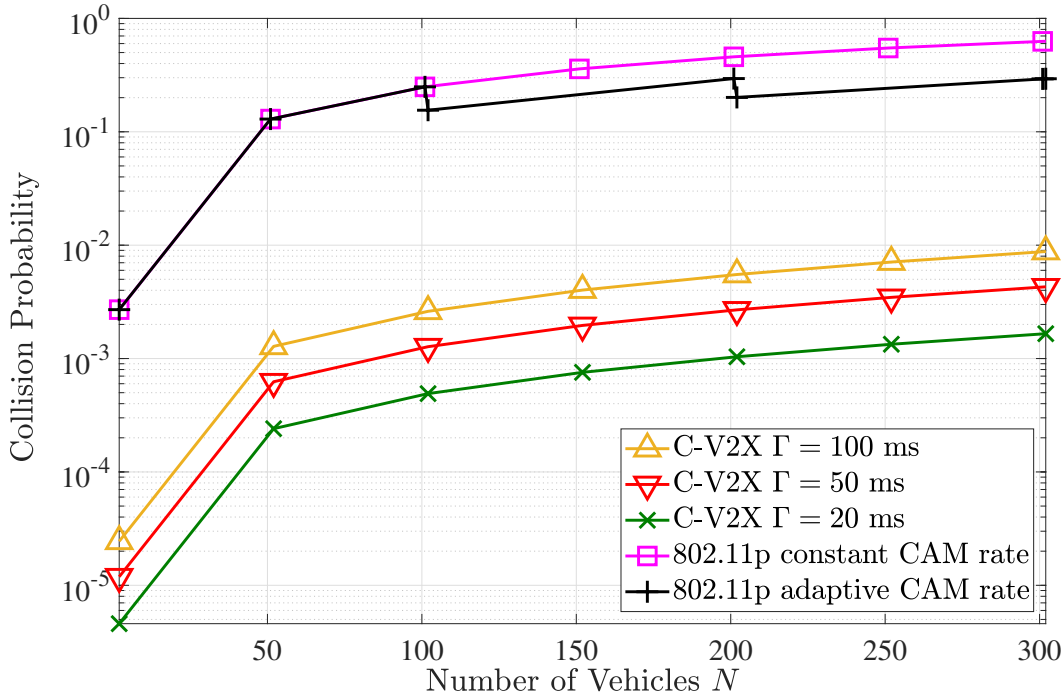

(a) Collision probability vs N.

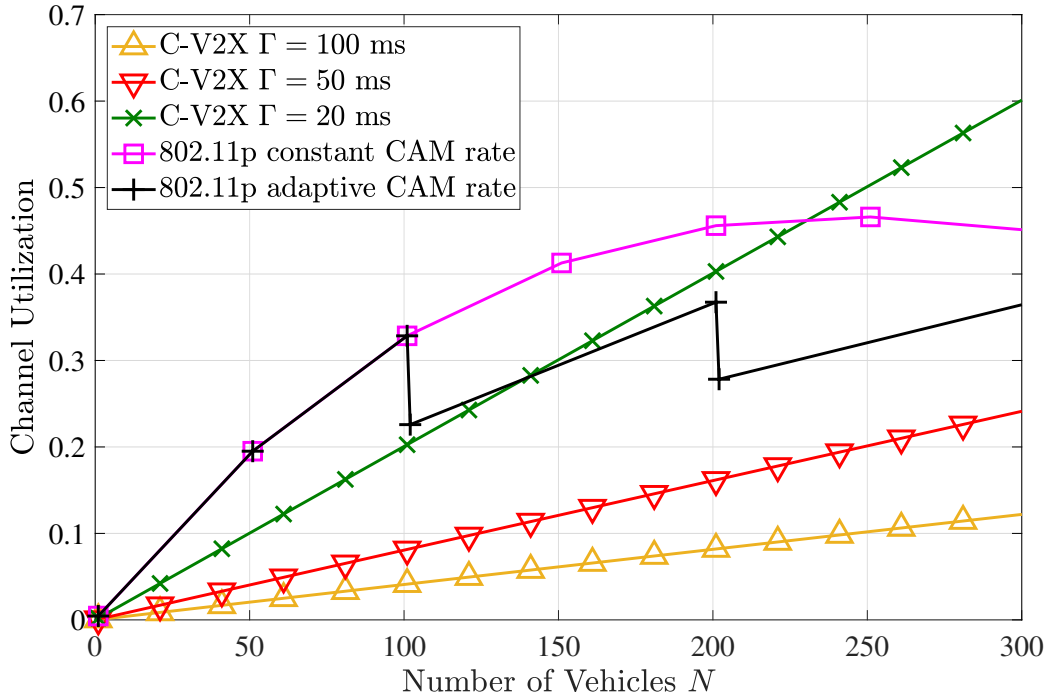

(b) Average channel utilization vs N.

Figure 3.9: The behavior of the collision probability and the average channel utilization with N, where $\lambda = 1$, $T_C = T_D = 100$ ms, $P_{rk} = 0.4$, and $K = 5$.

erage channel utilization increases with N up to about 200 and then saturates due to reaching the contention access based conditional stability region boundary. The average channel utilization of IEEE 802.11p can be improved with adaptive packet arrival. However, in general, it is always higher than C-V2X Mode 4. This shows that selecting a proper repetition interval for CAM packets can also be used for better channel utilization in IEEE 802.11p. The average channel utilization of both technologies decreases monotonically with T_C as the number of packets transmitted per second reduces when T_C increases. Similar behavior can be observed in the channel busy ratio. To this end, for $N = 300$, $\lambda = 1$ packet/s, $T_D = 100$ ms, $P_{rk} = 0.4$ and $K = 5$, the reduction in average channel utilization when T_C is increased from 100 ms to 1 s is 17.95% for IEEE 802.11p. For C-V2X, this reduction is significantly small, *e.g.*, for $\Gamma = 100$ ms, the reduction is 2.80%.

3.6 Conclusions

This chapter has presented multi-dimensional DTMC models to compare the MAC layer performance of the ETSI ITS-G5 IEEE 802.11p and C-V2X Mode 4, considering CAM and DENM packets proposed for ITS. DTMC based traffic generators and a device-level queue model have been used to feed the packets to the aforementioned DTMCs for transmission. Closed-form solutions for the steady-state probabilities of the models have been obtained, and they have been then utilized to derive expressions for key MAC layer-specific performance indicators such as the average delay, the collision probability, and the average channel utilization. An application of the models has been used for numerical results. The results have shown how the performance metrics of each communication technology vary for different parameter selections. When comparing the two technologies, the average delay of C-V2X Mode 4 is comparatively higher than IEEE 802.11p. On the other hand, the collision probability of a vehicle communicating using C-V2X Mode 4 is lower than its counterpart. The results have also shown that the average delay of C-V2X has a locally optimal combination of CAM and DENM packet arrival rates, which can be utilized to reduce delays in C-V2X further. Moreover, the DCC algorithm's TRC technique can be used to regulate the collision probability and the channel utilization of a vehicle communicating using IEEE 802.11p.

3.7 Appendix

3.7.1 Derivations of collision probability

Proof of Lemma 1

The selection window initiates at reaching state $(1,0)$, and this is the scenario where a collision can occur. The cycle time of state $(1,0)$ is $1/\pi_{1,0}$. Consider that vehicle v initiated its selection window. The probability of a neighboring vehicle reaching state $(1,0)$ during vehicle v's selection window is given by $1-\prod_{i=0}^{\Gamma-1}\left(1-\frac{1}{1/\pi_{1,0}-i}\right)=\tilde{p}$. Similarly, the probability of a neighboring vehicle reaching state $(1,0)$ during vehicle v's selection window and selecting the same CSR as vehicle v is given by $\tilde{p}(1-P_{rk})/(CSR_{tot}-CSR_{exc})$, where CSR_{exc} denotes the number of CSRs excluded according to the SPS algorithm such that there are $CSR_{tot}-CSR_{exc}$ CSRs in L_1. Thus, the probability of all $N-1$ neighboring vehicles not selecting the same CSR as vehicle v is given by $[1-\tilde{p}(1-P_{rk})/(CSR_{tot}-CSR_{exc})]^{N-1}$, and

$$1-\left[1-\tilde{p}(1-P_{rk})/CSR_{tot}-CSR_{exc})\right]^{N-1}$$

gives us the collision probability.

Let ξ denote the ratio between the size of the sensing window and the selection window, and Φ denote the number of times we encounter $RC=1$ in a given sensing window. Since $\xi \leq 2R_l$ according to the standard [31], we have $\Phi \in \{0,1,2\}$. This means, depending on the value of Φ, the vehicle of interest v may either use 1 CSR, 2 CSRs or 3 CSRs. Thus, the average number of CSRs used by vehicle v is given by $P_1+2P_2+3P_3$, where P_i is the probability of using i CSR values. The number of CSRs used by the neighboring vehicles known through SCI is approximately $N-1$. Hence, $CSR_{exc}\approx N-1+P_1+2P_2+3P_3$. It is not hard to see that $P_1+2P_2+3P_3\leq 3 << N-1$. Thus, we consider $CSR_{exc}\approx N-1$, which completes the proof.

Proof of Lemma 2

Let $P_{suc}=\Pr\{\text{exactly one vehicle transmits} \mid \text{at least one vehicle transmits}\}$, which can be simplified as the ratio between $P_{suc}=\Pr\{\text{exactly one vehicle transmits}\}$ and $\Pr\{\text{at least one vehicle transmits}\}$. Successful transmission of a packet by vehicle v can be obtained from the steady-state probabilities of the DTMC model for IEEE 802.11p as $(1-\theta)(\pi_{I,0}+\pi_{A_\Omega})+\sum_{j=1}^{\vartheta}\pi_{Tx,j}$. Similarly, the prob-

ability of the $N-1$ neighbors not transmitting is given by

$$\Big[1-\bigg(\pi_{I,0}+\pi_{A_\Omega}+\sum_{j=1}^{\vartheta}\pi_{Tx,j}\bigg)\Big]^{(N-1)}.$$

Thus, the probability of exactly one vehicle transmitting is given by

$$N\Big[(1-\theta)(\pi_{I,0}+\pi_{A_\Omega})+\sum_{j=1}^{\vartheta}\pi_{Tx,j}\Big]\Big[1-(\pi_{I,0}+\pi_{A_\Omega}+\sum_{j=1}^{\vartheta}\pi_{Tx,j})\Big]^{(N-1)},$$

and the probability of at least one vehicle transmitting is given by

$$1-\bigg[1-\bigg(\pi_{I,0}+\pi_{A_\Omega}+\sum_{j=1}^{\vartheta}\pi_{Tx,j}\bigg)\bigg]^{N}.$$

The ratio of these probabilities gives us P_{suc}, and $P_{col}^{11p}=1-P_{suc}$ completes the proof.

3.7.2 Derivations of average delay

Proof of Lemma 3

From the steady-state probabilities of the queue model, $1/P_{txo}$ is the duration in milliseconds (cycle time) to serve one packet. For the first packet, we may not spend the total cycle time to serve the packet, as it depends on the state vehicle v is in. Thus, we consider the service time to be $\frac{1}{2P_{txo}}$ (half the cycle time) for the first packet. From the second packet onwards, we add $\frac{1}{P_{txo}}$ to the service time of the previous packet to obtain the delay. For example, the service times of the second and the third packets are calculated as $\frac{3}{2P_{txo}}$ and $\frac{5}{2P_{txo}}$, respectively. We consider a queue of length M, and the averaging is done by utilizing the steady-state probability of each state, conditioned on the fact that the queue is not empty. Thus, the average delay is given by

$$d_{ave}^{v2x}=\sum_{i=1}^{M}\frac{2i-1}{2P_{txo}}\pi_i/(1-P_{qe}),$$

which completes the proof.

Proof of Lemma 4

Since unit time is considered to be $aSlotTime$, the delay associated with the transmit states is ϑ. The delay associated with states A_i where $i \in \{1, \ldots, \Omega\}$ is $1 + \sum_{i=1}^{\Omega-1}(1-\theta)^i$. The delay associated with the remaining states, *i.e.*, state $i \in S^{11p} - \left\{Idle, \bigcup_{j=1}^{\vartheta} Tx, j, \bigcup_{i=1}^{\Omega} A_i\right\}$ can be calculated by utilizing the product of the corresponding delay of each state (D_i) with the steady-state probability of each state conditioned on the fact that $i \in S^{11p} - \left\{Idle, \bigcup_{j=1}^{\vartheta} Tx, j, \bigcup_{i=1}^{\Omega} A_i\right\}$. Sum of the three delay values completes the proof.

Chapter 4

The EFFECT OF CONCURRENT MULTI-PRIORITY DATA STREAMS ON THE MAC LAYER PERFORMANCE OF C-V2X MODE 4 AND IEEE 802.11P

Supporting parallel multi-priority data streams is vital for maintaining the QoS in V2X communication. Hence, the ETSI has defined four packet types, with varying priority levels, to be used as broadcast packets in such communication. This chapter studies the MAC layer performance of IEEE 802.11p and cellular-V2X (C-V2X) Mode 4 using DTMC based models, while considering parallel multi-priority data streams. The overall model consists of four queue models with their respective traffic generators, which are appropriately linked with the DTMCs modeling the MAC layer operations of IEEE 802.11p and C-V2X Mode 4. Closed-form solutions for the steady-state probabilities of the models are obtained, which are then utilized to derive expressions for key performance indicators at the MAC layer. Numerical results are provided to draw insights on the MAC layer performance of the two technologies. IEEE 802.11p is comparatively superior in average delay, and at maintaining fairness among multi-priority data streams, whereas C-V2X Mode 4 exhibits better collision resolution, which leads to its higher throughput. The chapter also includes design insights on possible performance enhancements for future releases.

4.1 Introduction

4.1.1 Background and Motivation

Supporting multi-priority data streams plays a pivotal role in satisfying the stringent QoS requirements set for V2X communications. Against this backdrop, the ETSI ITS G5 [32] has defined four traffic classes that utilize different broadcast packets, namely, DENM, HPD, CAM, and MHD, for V2X communication. Each packet type has its own frequency of generation, number of repetitions, latency

constraints, and a level of priority. The different packet types allow the two enabling technologies of V2X, which are IEEE 802.11p and cellular-V2X (C-V2X), to cater a multitude of ITS applications having varying QoS requirements.

The periodic transmission of CAM packets governs information sharing, such as position, dynamics and attributes, and facilitates cooperative awareness [84]. HPD, DENM, and MHD, on the other hand, are event-driven messages utilized to communicate random events such as human or environment initiated disturbances [85]. DENM are used in comparatively less critical scenarios, such as roadwork warnings and safety function out of normal condition warnings, compared to HPD, which are utilized for highly critical scenarios such as emergency electronic brake light warnings. MHD are the relayed DENM packets from other vehicles, and they get the lowest priority upon transmission because a vehicle gives more priority for its own packets. The parallel operation of multi-priority broadcast data streams and the strict latency and reliability constraints in V2X communications make the MAC layer operation of the two enabling technologies of V2X crucial, which triggers our motivation for this study.

IEEE 802.11p [18] is the first WiFi-based standard designed explicitly for vehicular communications. The MAC layer operation of IEEE 802.11p stems from the well-known CSMA/CA technique. The EDCA mechanism [20] was introduced for IEEE 802.11p to allow the vehicle to accommodate differential QoS levels through four access categories (ACs), namely voice AC_{vo}, video AC_{vi}, best-effort AC_{be}, and background AC_{bk}. These ACs have different parameters for channel contention such that the QoS requirements of multiple data traffic classes can be met. Each AC also has an associated packet type, with a defined priority level [32]. In this chapter, we focus on the European version of 802.11p termed as the ETSI ITS-G5 IEEE 802.11p. C-V2X Mode 4 introduced in 3GPP Release 14, that has similar capabilities to IEEE 802.11p, can be considered to be the main competing technology [30, 86]. C-V2X Mode 4 uses the distributed sensing mechanism called SPS [31] to forecast and schedule free radio resources. However, there is no special mechanism to support multi-priority data streams in C-V2X Mode 4 similar to EDCA in IEEE 802.11p. Differential QoS is achieved by giving preference to higher priority packets, upon a transmission opportunity. This chapter primarily focuses on utilizing DTMCs for analytical modeling of the MAC layer operations of ETSI ITS-G5 IEEE 802.11p and C-V2X Mode 4, in the presence of parallel multi-priority data streams.

4.1.2 Related Works and Novel Contributions

Several research works that focus on the MAC layer performance of IEEE 802.11p in the presence of parallel multi-priority data streams can be identified in the literature [59,60,79–81]. The initial work on the MAC layer performance modeling of the IEEE 802.11p EDCA mechanism considered only a selective subset of the four ACs [79–81]. Subsequently, the authors of [59] and [60] considered the parallel operation of all four ACs in their DTMC-based modeling, and can be considered to be closely related to our work. Our model firstly improves slight inconsistencies of [59] and [60] with the standard, in terms of broadcast traffic. However, the main novelty in our work is the increased modeling granularity. This allows us to study the MAC layer operations for each $aSlotTime$, which is the smallest time unit in the IEEE 802.11p standard, similar to Chapter 3. The increased granularity makes our model more complex, but in turn, more accurate than [59] and [60]. We precisely model the waiting times of different ACs before resuming channel contention, enabling us to correctly capture the effect of prioritization among the ACs, which are not done in [59] and [60]. An AC bearing a higher priority can initiate transmission during the long waiting period of an AC with lower priority. Transmission delays are also calculated more accurately than in [59] and [60] by taking the payload size into account.

Performance analysis of C-V2X Mode 4 has become an active research area recently. The related works can be mainly categorized as simulation [22, 74] and analytical modeling based studies [75, 76, 96, 101]. The authors of [22] present the first open-source simulator for C-V2X Mode 4 by utilizing the NS3 software, and study the performance of the technology. A similar study using the VEINS open-source framework is presented in [74]. The first analytical model for the MAC layer operations of C-V2X Mode 4 is proposed in [75]. The chapter considers a PHY layer model to capture the effect of distance between the vehicles, and the MAC layer operation is handled by the SPS algorithm [31]. The authors then obtain analytical expressions for several performance measures at the MAC layer as a function of the distance between the communicating nodes. In [76], the authors compare the MAC layer performance of C-V2X Mode 4 with IEEE 802.11p for the transmission of periodic and aperiodic messages, having both fixed and variable sizes. The chapter highlights certain inefficiencies of the SPS algorithm when transmitting aperiodic messages with variable sizes. The first DTMC-based analytical model for the MAC layer operations of C-V2X Mode 4 is proposed in [96, 101]. The overall model in this chapter stems on this model,

while additionally capturing the effect of parallel multi-priority data streams. The model also considers the requirement of adjusting the selection window size based on the number of vehicles, to facilitate the radio resource selection process according to the SPS algorithm. To the best of our knowledge, this is the first work that focuses on the MAC layer performance of C-V2X Mode 4 in the presence of parallel multi-priority data streams.

The main contributions of this chapter can be summarized as follows:

- **Modeling multi-priority packets:** We model the generation of multi-priority data packets, namely HPD, DENM, CAM, and MHD, by utilizing four DTMCs. The separate DTMCs provide us the flexibility of altering the traffic arrival patterns of the individual packet types, and create a more realistic V2X communication scenario compared to the simpler models with predefined traffic rates used in [59] and [60]. We use four more DTMCs to model the device-level packet queues of the generated packet types, and each generator model is appropriately coupled with its queue model.

- **Modeling the MAC layer operations:** We then model the MAC layer operations of each V2X enabling technology using DTMCs. These models are appropriately coupled with the generator and queue models while taking priority levels among data streams into consideration. The priority management makes this work significantly different from Chapter 3, in terms of the overall models, as well as the results and the drawn insights. Since Chapter 3 neglects the priority levels of the packets, the generated packets are transmitted in the order of generation.

- **Performance analysis:** We utilize the closed-form steady-state probabilities of the DTMCs to derive expressions for the average delay, collision probability, throughput, and the channel utilization.

- **Comparison of the two technologies:** We then present an application of the models. We first highlight the importance of taking all four parallel data streams into consideration when studying the MAC layer performance of the two technologies, by comparing with a scenario where only a subset of the packet types is utilized for communication. We compare the two technologies using the derived performance measures while providing insights on the synchronous operation of multi-priority data streams. In particular, IEEE 802.11p is superior in average delay, but exhibits a higher number of collisions compared to C-V2X Mode 4. Also, it can be seen that

IEEE 802.11p treats multi-priority data streams more fairly compared to its counterpart, thanks to its inbuilt EDCA mechanism.

- **Insights on performance enhancements:** The numerical evaluations are used to draw insights on how the performance of each technology can be enhanced in the presence of parallel multi-priority data streams. We also present comparisons with similar results obtained according to the models in Chapter 3 to highlight the significance of priority management in the MAC layer performance. These insights can contribute in the evolution of these two technologies into new radio V2X (NR-V2X) and IEEE 802.11bd [57,58].

The chapter is organized as follows. The DTMCs and the evaluation of the dependencies among the DTMCs are presented in Section 4.2 and Section 4.3, respectively. The performance analysis follows in Section 4.4. Section 4.5 consists of the numerical results and discussion, and Section 4.6 concludes the chapter.

4.2 Analytical Models

This section presents the DTMC-based analytical models utilized to study the effect of concurrent multi-priority data streams on the MAC layer performance of IEEE 802.11p and C-V2X Mode 4. A DTMC is a stochastic model that describes a random process utilizing a discrete set of states in discrete-time, and follows the Markov property, *i.e.,* the future evolution of the process depends only on the present state. A state change in a DTMC is called a transition, and the associated probability is called the transition probability. DTMCs have been studied for decades to model a wide range of real-world applications [69]. There are two main reasons for using DTMC for this study. Firstly, DTMC-based modeling facilitates improved granularity in the models. This enables us to precisely model the MAC layer operations in discrete time. Secondly, the memoryless property of DTMCs makes the analysis mathematically tractable. All DTMCs in this chapter are aperiodic and irreducible, thus they are ergodic. Hence, a steady-state distribution for each model exists [97]. The models cater for both periodic and event-driven traffic (non-saturated transmission conditions), but do not account for phenomena at the PHY layer such as mobility, distance, and speed. We consider a vehicular network of N vehicles, and we use v to denote the target vehicle.

The overall models for IEEE 802.11p and C-V2X Mode 4 are presented in Figs. 4.1a and 4.1b, respectively. In our notations, we use subscripts H, D, C,

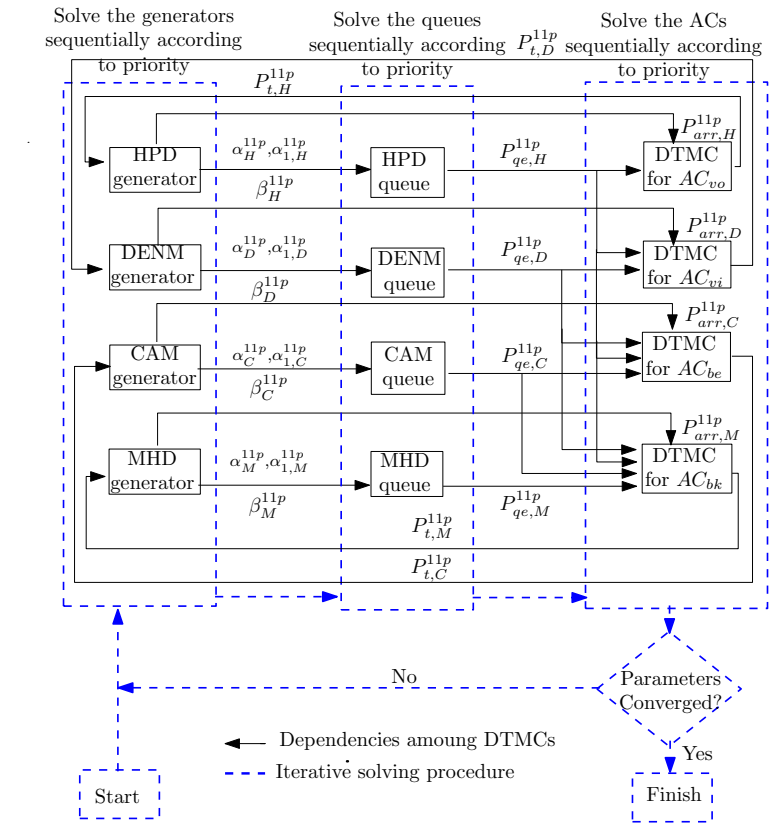

(a) IEEE 802.11p.

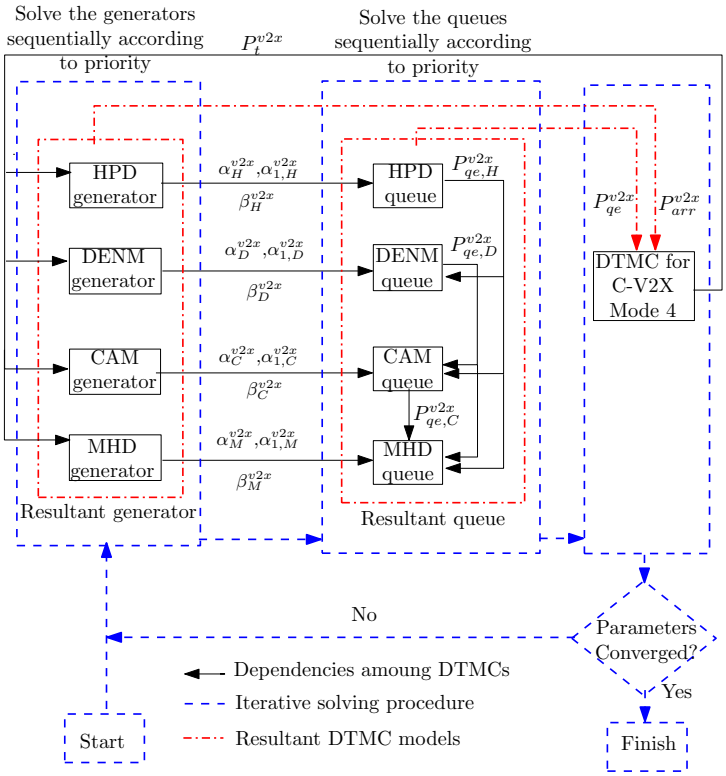

(b) C-V2X Mode 4.

Figure 4.1: Flowchart illustrating the overall models.

and M to differentiate between HPD, DENM, CAM, and MHD, respectively, and superscripts $11p$ and $v2x$ to differentiate between IEEE 802.11p and C-V2X Mode 4. The overall models consist of multiple interrelated DTMCs. The parameters that introduce dependencies among the DTMCs, (*e.g.*, α_l^k, $\alpha_{1,l}^k$, β_l^k, $P_{qe,l}^k$, $P_{t,l}^{11p}$, P_t^{v2x}, $P_{arr,l}^{11p}$, P_{qe}^{v2x}, P_{arr}^{v2x}, for $l \in \{H, D, C, M\}$, $k \in \{11p, v2x\}$), are introduced formally later in the section, while discussing the related DTMCs. Firstly, we use a common structure of four DTMCs to model the generation of HPD, DENM, CAM, and MHD packets, for both technologies. We refer to them as packet generators, and the priority order of serving these packets is as follows: HPD > DENM > CAM > MHD. The common structure for packet generation facilitates a fair performance comparison of the two technologies. Secondly, we use four DTMCs to model the device-level packet queues of the generated packet types. The queue models introduced for the two technologies are slightly different from one another.

The overall models differ significantly in the third stage that consists of the DTMCs modeling the MAC layer operations. IEEE 802.11p allows the vehicle to accommodate differential QoS levels through four ACs, namely, voice AC_{vo} utilized for HPD packets, video AC_{vi} utilized for DENM packets, best-effort AC_{be} utilized for CAM packets, and background AC_{bk} utilized for MHD packets [32]. Thus, the MAC layer operations of IEEE 802.11p are modeled using four separate DTMCs (one for each AC), as shown in Figure 4.1a, while incorporating the effect of priority. On the other hand, the MAC layer operation of C-V2X Mode 4 does not directly consider priority levels upon transmission. Therefore, a single DTMC is used to model the MAC layer operation, while considering the resultant effect of the generators and the queues, as shown in Figure 4.1b. The priority management is incorporated in the queues, which leads to the aforementioned difference in the queue models of the two technologies. Figs. 4.1a and 4.1b also illustrate the iterative solving procedure of these models, which we explain in detail in Section 4.5. Next, we present further details on the individual DTMCs.

4.2.1 Packet Generators

HPD, DENM, and MHD are all randomly generated packets, thus we model their arrivals through Poisson arrival processes of intensity λ_m, where $m \in \{H, D, M\}$. Due to their critical nature, HPD and DENM packets are repeated at fixed periods of T_H and T_D, respectively, for added reliability [78]. This means the HPD and DENM generators capture two distinct packet types: a Poisson-based triggered generation and the subsequent fixed-period repeat packet generation. Upon

a trigger, an HPD packet is transmitted K_H times, and a DENM packet is transmitted K_D times, periodically. MHD packets are generated by neighboring vehicles, and supposed to be forwarded by vehicle v with the lowest priority. Hence, these packets are not repeated, and the number of repetitions of an MHD packet K_M is set at one. CAM packets, on the other hand, have a periodic packet arrival pattern, and the inter-arrival time T_C takes a value between 100 ms and 1000 ms [84].

The four generator models are illustrated using a single figure (Figure 4.2). DTMCs for the generation of CAM and DENM packets are introduced in Chapter 3, and in this chapter, we have included two more variants of DENM, which are HPD and MHD. All four models are presented in this chapter for completeness and consistency in notations. The parts common to all generators are represented using solid lines, and different line styles are used to highlight the parts specific to a certain generator appropriately. The three event-driven generators consist of state $(Idle)$ to account for the periods with no generated packets. Note that since $K_M = 1$, the MHD generator simplifies into a two state DTMC model which consists of $(idle)$ and $(tx, 0)$ states. The triggered generation of MHD packets is represented by the transition from state $(idle)$ to $(tx, 0)$ with probability $1 - e^{-\lambda_M \tilde{T}}$. State $(tx, 0)$ represents packet generation, and since $K_M = 1$, the transition back to $(Idle)$ happens with probability 1.

The other three packet types (HPD, DENM, and CAM) share similarities with regards to the periodicity. In these generators, states $(i, 0)$, $i \in \{tx, tx'\}$, represent the packet generation, where tx and tx' are used to represent whether the previously generated packet has been transmitted, or not, respectively. The waiting time between the generation of two packets, denoted by T_n ms, $n \in \{H, D, C\}$, is represented by states (i, j), $i \in \{tx, tx'\}$ and $j \in [0, T_n - 1]$, with a modeling granularity of $aSlotTime$ =13 μs for IEEE 802.11p, and a subframe of 1 ms for C-V2X Mode 4. Not having a transmission opportunity upon generation requires the packet to wait for an opportunity, which is represented by states (tx', j), $j \in [1, T_n - 1]$. A state transition from (tx', j) to $(tx, j - 1)$, $j \in [1, T_n - 1]$, represents a successful transmission. For each technology, we use $\mathcal{P}_n^k$, where $n \in \{H, D, C\}$ and $k \in \{11p, v2x\}$, to capture the effect of the respective packet transmitting probabilities in the generator models. To this end, for $n \in \{H, D, C\}$, $\mathcal{P}_n^{11p} = P_{t,n}^{11p}$, and $\mathcal{P}_n^{v2x} = P_t^{v2x}$, as shown in Figs. 4.1a and 4.1b. These parameters link the generators with the DTMCs modeling the MAC layer operation. The variables associated with the generator models are tabulated in Table 4.1 at the end of this section for the ease of reference.

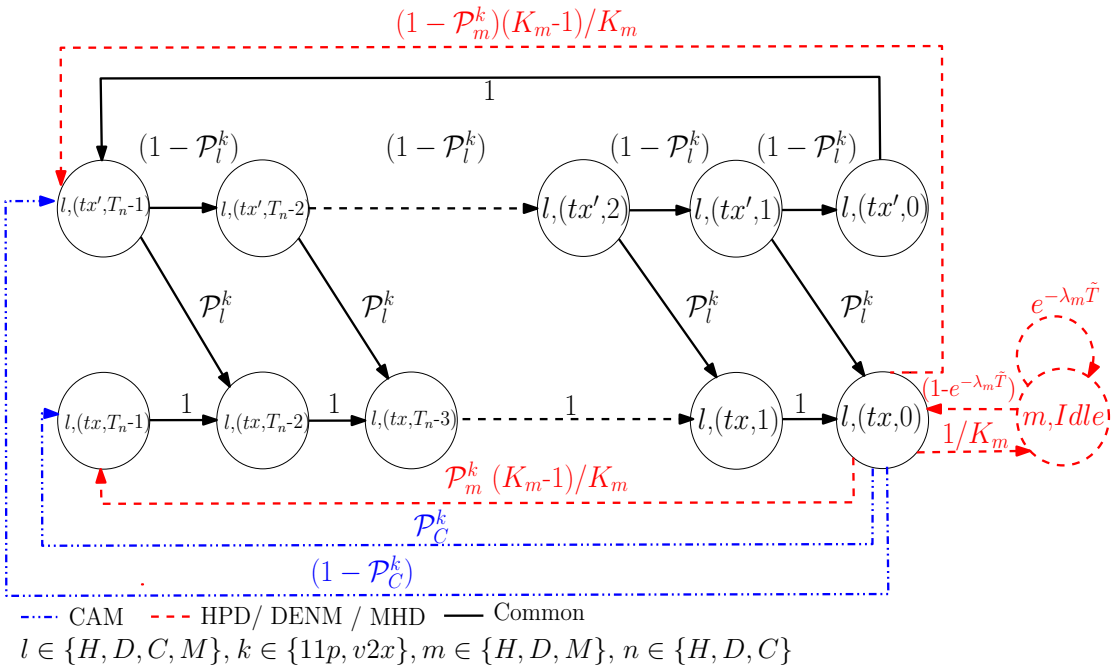

Figure 4.2: HPD, DENM, CAM, and MHD packet generators.

4.2.2 Packet Queues

Each packet type has its own queue with the common general structure similar to the one introduced in Chapter 3, as shown in Figure 4.3. State (i, l), $i \in [0, Q^{\max}]$ and $l \in \{H, D, C, M\}$, represents a queue of length i, such that $Q^{\max}$ is the maximum length. A transition from state (i, l) to state $(i + 1, l)$, which is incrementing the queue, or state $(i - 1, l)$, which is decrementing the queue, depends on packet generation and transmission, respectively. For $l \in \{H, D, C, M\}$ and $k \in \{11p, v2x\}$, $P^k_{qe,l}$ denotes the probability of having an empty queue, $P^k_{qne,l} = 1 - P^k_{qe,l}$, and $P^k_{arr,l}$ denotes the conditional probability of a new packet of type l arriving given its respective queue is empty. Note that although having the same structure, the transition probabilities of the queue models differ according to the packet type and the technology.

The overall device-level packet queues for the two technologies are different from each other as stated earlier, and they are significantly different to the one presented in Chapter 3. Since Chapter 3 does not consider any priority management among the packets, the generated packets are stored in a composite queue in the order of generation, for transmission. The priority handling in this chapter is incorporated through the ACs in IEEE 802.11p, thus the queue models can be directly coupled with the appropriate ACs as shown in Figure 4.1a. On the other hand, there is only one DTMC to model the MAC layer operations in

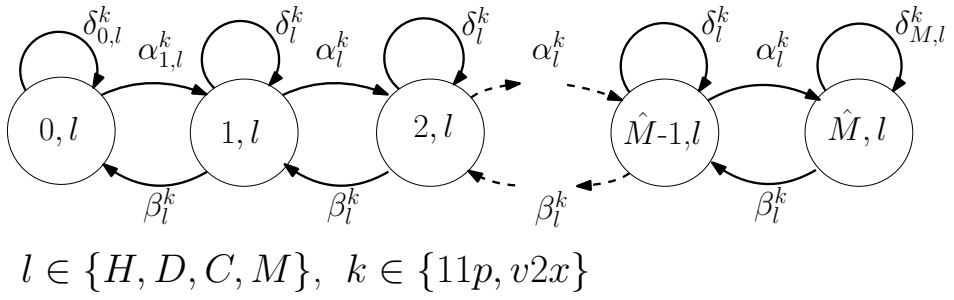

Figure 4.3: The common queue structure for HPD, DENM, CAM, and MHD packets.

C-V2X Mode 4. Thus, the four packet-level queues are incorporated such that a resultant queue which simultaneously considers priority levels, is coupled with the DTMC modeling the MAC layer operations, as shown in Figure 4.1b. The resultant queue also takes the same structure shown in Figure 4.3, and the priority is incorporated through appropriately setting the transition probabilities, which we discuss in detail in Section 4.4. Similar to the individual queues, P^{v2x}_{qe} and P^{v2x}_{arr} denote the queue empty and conditional packet arrival probabilities of the resultant queue, respectively, and $P^{v2x}_{qne} = 1 - P^{v2x}_{qe}$. The variables associated with the queue models are tabulated in Table 4.1 at the end of this section for the ease of reference.

4.2.3 DTMC Models for the Four ACs of IEEE 802.11p

In this subsection, we present the DTMCs used to model the behavior of each AC in IEEE 802.11p. We use index $i \in \mathcal{AC} = \{vo, vi, be, bk\}$ to differentiate between the parameters related to voice (HPD), video (DENM), best-effort (CAM), and background (MHD), respectively, and the DTMC model illustrated in Figure 4.4 is used to describe the MAC layer operations of AC_i. To this end, vehicle v is at state $(Idle_i)$, and remains in this state if the packet queue for AC_i is empty[1]. When a packet arrives, vehicle v listens for an $AIFS$ duration. The $AIFS$ duration for AC_i, denoted by $AIFS_i$, is calculated according to $AIFS_i = aSIFSTime + AIFSN_i \times aSlotTime$, where $aSlotTime$ is 13 μs, $aSIFSTime$ is 32 μs, and arbitration inter-frame spaces number of AC_i ($AIFSN_i$) is selected according to the AC from the standard [1]. For AC_i, let C_i denote the minimum contention window size, and $\Omega_i = \lceil AIFS_i/aSlotTime \rceil$. States (A^j_i) for $j \in \{1, \ldots, \Omega_i\}$ represent this listening time. If the channel stays idle in this duration, the vehicle transmits, which is represented by states (T_i, j), $j \in \{1, \ldots, \vartheta\}$, in

[1]This chapter presents a more precise definition of state $(Idle_i)$ compared to the one in [102]. The subsequent derivations and the expressions for performance indicators differ accordingly.

which $\vartheta \times aSlotTime$ is the time taken for the transmission. This is in fact the time taken to transmit 134 bytes over a 6 Mbps control channel (CCH) [32]

However, if the channel is found to be occupied within the listening period, the vehicle waits for the transmission to end. This $\vartheta \times aSlotTime$ duration is modeled by states (B_i, j), $j \in \{1, \ldots, \vartheta\}$. State (A_i^1) depicts the special case of a packet arrival while the channel is busy. In such a case, the vehicle may not have to wait for $\vartheta \times aSlotTime$ until the channel becomes free again. Thus, the waiting duration can be written as $J \times aSlotTime$, where integer J is random and uniform in $[1, \vartheta]$. Therefore, the transition from state (A_i^1) is different from the transitions from (A_i^j) for $j \in \{2, \ldots, \Omega_i\}$. We can also notice a difference in the transition probabilities. The two transition probabilities represent slight variations of the probability of the channel being busy. At states (A_i^j), where $j \in \{2, \ldots, \Omega_i\}$, the channel has remained idle for at least one $aSlotTime$ interval. Thus, if vehicle v can sense transmission at one of these states, the transmission from a neighboring vehicle must have just initiated. Hence, the transmitting vehicle should be at the first transmitting state. This restriction does not exist at (A_i^1), and the transmitting vehicle can be at any transmitting state.

After vehicle v reaches (B_i, ϑ), where the channel is supposed to be idle again, it initiates a backoff by randomly and uniformly selecting a backoff counter value from $[0, C_i]$. Each counter value gives rise to a specific backoff stage with both counter values zero and one leading to stage zero, according to the standard. During backoff, the vehicle waits for an $AIFS$ duration before sensing the channel again, and this wait is represented by states (b, A_i^j), $j \in \{1, \ldots, (\Omega_i - 1)\}$, for counter value $b \in \{0, \ldots, (C_i - 1)\}$. During the wait, the vehicle senses the channel after each $aSlotTime$ interval. If it finds the channel to be busy, it waits $\vartheta \times aSlotTime$ for the transmission of the neighboring vehicle to end. This duration is represented by states (Δ_i^b, j), for $j \in \{1, \ldots, \vartheta\}$. Upon the completion of the transmission of the neighboring vehicle, the vehicle waits for another $AIFS$ duration at the same backoff stage. The process continues until the channel is found to be free at state (I_i, b). Observation of a free channel at state (I_i, b) leads to decrementing the backoff counter to arrive at state $(I_i, b - 1)$. The channel being free at state $(I_i, 0)$ gives the vehicle the opportunity to transmit.

The ACs with a higher priority have a shorter $AIFS$ duration, and AC_{bk}, which is the AC with the lowest priority, has the longest duration. Thus, Figure 4.4 in fact illustrates the DTMC model for AC_{bk}. The DTMC models for the other three ACs that have shorter $AIFS$ duration values can be obtained by appropriately excluding states and transitions (as illustrated) from Figure 4.4.

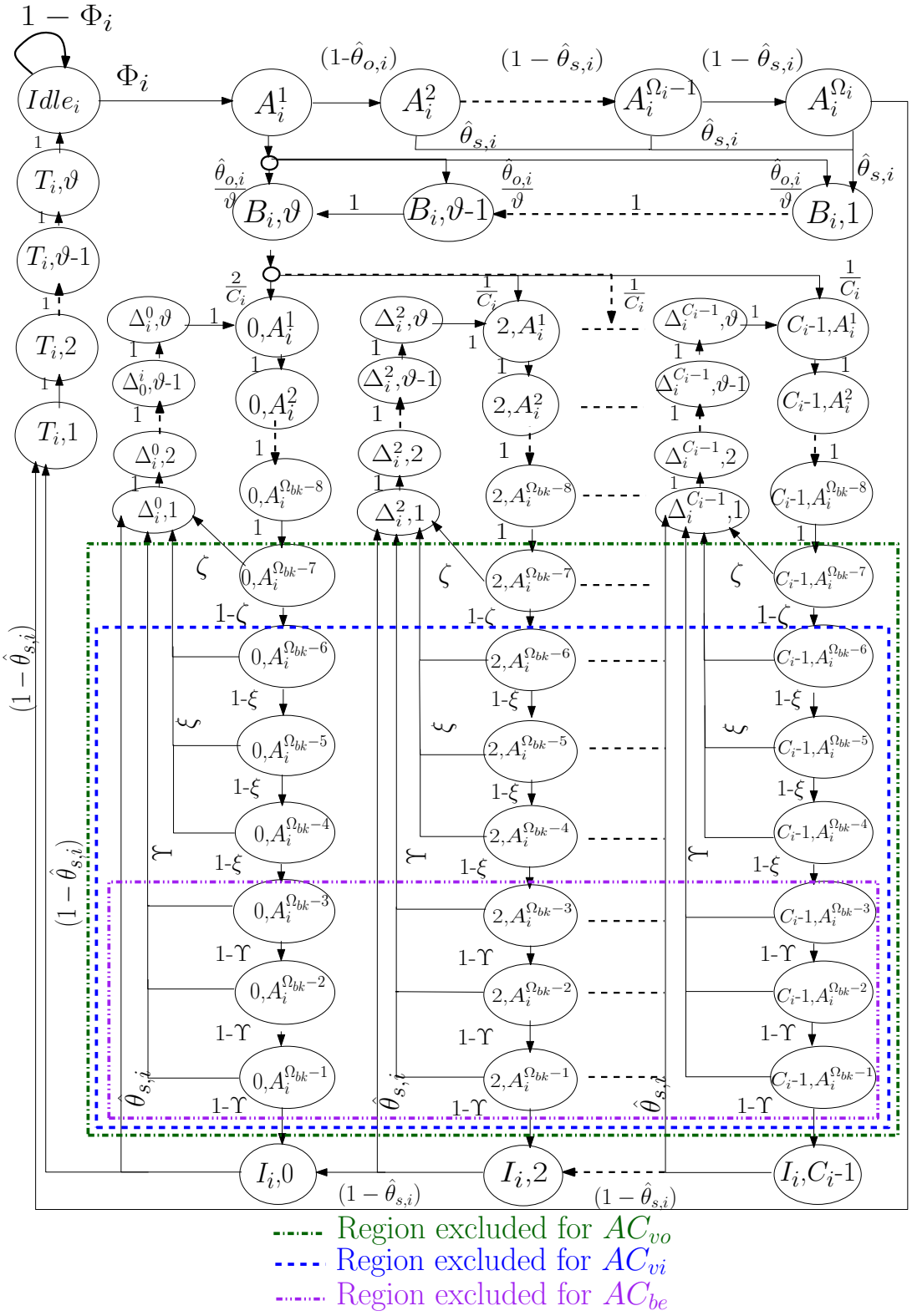

Figure 4.4: DTMC models for the MAC layer operations of the four ACs in IEEE 802.11p.

For the backoff stage value b, the transition from states $(b, A_i^{\Omega_{bk}-j})$, where $j \in \{1, \ldots, (\Omega_{bk} - \Omega_{vo})\}$, to state $(\Delta_i^b,1)$, can only happen due the arrival of a higher priority packet. As an example, for AC_{bk}, this can happen due to the arrival of a HPD, DENM or CAM packet. Let the channel busy ratio θ_i denote the probability of the channel being busy for AC_i. Then, $\zeta = \theta_{vo}$, $\xi = (\theta_{vo} + \theta_{vi})$, and $\Upsilon = \sum_{i \in \mathcal{AC} \setminus \{bk\}} \theta_i$. The variables associated with the DTMC are tabulated in Table 4.1 at the end of this section for the ease of reference.

4.2.4 DTMC Model for C-V2X Mode 4

C-V2X Mode 4 utilizes the SPS algorithm for radio resource allocation [31]. The SPS algorithm is specially designed for identifying the available CSRs and allocating them for communication without the aid of the cellular infrastructure. Upon allocation, the vehicle uses the radio resource RC times, where RC is called the reselection counter. The value RC is selected uniformly and randomly from $[R_l, R_h]$, where R_l and R_h denote the lower and upper bounds for RC, respectively. Let P_{sch} denote the probability of allocating a suitable CSR for a vehicle by utilizing the SPS algorithm. Γ denotes the length of the selection window. This is the time allocated for CSR selection, and is defined as the maximum tolerable latency in the standard [30]. Each selection window size has its respective range for RC. According to the standard, the three selection window sizes are, $\Gamma = 100$ ms with $RC \in [5, 15]$, $\Gamma = 50$ ms with $RC \in [10, 30]$ and $\Gamma = 20$ ms with $RC \in [25, 75]$ [86].

We assume that $P_{sch} = 1$ without any loss of generality as it is unlikely that a vehicle ends up without any radio resources to transmit according to the standard. However, the selection window size should be appropriately increased with the number of vehicles in the network to maintain this condition. Let $CSR_{tot,\Gamma}$ denote the total number of CSRs in a selection window of Γ duration. For example, according to [30], a 1 ms subframe contains 100 RB. Transmitting a payload of 100 bytes using 64 QAM modulation requires at least 4 RBs. Thus, a subframe can hold 25 CSRs, which means $CSR_{tot,20} = 500$. The maximum number of vehicles that the system can support for each selection window size while maintaining $P_{sch} = 1$ is denoted by $N_{m,\Gamma} = 0.8 \times CSR_{tot,\Gamma}$ according to the standard [31]. The DTMC model for the MAC layer operations is illustrated in Figure 4.5. We note that this model for C-V2X Mode 4 was first introduced in Chapter 3. We present a summary of this model for completeness.

State *Idle* represents the idle state with either no packets or no CSRs to transmit. The waiting time before transmitting a newly arrived packet is modeled using

states $(w,\ j)$, $j \in [0, \Gamma - 2]$, and these states are assumed equiprobable. The vehicle uniformly selects a random value for RC after this waiting period. States $(i, 0)$, where $i \in [1, R_h]$ depicts the current RC value, represent transmission opportunities. Upon a transmission opportunity, the system stays in the current RC value for Γ ms if the queue is empty, or otherwise, transmits and moves to $(RC - 1,\ \Gamma - 1)$. If the queue is not empty at $(1,\ 0)$, the vehicle opts for a new radio resource with probability $1 - P_{rk}$, or else continue using the same radio resource, where $P_{rk} \in [0, 0.8]$ according to the standard [31]. The variables associated with all the DTMCs presented in this section are tabulated in Table 4.1 for the ease of reference.

4.3 Evaluation of the Dependencies among the DTMCs

In this section, we derive expressions for the parameters that introduce dependencies among the DTMCs as shown in Figs. 4.1a and 4.1b, by utilizing the steady-state solutions of each DTMC. We denote the steady-state probability of an arbitrary state (A) by π^k_A, where $k \in \{11p, v2x\}$. We first focus on the generator models.

4.3.1 Generator Models

The parameters that introduce dependencies among the generators and the queue models are the queue advancing transition probabilities α^k_l and $\alpha^k_{1,l}$, and the queue servicing transition probabilities β^k_l, for $l \in \{H, D, C, M\}$ and $k \in \{11p, v2x\}$. To this end, we have

$$
\begin{aligned}
\alpha^k_i &= \pi^k_{i,(tx',0)}, \\
\alpha^k_{1,i} &= \pi^k_{i,(tx,0)} \left(1 - \frac{1}{K_i}\right)(1 - \mathcal{P}^k_i), \quad \text{for } i \in \{H, D\}, \\
\alpha^k_C &= \pi^k_{C,(tx',0)}, \\
\alpha^k_{1,C} &= \pi^k_{C,(tx,0)}(1 - \mathcal{P}^k_C), \\
\alpha^k_{1,M} &= \alpha^k_M = (1 - e^{-\lambda_M \tilde{T}}), \text{ where } k \in \{11p, v2x\}.
\end{aligned}
$$

$\tilde{T}$ is $aSlotTime$ for IEEE 802.11p, and $subframe$ for C-V2X Mode 4. Moreover, $\mathcal{P}^{11p}_n = P^{11p}_{t,n}$ and $\mathcal{P}^{v2x}_n = P^{v2x}_t$ for $n \in \{H, D, C\}$, and the expressions for the steady-state probabilities of the generator models are presented in Appendix 4.7.1.

The queue servicing transition probabilities related to the four queue models associated with IEEE 802.11p are given by $\beta^{11p}_n = P^{11p}_{t,n} \sum_{j=1}^{T_n - 1} \pi^{11p}_{n,(tx',j)}$, for $n \in$

Table 4.1: The parameters of the analytical models.

Parameters	Description
For $i \in \{vo, vi, be, bk\}$, $m \in \{H, D, M\}$, $l \in \{H, D, C, M\}$, $n \in \{H, D, C\}$, **and** $k \in \{11p, v2x\}$**:**	
Generator models	
λ_m	Arrival rate of packet m.
$\mathcal{P}_l^k$	The transmission probability of packet l.
K_m	Number of repetitions of packet m.
T_n	Repetition interval of packet n.
Queue models	
Q^{max}	The maximum queue length.
$P_{qe,l}^k$	Queue empty probability of packet l.
P_{qe}^{v2x}	Queue empty probability of the C-V2X resultant queue.
$P_{qne,l}^k$	$1 - P_{qe,l}^k$.
P_{arr}^{v2x}	Conditional packet arrival probability of the C-V2X resultant queue.
IEEE 802.11p model	
$AIFSN_i$	Arbitration inter-frame spacing number of AC_i.
$AIFS_i$	Arbitration inter-frame spacing of AC_i.
$aSlotTime$	The smallest time unit of the IEEE 802.11p protocol (13 μs).
Ω_i	$AIFS_i/aSlotTime$.
ϑ	The number of $aSlotTime$ taken to transmit a 134 bytes packet over a 6 Mbps CCH.
C_i	The minimum contention window size for AC_i.
C-V2X Mode 4 model	
Γ	The selection window size.
P_{rk}	The probability of using the same radio resource.
P_{sch}	The probability of allocating a suitable CSR for a vehicle by utilizing the SPS algorithm.
R_h	The upper bound for RC.
R_l	The lower bound for RC.
RC	The reselection counter value.

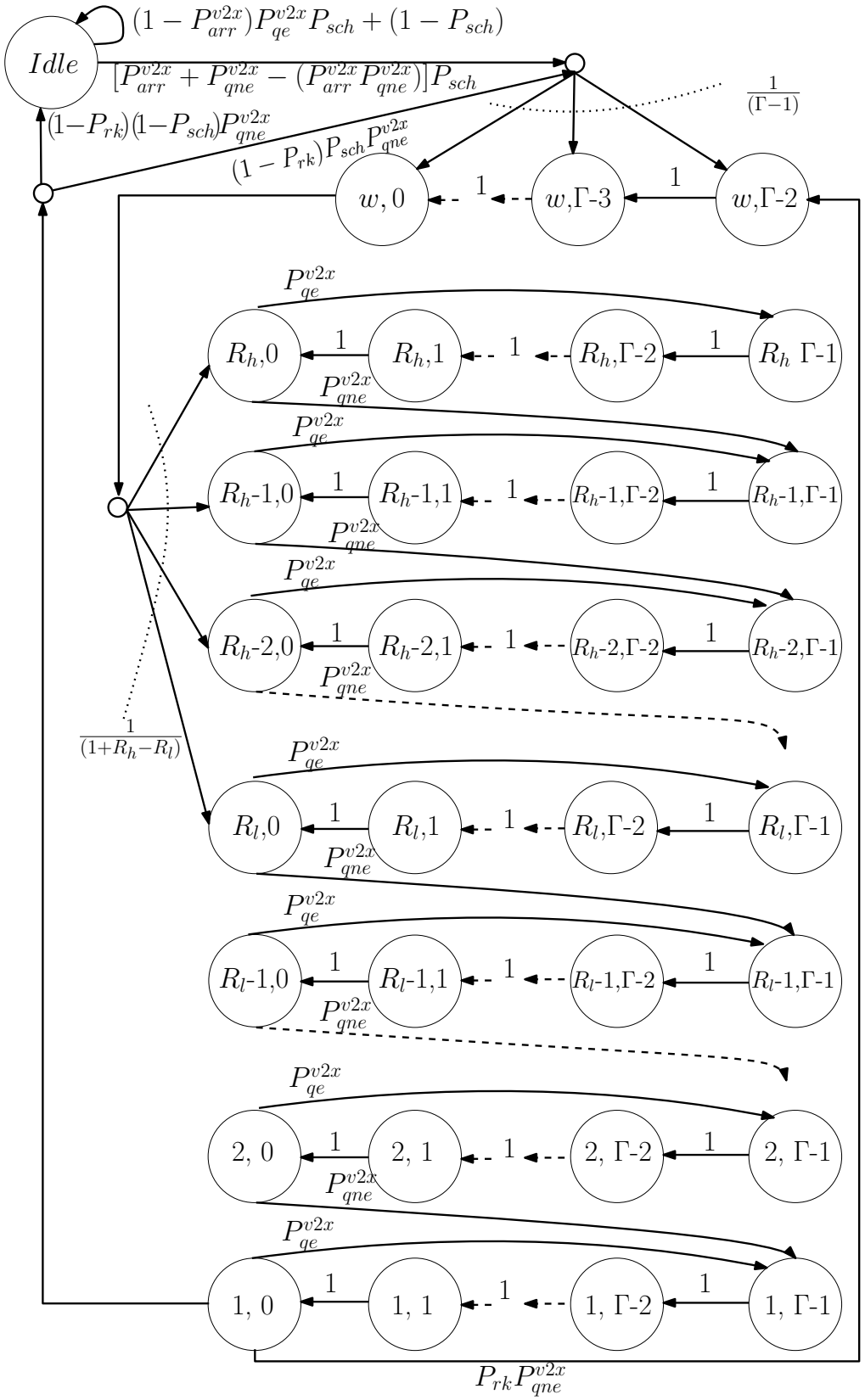

Figure 4.5: DTMC model for the MAC layer operations of C-V2X Mode 4.

$\{H, D, C\}$, and $\beta_M^{11p} = P_{t,M}^{11p}$, where $P_{t,M}^{11p}$ denotes the transmit probability of MHD packet in IEEE 802.11p. Although the queue advancing transition probabilities are of similar form for both enabling technologies, there is a variation in the queue servicing transition probabilities since the priority management is incorporated in the queue models for C-V2X Mode 4. This means, the packets in the lower priority queues are only served if there are no packets in the higher priority queues, thus we have

$$\begin{aligned}
\beta_H^{v2x} &= \sum_{j=1}^{T_H-1} \pi_{H,(tx',j)}^{v2x} P_t^{v2x}, \\
\beta_D^{v2x} &= \sum_{j=1}^{T_D-1} \pi_{D,(tx',j)}^{v2x} P_t^{v2x} P_{qe,H}^{v2x}, \\
\beta_C^{v2x} &= \sum_{j=1}^{T_C-1} \pi_{C,(tx',j)}^{v2x} P_t^{v2x} P_{qe,H}^{v2x} P_{qe,D}^{v2x}, \\
\beta_M^{v2x} &= P_t^{v2x} \prod_{n\in\{H,D,C\}} P_{qe,n}^{v2x}.
\end{aligned}$$

We can also observe dependencies between the generator models and the DTMCs introduced for the MAC layer operations. To this end, for $k \in \{11p, v2x\}$, we have $P_{arr,m}^k = (1 - e^{-\lambda_m \tilde{T}})$ for $m \in \{H, D, M\}$, and $P_{arr,C}^k = \pi_{tx,0}^C + \pi_{tx',0}^C$. The packet arrival probability for the resultant queue in C-V2X Mode 4 is given by

$$P_{arr}^{v2x} = P_{arr,H}^{v2x} + P_{arr,D}^{v2x} P_{qe,H}^{v2x} + P_{arr,C}^{v2x} P_{qe,H}^{v2x} P_{qe,D}^{v2x} + P_{arr,M}^{v2x} \prod_{n\in\{H,D,C\}} P_{qe,n}^{v2x}.$$

4.3.2 Queue Models

Next, we focus on the dependencies among the queue models and the DTMCs for the MAC layer operations, which are the probabilities of the queues being empty. These values can be obtained through the steady-state probability of the zeroth state in each queue, and can be written as

$$\pi_{0,l}^k = \left[1 + \alpha_{1,l}^k \left(\frac{1 - (\beta_l^k)^{-Q^{\max}} (\alpha_l^k)^{Q^{\max}}}{\beta_l^k - \alpha_l^k}\right)\right]^{-1} = P_{qe,l}^k,$$

for $l \in \{H, D, C, M\}$ and $k \in \{11p, v2x\}$. The queue empty probability of the resultant queue in C-V2X Mode 4 is given by $P_{qe}^{v2x} = \prod_{l\in\{H,D,C,M\}} P_{qe,l}^{v2x}$.

4.3.3 Models for the MAC Layer Operations

The transmission probabilities introduce the dependencies between the DTMCs modeling the MAC layer operations and their associated generator models. Further evaluation of these parameters requires the steady-state solutions and the transition probabilities of the DTMCs modeling the MAC layer operations. The steady-state solutions of the DTMCs modeling the different ACs in IEEE 802.11p are presented in Appendix 4.7.1. With regards to the transition probabilities in Figure 4.4, it is not hard to show that

$$\begin{aligned}
\Phi_{vo} &= [1-(1-P^{11p}_{arr,H})P^{11p}_{qe,H}],\\
\Phi_{vi} &= [1-(1-P^{11p}_{arr,D})P^{11p}_{qe,D}],\\
\Phi_{be} &= [1-(1-P^{11p}_{arr,C})P^{11p}_{qe,C}],\\
\Phi_{bk} &= [1-(1-P^{11p}_{arr,M})P^{11p}_{qe,M}].
\end{aligned}$$

These values can be computed utilizing the dependency parameters from the queue and generator models. Moreover, we consider

$$\hat{\theta}_{s,i} \approx 1-\left[\prod_{i\in\mathcal{AC}}(1-\pi_{T_i,1})\right]^{N-1}+\sum_{k\in\mathcal{AC}\setminus\{i\}}(\pi_{T_k,1})$$

and

$$\hat{\theta}_{o,i} \approx 1-\Big[\prod_{i\in\mathcal{AC}}\left(1-\sum_{j=1}^{\vartheta}\pi_{T_i,j}\right)\Big]^{N-1}+\Big[\sum_{k\in\mathcal{AC}\setminus\{i\}}\sum_{j=1}^{\vartheta}(\pi_{T_k,j})\Big],$$

which can be used subsequently to obtain expressions for θ_i for $i \in \mathcal{AC}$. For an example,

$$\theta_{vo}=\left(\sum_{i\in\mathcal{AC}}\hat{\theta}_{s,i}\right)\left(\pi_{A^{\Omega_{vo}}_{vo}}+\pi_{I_{vo},0}\right)/\Big[4\sum_{i\in\mathcal{AC}}\left(\pi_{A^{\Omega_i}_{i}}+\pi_{I_i,0}\right)\Big].$$

With these transition probabilities, the transmit probability of each packet type can be obtained by summing the steady-state probabilities of the transmit states of the appropriate AC, *i.e.*, $P^{11p}_{t,l}=\sum_{j=1}^{\vartheta}\pi_{T_i,j}$ for $l \in \{H, D, C, M\}$, where index i represents the appropriate AC such that $i \in \mathcal{AC}$.

A similar approach can be used to obtain an expression for P^{v2x}_t. Firstly, the transition probabilities can be calculated utilizing the dependency parameters from the queue and generator models. Then, the probability of transmission op-

portunity can be found by summing the steady state probabilities of the transmit states, *i.e.*, $P_{txo} = \sum_{j=1}^{R_h} \pi_{j,0}$, where the expressions for the steady-state probabilities are listed in Appendix 4.7.1. Finally, we have $P_t^{v2x} = P_{txo} \times P_{qne}^{v2x}$.

4.4 Performance Analysis

This section focuses on deriving expressions for few key performance metrics at the MAC layer.

4.4.1 Average Delay

Firstly, we focus on the average delay between generation and transmission. The delay value captures the waiting time in the queue (queuing delay), and the delay in accessing radio resources (access delay). This can be calculated through the cycle time of the DTMCs modeling the MAC layer operations, and the steady-state probabilities of the DTMCs modeling the queues. We present expressions for the average delay through the following lemma.

Lemma 5. *Let index $i \in \mathcal{AC}$ represent the respective AC for $l \in \{H, D, C, M\}$. The average delay for multi-priority data streams in IEEE 802.11p is given by*

$$d_{avg,l}^{11p} = aSlotTime[(1 - \pi_{idle_i})/\pi_{T_i,1} + \vartheta - 1] \sum_{j=0}^{Q^{\max}} (j+1)\pi_{j,l}^{11p}.$$

For C-V2X Mode 4, it is given by

$$d_{avg,l}^{v2x} = \sum_{j=1}^{Q^{\max}} \frac{2j-1}{2P_{txo}} \pi_{j,l}^{v2x}/(1 - P_{qe,l}^{v2x}).$$

Proof. See Appendix 4.7.2. □

4.4.2 Probability of Collision

According to the IEEE 802.11p standard, a collision occurs when two or more vehicles initiate their transmission simultaneously, or two or more data streams of a given vehicle initiate the transmission simultaneously (self-collision). On the other hand, a collision occurs in C-V2X Mode 4 due to an overlap in the selection windows of nearby vehicles, as explained in Chapter 3. The overlap may lead to them choosing the same CSR for transmission. The expressions for collision probability are as follows.

Lemma 6. *The collision probability of IEEE 802.11p and C-V2X Mode 4 are given by*

$$P_{col}^{11p} = 2 - \left[\prod_{i\in\mathcal{AC}}(1-\pi_{T_i,1})\right]^{N} - N\sum_{i\in\mathcal{AC}}(\pi_{T_i,1}\theta_i)\left[\prod_{j\in\mathcal{AC}}(1-\pi_{T_j,1})\right]^{N-1} - \left[\prod_{i\in\mathcal{AC}}(1-\pi_{T_i,1})\right] - \sum_{i\in\mathcal{AC}}\pi_{T_i,1}\prod_{j\in\mathcal{AC}\setminus\{i\}}(1-\pi_{T_j,1})$$

and

$$P_{col}^{v2x} \approx 1 - \left[1 - \left[1 - \prod_{j=0}^{\Gamma-1}\left(1 - \frac{\pi_{1,0}}{1-j\pi_{1,0}}\right)\right]\frac{(1-P_{rk})}{(CSR_{tot,\Gamma} - N + 1)}\right]^{N-1},$$

respectively.

Proof. See Appendix 4.7.2. □

4.4.3 Average Channel Utilization and Throughput

The average channel utilization is the fraction of time any available channel resource is used for transmission by at least one vehicle. The channel resource is the shared channel in IEEE 802.11p and any CSR in C-V2X Mode 4. In IEEE 802.11p, the channel utilization captures the probability of at least one vehicle transmitting, thus it can be written as

$$CU_{avg}^{11p} = 1 - \left[\prod_{i\in\mathcal{AC}}(1 - \sum_{j=1}^{\vartheta}\pi_{T_i,j})\right]^{N}.$$

Moreover, the total throughput is the product of the bandwidth of the CCH and the probability of exactly one vehicle transmitting, which is given by

$$TP^{11p} = \textit{Bandwidth of CCH} \times N\sum_{i\in\mathcal{AC}}\left(\sum_{j=1}^{\vartheta}\pi_{T_i,j}\theta_i\right)\left[\prod_{i\in\mathcal{AC}}(1 - \sum_{j=1}^{\vartheta}\pi_{T_i,j})\right]^{(N-1)}.$$

For C-V2X Mode 4, we are interested in finding the average channel utilization within a single subframe. Therefore, channel utilization is normalized by $CSR_{tot,\Gamma}/\Gamma$, which is the total number of CSRs per subframe. Thus, the average channel utilization can be written as

$$CU_{avg}^{v2x} = P_t^{v2x}N(1 - P_{col}^{v2x})/[\textit{CSRs per Subframe}].$$

Moreover, the throughput can be written as

$$TP^{v2x} = \textit{Channel Bandwidth} \times CU_{avg}^{v2x}.$$

4.5 Numerical Results and Discussion

In this section, we present numerical results to compare the MAC layer performance of IEEE 802.11p and C-V2X Mode 4 in the presence of concurrent multi-priority data streams. The reference packet formats of HPD, DENM, CAM, and MHD are set according to [84, 85]. We set $T_H = 100$ ms and $K_H = 8$ for HPD, and $T_D = 500$ ms and $K_D = 5$ for DENM, to capture the difference in priority levels [85]. The standard in fact allows the vehicle to choose T_i and K_i, $i \in \{H, D\}$, based on the severity of the event. Moreover, we consider T_C to be between 100 ms and 1 s [84], and we set $K_M = 1$. Adjusting T_C dynamically according to network performance is termed as adaptive CAM rate. The value of λ_m, for $m \in \{H, D, M\}$, is set at 0.1 packets/s, by considering the example use case scenarios in [67]. For the purpose of maintaining $P_{sch} = 1$, we have $N_{m,20} = 400$, $N_{m,50} = 1000$ and $N_{m,100} = 2000$. We set $P_{rk} = 0.4$. In IEEE 802.11p, the CCH has a bandwidth of 10 MHz, and the transmission data rate is 6 Mbps [1]. C-V2X Mode 4 utilizes a channel bandwidth of 10 MHz with a transmission data rate of 20 Mbps [75].

Steady-state probabilities of the DTMCs are computed iteratively according to the flowcharts in Figs. 4.1a and 4.1b. For example, in IEEE 802.11p, we start solving the generator models sequentially according to their priority and then solve the queue models sequentially according to priority. Finally, we sequentially solve the AC models according to their precedence. This process is continued iteratively until the parameters converge. The rate of convergence was not found to be a bottleneck in the numerical evaluations, and all parameters in the models did exhibit fast convergence. For example, the values for $P_{qe,M}^{11p}$ and $P_{qe,M}^{v2x}$ converge after approximately 25 and 5 iterations, respectively, at $N = 50$. The convergence rate increases with N for IEEE 802.11p and reduces slightly in C-V2X Mode 4 with increasing N. It was also observed that the parameters of the C-V2X Mode 4 models converge faster than its counterpart.

The parameter values are used subsequently to calculate the performance measures introduced in Section 4.5, and we first compare the average delay. We validate the results obtained for IEEE 802.11p and C-V2X Mode 4 using simulation tools NS3 and Matlab, respectively. For the IEEE 802.11p model valida-

tion, we have used the NS3 code in [103], and we have modified it to support multi-priority packets and multiple queues. Then, we have obtained the data for validation through the simulation traces. For C-V2X Mode 4, we have first implemented the periodic and Poisson arrivals for packet generation. Then, we have used four arrays to model the queues of the generated packet types. The SPS algorithm is then implemented according to the standard [31], and the results are generated. Since C-V2X Mode 4 stems on a scheduling based access mechanism, a discrete-event simulator is not mandatory for the validation, and hence, we have resorted to a much simpler validation process using Matlab. For C-V2X Mode 4, we have first implemented the generation of HPD, DENM, and MHD packets by utilizing the inbuilt exponential random variable generation function of Matlab to ascertain the generation times. The CAM packets are generated periodically. Then we use four arrays to model the queues of the generated packet types. The SPS algorithm is then implemented according to the standard [31]. The code is executed for different values of N, and the performance parameters are appropriately averaged for validation of the models. In this validation process, we consider the parallel operation of all four data streams. The validation results are presented by considering the parallel operation of all four data streams. Please note that validation results for some curves have not been included as they affect the clarity of the figures.

4.5.1 Average delay

The average delay is calculated according to Lemma 5, and the results are illustrated in Figure 4.6. As discussed in Chapter 3, it is clear that IEEE 802.11p displays a lower average delay compared to C-V2X Mode 4, thanks to the relatively short $AIFS$ values when compared with the selection window sizes in C-V2X Mode 4. The figures clearly illustrate priority management, with the higher priority data streams experiencing lower average delays, in both technologies. In IEEE 802.11p, this is achieved by allocating lower $AIFS$ values and smaller contention window sizes for higher priority ACs, whereas in C-V2X Mode 4, this is achieved by giving preference to higher priority packets at every transmission opportunity.

In particular, Figure 4.6 illustrates the behavior of the average delay with N. We use the term *single stream* to refer to scenarios in which only one packet type is used for communication, as in [73, 75, 101], and the term *multiple streams* to refer to scenarios where the parallel operation of all four data streams is considered as per the models in this chapter. The plots clearly highlight the importance of

the motivation behind this work, as there is a large deviation, in particular for the lower priority packets. Figure 4.6a confirms the effectiveness of the EDCA mechanism in IEEE 802.11p [102]. According to ETSI standard [67], the maximum allowable latency in V2X communication is recommended to be less than 100 ms for most use cases. We can see that IEEE 802.11p satisfies this requirement on the average for packets of all priority levels, even in ultra-dense network settings. This is not the case with C-V2X Mode 4, as shown in Figure 4.6b. The lower priority data streams easily exceed this threshold value as soon as the network becomes dense. However, HPD and DENM packets, which have the most crucial latency constraints, satisfy the 100 ms delay constraints on the average, even in ultra-dense networks.

Being consistent with Chapter 3, it can be noted from Figure 4.6b that the average delay in C-V2X Mode 4 is mainly sensitive to Γ, exhibiting a step-wise increase when Γ switches from a shorter to a longer value. Increasing Γ reduces P_{txo}, which in turn increases $d^{v2x}_{avg,l}$ in Lemma 5. For the CAM and MHD curves, the average delay for the single stream is lower than multiple streams, which is rather intuitive. However, for HPD and DENM, we can observe the average delay slightly decreasing when switching from single to multiple streams. It has been shown in Chapter 3 that selecting new CSR values leads to a reduction in average delay compared to retaining the same CSR value. When considering multiple parallel data streams, there are more packets to transmit, thus the vehicle gets the chance to select new CSR values ($RC = 1$ condition) more frequently, which leads to this slight reduction. It is interesting to note that Figure 4.6b illustrates insignificant difference in average delay among data streams when $\Gamma = 20$ ms. Small values of Γ lead to frequent transmission opportunities, and negligible queue build up. This is not true when Γ is large, thus we can observe a significant variation in the queuing delays among the multi-priority data streams.

Note that the difference in the average delay between the highest (HPD) and the lowest (MHD) priority data streams is higher in C-V2X Mode 4 compared to IEEE 802.11p. Thus, IEEE 802.11p can be considered to be fairer among multi-priority data steams with regards to average delay. The ETSI ITS-G5 decentralized congestion control (DCC) algorithm for IEEE 802.11p proposes regulating T_C according to the utilization of the channel for congestion control. To this end, T_C can be increased to reduce the congestion. The reduction in congestion in turn further reduces the delay in all data streams as shown in Figure 4.6c. There is no built-in technique to control T_C in C-V2X Mode 4 adaptively. This is an interesting avenue that can be further explored in future releases of

C-V2X Mode 4.

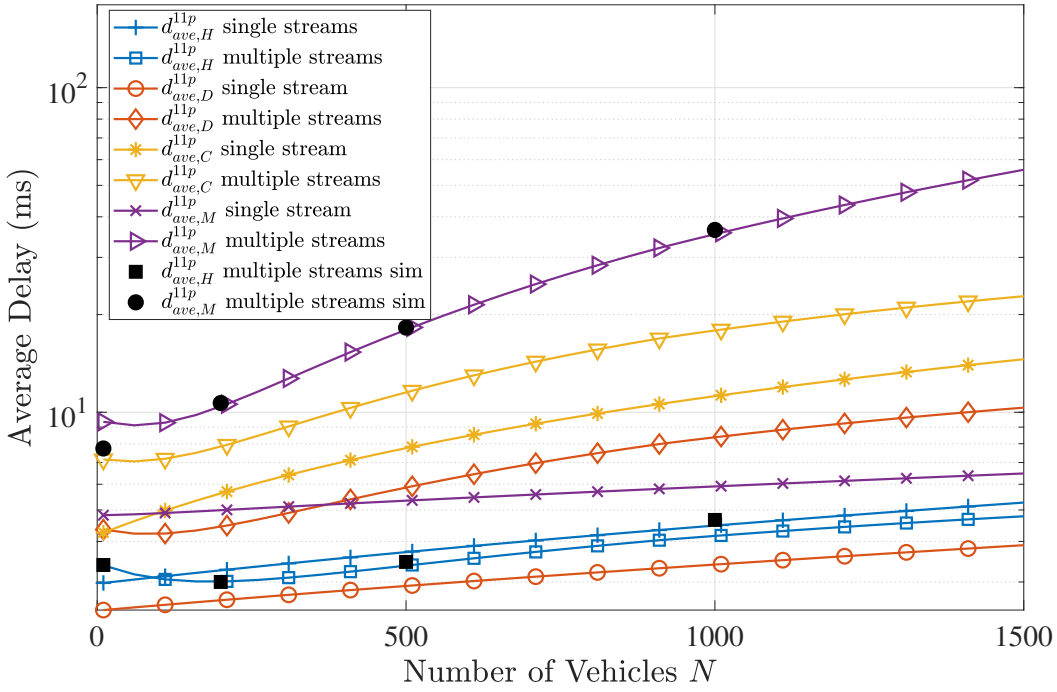

(a) IEEE 802.11p, where $T_C = 100$.

Figure 4.6: The behavior of the average delay with N.

4.5.2 Collision probability

The collision probability is calculated according to Lemma 6, and the results are illustrated in Figure 4.7. The collision probability obviously increases with N. However, it is interesting to note that C-V2X Mode 4 experiences a lower collision probability than IEEE 802.11p. This implies that the SPS algorithm is superior for collision resolution compared to its contention-based counterpart. Adaptive CAM rate leads to a marginal improvement in the collision probability of IEEE 802.11p, but it is still comparatively high for $N > 300$. The observations imply that C-V2X Mode 4 is the preferable choice for ultra-reliable communications.

The behavior of the collision probability of IEEE 802.11p with N is illustrated in Figure 4.7a. The figure also highlights the significance of the motivation behind this work, as there is a considerable deviation between the single and parallel multiple streams. The collision probabilities are expected to increase further with increasing packet generation rates. The equivalent results for C-V2X Mode 4 are illustrated in Figure 4.7b. We can observe the collision probability increasing

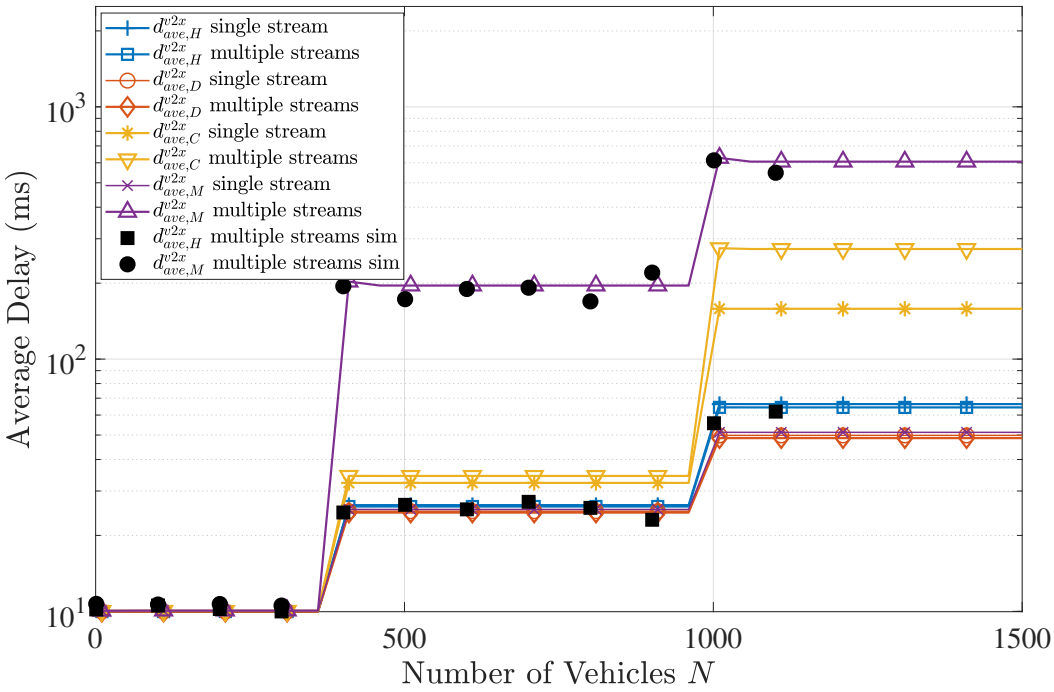

(b) C-V2X Mode 4, where $T_C = 100$.

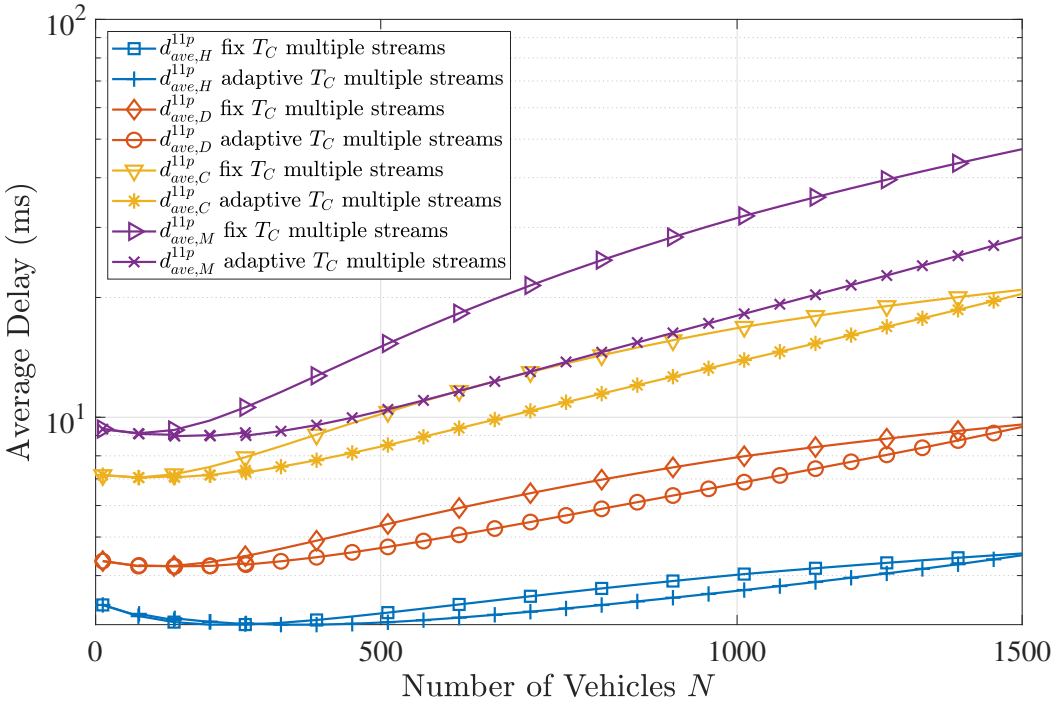

(c) IEEE 802.11p with adaptive CAM rates.

Figure 4.6: The behavior of the average delay with N (Cont.).

exponentially with N. When considering the single stream operations, there is no major variation among the collision probabilities of the four packet types. A similar observation can be made when comparing with parallel multiple streams. Thus, only two curves are presented for clarity. The minor variations are due to C-V2X Mode 4 using a schedule-based access mechanism. We note that Γ has a significant impact on the collision probability. When Γ is increased to preserve $P_{sch} = 1$, *i.e.*, at $N = 400$ and $N = 1000$, the collision probability reduces significantly, as $CSR_{tot,\Gamma}$ increases when a vehicle switches from a shorter to a longer selection window. The overall curve can be shifted down further if we reduce the values of N at which the selection window switches, *e.g.,* we switch it at $N = 300$ and $N = 800$. However, we should note that this in turn increases the average delay, thus, there is a clear trade-off. Therefore, the selection of these thresholds should be made by considering the QoS requirements of the V2X communication applications [67].

4.5.3 Throughput and Channel Utilization

The behavior of the throughput with N is illustrated in Figure 4.8. In IEEE 802.11p, we can observe that the throughput increases with N first, which is rather intuitive. However, when more vehicles contend for transmission simultaneously, the delay and the collisions increase, and hence, the throughput starts to decline. Although not seen in the figure, the curve for S_M^{11p} single stream tends to decrease at large N values as well. Due to having no repetitions, MHD has the lowest transmit rate, hence the lowest number of collisions. Thus, the value of N at which the collisions and the delay start dominating the throughput is comparatively large ($N \approx 3500$) for MHD. The value of N at which the declining stage begins reduces when the data rates increase, which is expected. This can be observed by comparing the single stream operations with the parallel multiple streams, which has more frequent packet transmissions and higher collision probability (see Figure 4.7a). The collisions also lead to lower throughput per vehicle when parallel multi-priority data streams are used for communication. Since we consider broadcast packets, the calculated average delay values in this chapter only capture the latency from packet generation to packet transmission, and not till successful packet reception. Hence, the probability of collision plays an important role in the performance of the protocols. For example, Figure 4.7a clearly exhibits that a small change in collision probability has a huge impact on the overall performance in terms of throughput. We can also observe that the throughput decreases further with the use of adaptive CAM rates. Adaptive

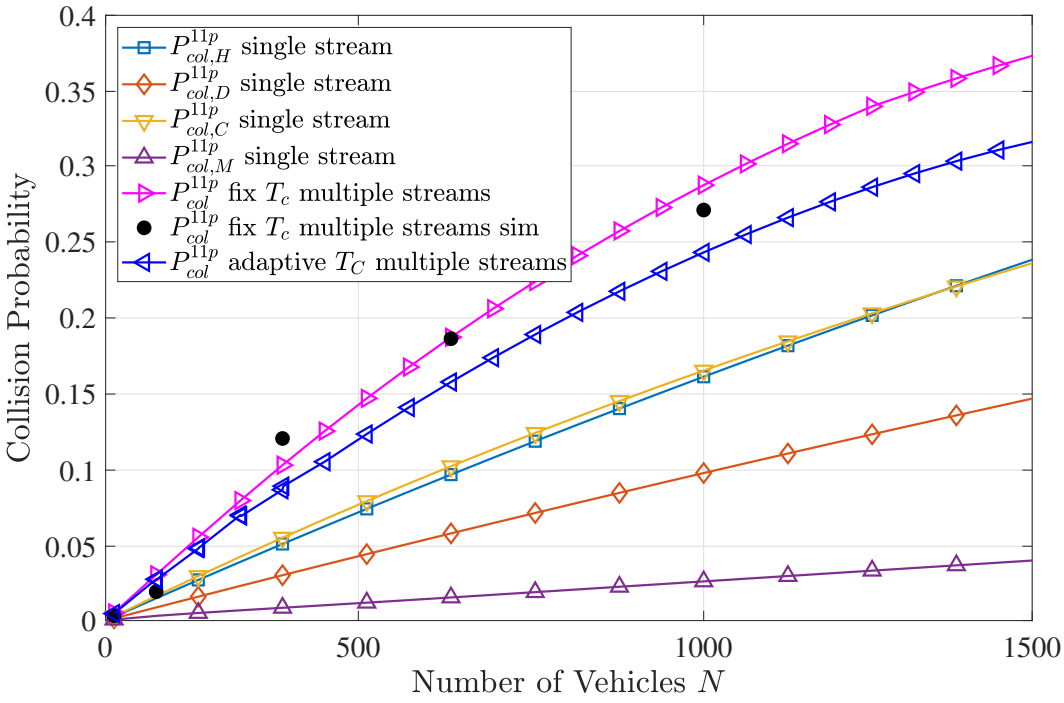

(a) IEEE 802.11p.

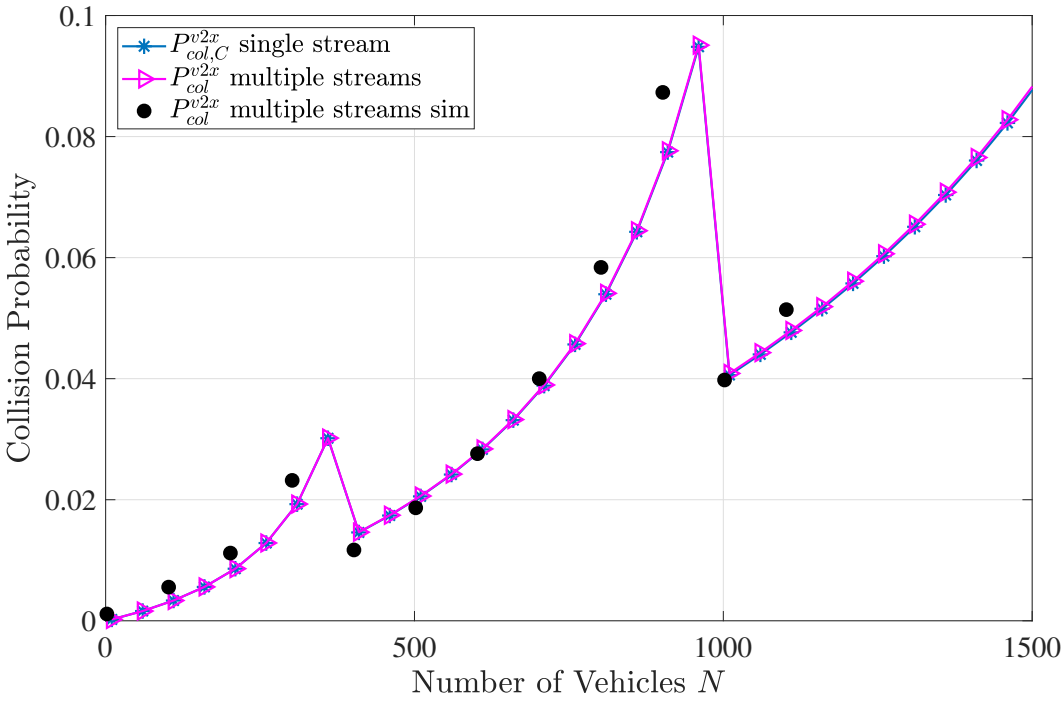

(b) C-V2X Mode 4.

Figure 4.7: The behavior of the collision probability with N, where $T_C = 100$ ms.

CAM reduces the CAM packet generation rate when the channel is congested, which in turn decreases the throughput.

On the other hand, in C-V2X Mode 4, we can observe that the throughput increases with N, with a sudden reduction when the vehicle switches from a shorter to a longer selection window size. This is due to the reduction in P_{txo}, which is proportional to P_t^{v2x}. It is interesting to note that the parallel multiple stream scenario of C-V2X Mode 4 exhibits higher throughput compared to the single stream operations, unlike IEEE 802.11p. The following can be used to explain this behavior. The collision probability in the scheduling based C-V2X Mode 4 is the same regardless of single or multiple streams. Therefore, multiple streams lead to higher throughput for C-V2X. On the other hand, multiple streams exhibit a higher collision probability compared to a single stream in contention based IEEE 802.11p. Therefore, there is a trade-off between higher number of packets and packet collisions. The collisions dominate, which leads to a single stream exhibiting superior performance compared to multiple streams in terms of throughput. Thus, it can be noted that C-V2X Mode 4 manages multi-priority data streams in a better manner with regards to throughput, when compared with IEEE 802.11p.

The behavior of the channel utilization with N is illustrated in Figure 4.9. The parallel operation of multiple streams depict higher channel utilization for both technologies. This implies that in an actual network, the channel is well utilized by both of these technologies, with C-V2X Mode 4 having a slightly lower utilization, comparatively. We can observe the channel utilization varying with adaptive CAM rates and with selection window sizes. The behavior can be explained using the same reasons provided for the throughput.

4.6 Conclusions

This chapter has presented analytical models for the MAC layer operations of ITS-G5 IEEE 802.11p and C-V2X Mode 4, considering four concurrent multi-priority data streams. Four DTMC-based traffic generators have been used to generate the HPD, DENM, CAM, and MHD packets. The packet generation parameters for each type of data stream have been selected according to ETSI standards. Four device-level queue models have been used to feed the generated multi-priority packets to the DTMCs modeling the MAC layer operations. The steady-state probabilities of the models have been utilized to derive expressions for key performance indicators at the MAC layer, which includes the average de-

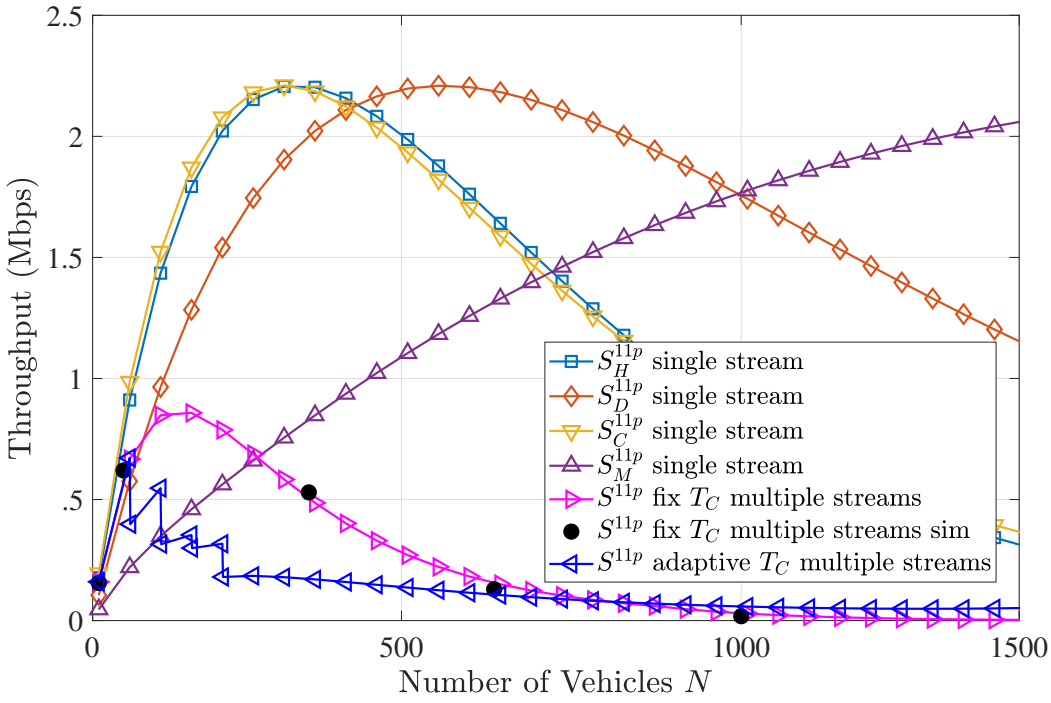

(a) IEEE 802.11p.

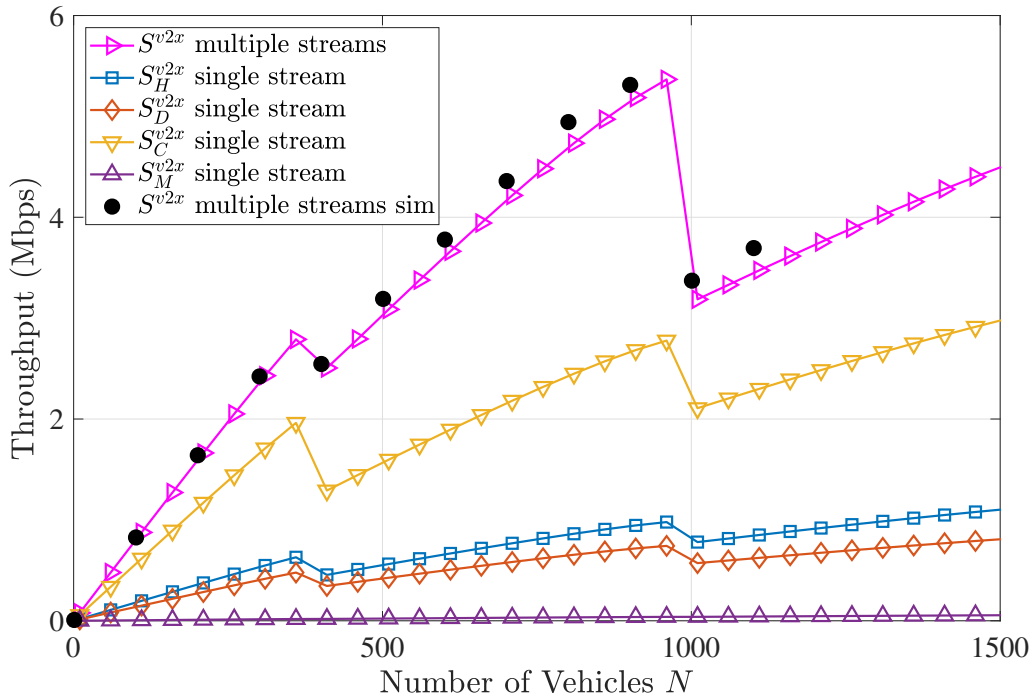

(b) C-V2X Mode 4.

Figure 4.8: The behavior of the throughput with N, where $T_C = 100$ ms.

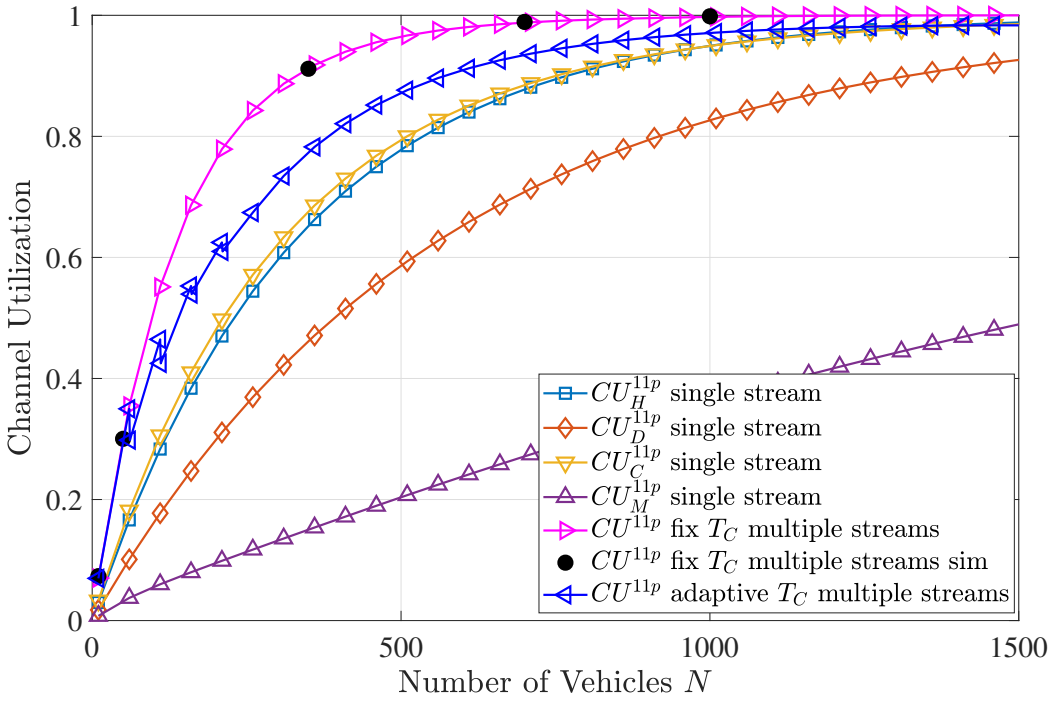

(a) IEEE 802.11p.

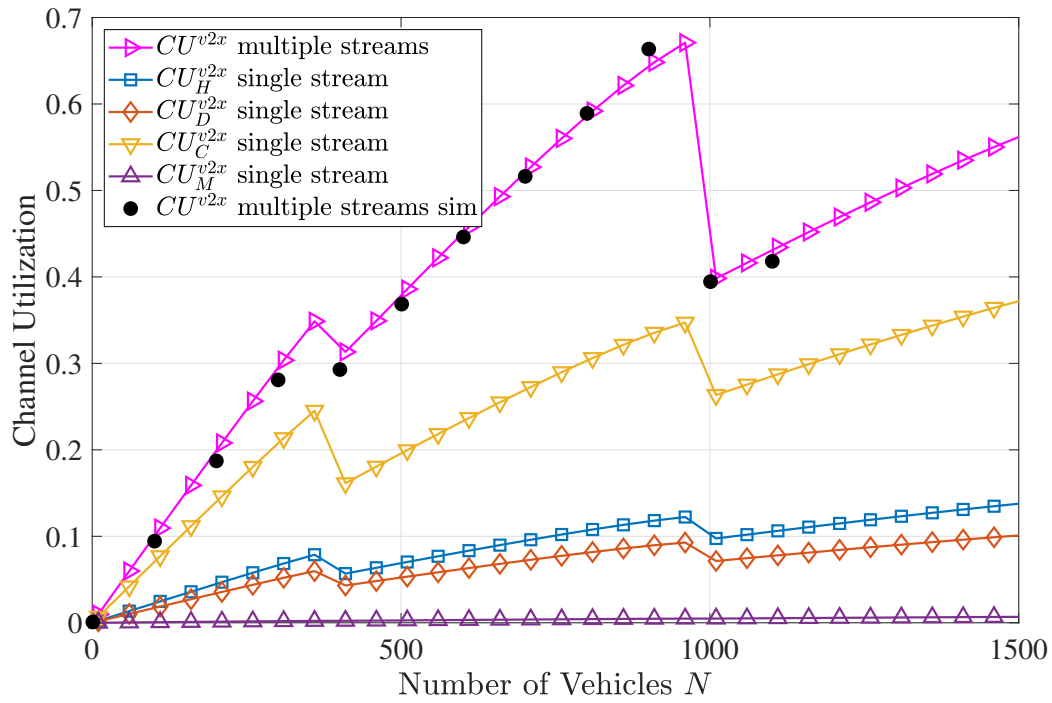

(b) C-V2X Mode 4.

Figure 4.9: The behavior of the channel utilization with N, where $T_C = 100$ ms.

lay, collision probability, throughput, and channel utilization. Numerical examples have been presented for further insights. The results have firstly highlighted the importance of considering all four parallel data streams when studying the MAC layer performance of the two technologies. Priority management is implemented successfully in both technologies, but it can be seen that IEEE 802.11p treats multi-priority data streams more fairly compared to its counterpart, thanks to its inbuilt EDCA mechanism. IEEE 802.11p is also superior in average delay, but C-V2X Mode 4 exhibits better performance in terms of collision resolution, in turn leading to higher throughput values as well. Further insights have been presented on the possible improvements of both technologies.

4.7 Appendix

4.7.1 The Steady-state Solutions for the DTMCs

Generator Models

For $i \in \{H, D\}$ and $k \in \{11p, v2x\}$, we have

$$\pi^k_{i,(tx,0)} = \Big[T_i\Big(1-\frac{1}{K_i}\Big)\Big[1-\mathcal{P}^k_i\left(1-\mathcal{P}^k_i\right)^{T_i-1}\Big]\Big[1-\left(1-\mathcal{P}^k_i\right)^{T_i-1}\Big]^{-1}+1/K_i+\big[K_i(1-e^{-\lambda_i\tilde{T}})\big]^{-1}\Big]^{-1},$$

$$\pi^k_{i,(tx,j)} = \mathcal{P}^k_i\Big[\big(1-\frac{1}{K_i}\big)\pi^k_{i,(tx,0)} + \sum_{m=j+1}^{T_i-1}\pi^k_{i,(tx',m)}\Big] \text{ for } j \in [1, T_i-2],$$

$$\pi^k_{i,(tx,T_i-1)} = \pi^k_{i,(tx,0)}\Big(1-\frac{1}{K_i}\Big)\mathcal{P}^k_i,$$

$$\pi^k_{i,(tx',j)} = \pi^k_{i,(tx,0)}\Big(1-\frac{1}{K_i}\Big)\Big(1-\mathcal{P}^k_i\Big)^{T_i-j}\Big[1-(1-\mathcal{P}^k_i)^{T_i-1}\Big]^{-1} \text{ for } j \in [0, T_i-1].$$

For the CAM generator, for $k \in \{11p, v2x\}$,

$$\pi^k_{C,(tx,0)} = [1-(1-\mathcal{P}^k_C)^{T_C-1}]\big[T_C\big[1-\mathcal{P}^k_C(1-\mathcal{P}^k_C)^{T_C-1}\big]\big]^{-1},$$

$$\pi^k_{C,(tx,j)} = \mathcal{P}^k_C\big(\pi^k_{C,(tx,0)} + \sum_{m=j+1}^{T_C-1}\pi^k_{C,(tx',m)}\big) \text{ for} j \in [1, T_C-2],$$

$$\pi^k_{C,(tx,T_C-1)} = \pi^k_{C,(tx,0)}\mathcal{P}^k_C,$$

$$\pi^k_{C,(tx',j)} = \pi^k_{C,(tx,0)}[(1-\mathcal{P}^k_C)^{T_C-j}][1-(1-\mathcal{P}^k_C)^{T_C-1}]^{-1} \text{ for } j \in [0, T_C-1].$$

IEEE 802.11p ACs Models

Steady-state Solutions for the States Common to All ACs:
For $i \in \mathcal{AC}$,

$$\pi_{A^j_i} = \pi_{idle_i}\Phi_i \text{ for } j = 1,$$

$$\pi_{A^j_i} = \pi_{idle_i}\Phi_i\left(1-\hat{\theta}_{o,i}\right)\left(1-\hat{\theta}_{s,i}\right)^{(j-2)} \text{ for } j\in[2, (\Omega_i-1)],$$

$$\pi_{I_i,j} = \pi_{B_{vo},\vartheta}(C_{vo}-j)/\left[C_{vo}\left(1-\hat{\theta}_{s,i}\right)\right] \text{ for } j \in [0, (C_{vo}-1)],$$

$$\pi_{B_i,j} = \pi_{Idle_i}\Phi_i\Big[j\frac{\hat{\theta}_{o,i}}{\vartheta} + \left(1-\hat{\theta}_{o,i}\right)\left[1-\left(1-\hat{\theta}_{s,i}\right)^{\Omega_i-1}\right]\Big],$$

$$\pi_{T_i,j} = \pi_{Idle_i}\Phi_i \text{ for } j \in [1, \vartheta].$$

Steady-state Solutions for States Specific to AC_{vo}:

$$\pi_{\Delta^b_{vo},j}=\pi_{B_{vo},\vartheta}\left(C_{vo}-k\right)\hat{\theta}_{s,vo}/\left[C_{vo}\left(1-\hat{\theta}_{s,vo}\right)\right] \text{ for } b\in[0,(C_{vo}-1)],\, j\in[1,\vartheta].$$

$$\pi_{b,A^j_{vo}}=\pi_{B_{vo},\vartheta}\left[1+\left(C_{vo}-b-1\right)\hat{\theta}_{s,vo}\right]/\left[C_{vo}\left(1-\hat{\theta}_{s,vo}\right)\right] \text{ for } j\in[1,(\Omega_{bk}-8)],$$

$$b\in[2,(C_{vo}-1)],$$

$$\pi_{b,A^j_{vo}}=\pi_{B_{vo},\vartheta}(2-2\hat{\theta}_{s,vo}+C_{vo}\hat{\theta}_{s,vo})/\left[C_{vo}(1-\hat{\theta}_{s,vo})\right] \text{for } b=0.$$

Steady-state Solutions for States Specific to AC_{vi}:

For $j\in[1,\vartheta]$,

$$\pi_{\Delta^b_{vi},j}=\pi_{B_{vi},\vartheta}[\theta_{vo}+\left(C_{vi}-b-\theta_{vo}\right)\hat{\theta}_{s,vi}]/\left[C_{vi}(1-\theta_{vo})(1-\hat{\theta}_{s,vi})\right]$$

$$\text{for } b\in[2,(C_{vi}-1)],$$

$$\pi_{\Delta^b_{vi},j}=\pi_{B_{vi},\vartheta}[2\theta_{vo}+(C_{vi}-2\theta_{vo})\hat{\theta}_{s,vi}]/\left[C_{vi}\left(1-\theta_{vo}\right)\left(1-\hat{\theta}_{s,vi}\right)\right] \text{ for } b=0.$$

For $j\in[1,(\Omega_{bk}-7)]$,

$$\pi_{b,A^j_{vi}}=\pi_{B_{vi},\vartheta}[1+(C_{vi}-b-1)\hat{\theta}_{s,vi}]/\left[C_{vi}(1-\hat{\theta}_{s,vi})\left(1-\theta_{vo}\right)\right]$$

$$\text{for } b\in[2,(C_{vi}-1)],$$

$$\pi_{b,A^j_{vi}}=\pi_{B_{vi},\vartheta}\left(2-2\hat{\theta}_{s,vi}+C_{vi}\hat{\theta}_{s,vi}\right)\left[C_{vi}\left(1-\hat{\theta}_{s,vi}\right)(1-\theta_{vo})\right] \text{ for } b=0.$$

Steady-state Solutions for States Specific to AC_{be}:

For $j\in[1,\vartheta]$, $G_1=\theta_{vo}+(1-\theta_{vo})\left[1-(1-\theta_{vo}-\theta_{vi})^3(1-\hat{\theta}_{s,be})\right]$,

$$\pi_{\Delta^b_{be},j}=\left[G_1+(C_{be}-b-1)\hat{\theta}_{s,be}\right]/\left[C_{be}(1-\theta_{vo})(1-\theta_{vo}-\theta_{vi})^3(1-\hat{\theta}_{s,be})\right]$$

$$\text{for } b\in[2,(C_{be}-1)],$$

$$\pi_{\Delta^b_{be},j}=\left[2G_1+\left(C_{be}-2\right)\hat{\theta}_{s,be}\right]/\left[C_{be}\left(1-\theta_{vo}\right)\left(1-\theta_{vo}-\theta_{vi}\right)^3(1-\hat{\theta}_{s,be})\right] \text{ for } b=0.$$

For $j\in[1,(\Omega_{bk}-1)]$, $G_2(b)=\pi_{B_{be},\vartheta}[1+(C_{be}-b-1)\hat{\theta}_{s,be}]/\left[C_{be}\left(1-\hat{\theta}_{s,be}\right)(1-\theta_{vo})(1-\theta_{vo}-\theta_{vi})^3\right]$,

$$f_1(j)=\begin{cases}1/(1-\theta_{vo}) \text{ for } j\in[1,(\Omega_{bk}-4)]\\ (1-\theta_{vo}-\theta_{vi})^b \text{ for } j=(\Omega_{bk}-3+b) \text{ and } b\in\{0,1,2\}\end{cases}.$$

$$\pi_{b,A^j_{be}}=G_2(b)f_1(j)(1-\theta_{vo}) \text{ for } b\in[2,C_{be}-1],$$

$$\pi_{b,A^j_{be}}=G_2(b)[2+(C_{be}-2)\hat{\theta}_{s,be}]/[1+(C_{be}-b-1)\hat{\theta}_{s,be}] \text{ for } b=0.$$

Steady-state Solutions for States Specific to AC_{bk}:
For $j \in [1, \vartheta]$, $G_3 = \theta_{vo}+(1-\theta_{vo})\big[1-(1-\theta_{vo}-\theta_{vi})^3[(1-\sum_{l\in\mathcal{AC}\setminus\{bk\}}\theta_l)^3+(1-\hat{\theta}_{s,bk})]\big]$,

$$\pi_{\Delta^b_{bk},j}=[G_3+(C_{bk}-b-1)\hat{\theta}_{s,bk}]/\Big[C_{bk}(1-\theta_{vo}(1-\theta_{vo}-\theta_{vi})^3(1-\sum_{l\in\mathcal{AC}\setminus\{bk\}}\theta_l)^3$$

$(1-\hat{\theta}_{s,bk})\Big]$ for $b \in [2,(C_{bk}-1)]$,

$\pi_{\Delta^b_{bk},j} = \Big[2G_3+(C_{bk}-2)\hat{\theta}_{s,bk}\Big]/[C_{bk}(1-\theta_{vo})(1-\theta_{vo}-\theta_{vi})^3(1-\theta_{vo}-\theta_{vi}-\theta_{be})^3$
$(1-\hat{\theta}_{s,bk})]$ for b=0.

For $j \in [1,(\Omega_{bk}-1)], G_4(b) = \pi_{B_{bk},\vartheta}[1+(C_{bk}-b-1)\,\hat{\theta}_{s,bk}]/[C_{bk}(1-\hat{\theta}_{s,bk})(1-\theta_{vo})(1-\theta_{vo}-\theta_{vi})^3(1-\sum_{l\in\mathcal{AC}\setminus\{bk\}}\theta_l)^3]$,

$$f_2(j)=\begin{cases}1/(1-\theta_{vo}) \text{ for } j\in[1,(\Omega_{bk}-7)]\\ (1-\theta_{vo}-\theta_{vi})^b \text{ for } j=(\Omega_{bk}-6+b) \text{ and } b\in\{0,1,2,3\}\\ (1-\theta_{vo}-\theta_{vi})^3(1-\theta_{vo}-\theta_{vi}-\theta_{be})^{b+1} \text{ for } j=(\Omega_{bk}-2+b) \text{ and } b\in\{0,1\}\end{cases}.$$

$\pi_{b,A^j_{bk}} = G_4(b)\times f_2(j)$ for $b\in[2,C_{bk}-1]$,
$\pi_{b,A^j_{bk}} = f_2(j)(1-\theta_{vo})G_4(b)[2+(C_{bk}-2)\hat{\theta}_{s,bk}]/\Big[1+(C_{bk}-b-1)\hat{\theta}_{s,bk}\Big]$ for $b=0$.

By using the sum of steady-state probabilities, and appropriately substituting the above derived steady-state probabilities, we can obtain π_{idle_i} for $i\in\mathcal{AC}$, which can then be used to calculate all steady-state probabilities of interest.

C-V2X Mode 4 Model

State$(Idle)$:

$$\pi_{Idle} = \gamma\pi_{w,0},$$

where $\gamma = (1-P_{rk})\big[(1/P_{sch})-1\big]\big[P^{v2x}_{arr}+P^{v2x}_{qne}\big(1-P_{arr}\big)\big]^{-1}$.
States (w,i) for $i\in[0,\Gamma-2]$:

$$\pi_{w,j} = \Big[1-\frac{j}{(\Gamma-1)}\Big]\Big[a\pi^{v2x}_{Idle}+(1-P_{rk})P_{sch}\pi_{1,0}P_{qne}\Big]+P_{rk}\pi_{1,0}P_{qne},$$

where $a = \big(P^{v2x}_{arr}+P^{v2x}_{qne}-P^{v2x}_{arr}P^{v2x}_{qne}\big)\,P_{sch}$.
States (i,j):

$$\pi_{i,j} = \pi_{w,0}(R_h-i+1)/\big[(P^{v2x}_{qne})^2(1+R_h-R_l)\big] \text{ for } i\in[R_l,R_h]\,,\ j\in[1,\Gamma-1]\,.$$

States $(i, 0)$:

$$\pi_{i,0} = \pi_{w,0}(R_h - i + 1)/\left[P_{qne}^{v2x}(1 + R_h - R_l)\right] \text{ for } i \in [R_l, R_h]\,.$$

States (i, j):

$$\pi_{i,j} = \pi_{w,0}/P_{qne}^{v2x}, \text{for } i \in [1, R_l - 1]\,,\ j \in [0, \Gamma - 1]\,.$$

Since the sum of probabilities is one, we have

$$\pi_{w,0} = \left[1 - \Gamma + \gamma + \left(\frac{\Gamma - 2}{2}\right)[a\gamma + 2P_{rk} + (1 - P_{rk})P_{sch}] + \left[\Gamma(R_h + R_l)/2P_{qne}^{v2x}\right]\right]^{-1}.$$

4.7.2 Performance Metric Derivations

Average Delay Derivations: Proof of Lemma 5

For AC_i, the cycle time of state $(T_i, 1)$ can be written as $aSlotTime/\pi_{T_i,1}$, which gives the average time taken to initiate two consecutive transmissions. We modify this cycle time by scaling it by $(1 - \pi_{idle_i})$, which eliminates the time spent at state $(idle_i)$ without any packets to transmit, as this cannot be considered to be a part of the delay. We add $(\vartheta - 1)aSlotTime$ to this value to account for the further time spent in transmission similar to Chapter 3. The delay will vary depending on the length of the queue. Since we are dealing with the average delay, we multiply by the resulting delay by the average queue length, which is given by $\sum_{j=0}^{Q^{\max}}(j + 1)\pi_{j,l}^{11p}$, where $\pi_{j,l}^{11p}$ is the steady state probability of state j of queue l. The proof for $d_{avg,l}^{v2x}$ can be obtained by following similar lines as in Chapter 3, thus omitted in this chapter due to space limitations.

Collision Probability Derivations: Proof of Lemma 6

According to the IEEE 802.11p standard, a collision occurs when multiple vehicles initiate their transmission simultaneously, or in the case of a self-collision. Firstly, by eliminating the probabilities of no vehicles initiating transmission or exactly one vehicle initiating transmission from the total probability, we get the probability of two or more vehicles initiating their transmission simultaneously. Then, we calculate the self-collision probability by considering a single vehicle, and eliminating the probabilities of no data transmission or exactly one data stream initiating transmission from the total probability. The summation of these two probabilities gives the expression for P_{col}^{11p}. The proof for P_{col}^{v2x} can be

obtained by following similar lines as in Chapter 3, thus omitted in this chapter due to space limitations.

Chapter 5

PERFORMANCE ENHANCEMENT OF C-V2X MODE 4 UTILIZING MULTIPLE CANDIDATE SINGLE-SUBFRAME RESOURCES

Prioritization of data streams in cellular vehicle-to-everything (C-V2X) may lead to unfavorable packet delays in low-priority streams. This chapter studies allocating multiple candidate single-subframe resources (CSRs) per vehicle as a solution. It proposes a methodology to determine the number of CSRs for each vehicle based on the total number of neighboring vehicles, and to assign the multiple data streams among them for simultaneous transmission. The numerical results highlight the achievable delay gains of the proposed approach, and its negligible impact on packet collisions.

5.1 Introduction

In Release 14, the 3GPP introduced C-V2X Mode 4 to support vehicular communications without the support of cellular infrastructure. Therein, the MAC layer plays a crucial role in handling stringent, but varying, delay and reliability constraints of different V2X applications. The variable delay constraints have necessitated the technologies to support multi-priority data streams [32]. In Chapter 4, it has been shown that in the presence of multi-priority data streams, the competing technology IEEE 802.11p [20] outperforms C-V2X Mode 4 in terms of delay and priority management, thanks to its EDCA mechanism. Thus, addressing this issue is of importance for C-V2X Mode 4, specifically in avoiding stale packets in lower priority data streams.

Limited work on enhancing the performance of C-V2X Mode 4 can be found in the literature. Performance enhancement through variations in the transmit power is studied in [83]. The work in [82] and [74] are more related, and they focus on spectrum management and the SPS algorithm. In C-V2X Mode 4, vehicles use the SPS algorithm in a distributed manner to sense the radio resources (called

candidate single-subframe resources (CSRs) utilized by other vehicles in a sensing window, and to select a CSR for its own transmission. To this end, [82] introduces a weighted power averaging methodology for sensing the CSRs in the sensing window. The authors of [74] show that re-selecting the same CSR used for the previous transmission (reusing) more frequently, and using exponential sensing window sizes under high channel load levels can lead to enhanced performance. Both works limit their study to a single data stream at each vehicle. Moreover, as the performance metric, they focus mainly on the packet reception ratio of C-V2X Mode 4, which is known to be superior compared to its competing technology in Chapter 4. Chapter 4 further highlight the lower channel utilization exhibited by C-V2X Mode 4, which we try to exploit to ameliorate the pressing concerns on delay and priority management.

In this chapter, we focus on multi-priority data streams, and study the possibility of enhancing the performance of C-V2X Mode 4 by allocating multiple CSRs for each vehicle, which in turn increases the channel utilization. The procedure leads to two fundamental problems.

- **Determining the number of CSRs for each vehicle:** We determine how many CSRs can be allocated to each vehicle based on the total number of vehicles in the system.
- **Allocating the multi-priority data streams among the CSRs:** Having established the number of CSRs, we introduce a procedure for allocating the multi-priority data streams among the allocated CSRs.

We evaluate the performance of the proposed method using the DTMC-based models in Chapter 4. The results show that the parallelism achieved by allocating multiple CSRs leads to significant reductions in the average delay, specially in the low priority data streams. In general, this is achieved by allocating separate CSRs for low priority data streams and allowing them more frequent transmission opportunities, opposed to waiting till all higher priority queues are empty. We can observe that the optimal group selection depends on the number of CSRs available and the generation rates of each data stream. It should be noted that increased packet collisions is the tradeoff of allocating multiple CSRs. However, since C-V2X Mode 4 inherently has superior collision resolution, the increase is incremental, and can be considered insignificant when compared with the perceived benefits in terms of delay and priority management.

The chapter is organized as follows. The system model is presented in Section 5.2. Section 5.3 studies the allocation of multiple CSRs to a vehicle. Section 5.4

presents the numerical results and the discussion, and Section 5.5 concludes the chapter.

5.2 System Model

We consider a network where the target vehicle has N neighbouring vehicles, and each vehicle transmits DENM, HPD, MHD and CAM. The priority order of serving these packets according to the standard is as follows: HPD > DENM > CAM > MHD. We use subscripts $i \in \mathcal{I} = \{H, D, C, M\}$ to differentiate between the parameters for HPD, DENM, CAM, and MHD, respectively. The CAM packets are generated periodically with a generation interval T_C. HPD, DENM, and MHD are randomly generated at an average generation rate of λ_m, for $m \in \mathcal{I} \setminus \{C\}$, based on events initiated by human activity or environmental conditions. Thus, the parameters related to packet generation can be written as $\mathcal{P} = \{\lambda_H, \lambda_D, \lambda_M, T_C\}$. The generated packets are queued separately, and transmitted according to their level of priority, based on the SPS algorithm. For the simplicity of the study, we assume that the packet generation rates are the same among all vehicles in the network [75]. Let n_{CSR} denote the number of CSRs allocated to each vehicle such that $n_{CSR} \in \{1, 2, 3, 4\}$ [1]. To this end, CSRs are adjacent sub-channel sets within the subframe that are large enough to fit in the SCI and the TB to be transmitted.

In Chapter 4, a similar setup is modeled using DTMCs for $n_{CSR} = 1$. The overall model in Chapter 4 consists of four separate DTMCs that model the generation of the packet types of interest, four DTMCs that model their device-level packet queues, and one DTMC that models the MAC layer operations related to the transmission. We directly resort to the modeling techniques and the derived performance measures in Chapter 4 to evaluate the performance achieved when $n_{CSR} \geq 1$. For a given CSR, $A \subset \mathcal{P}$, N, and Γ, which is called the selection window size in the SPS algorithm, act as the inputs to the model, as illustrated in Figure 5.1. A is based on the data streams allocated to that particular CSR, and the respective performance metrics which are functions of A act as the outputs of the model. To this end, we obtain the average delay of the l-th data stream $d_{avg,l}(A)$, for each $l \in B$, the collision probability $P_{col}(A)$, and the channel utilization $CU(A)$ as outputs, where $B \subset \mathcal{I}$ is the corresponding set of indices for A, *e.g.*, $A = \{\lambda_H, T_c\} \rightarrow B = \{H, C\}$.

[1] We have selected the maximum value of n_{CSR} to be four for simplicity as we consider four multi-priority data streams. Conceptually, more than four CSRs can be allocated to a vehicle given it has the necessary capabilities of handling the simultaneous transmissions.

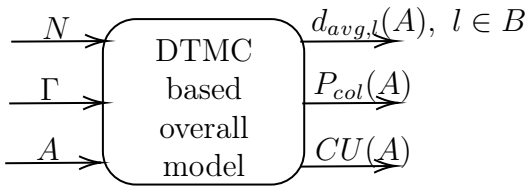

Figure 5.1: The DTMC based overall model for a given CSR based on the modeling techniques in Chapter 4.

We use an example scenario to further elaborate the inputs, outputs, and the usage of the DTMCs. Consider an example where two CSRs are used at each vehicle. Moreover, HPD and DENM data are allocated for the first CSR, and the other two data streams are allocated for the second, as illustrated in Figure 5.2. With regards to the first CSR, N, Γ, and $A = \{\lambda_H, \lambda_D\}$ act as the inputs, and $d_{avg,H}(\lambda_H, \lambda_D)$, $d_{avg,D}(\lambda_H, \lambda_D)$, $P_{col}(\lambda_H, \lambda_D)$ and $CU(\lambda_H, \lambda_D)$ act as the outputs. Further on the DTMCs, two DTMCs model the generation of HPD and DENM packets, and two DTMCs model their device-level packet queues. The priority management is incorporated in the queue models such that a resultant queue is connected with the next DTMC that models the transmission of these packets. The dependencies among these DTMCs are appropriately modeled according to Chapter 4, and illustrated in Figure 5.2. We obtain expressions for the steady state probabilities of the DTMCs and solve them iteratively until convergence is achieved. Upon convergence, the performance metrics are calculated using the steady state probabilities, which act as the outputs. A similar procedure is followed for the second CSR. It is not hard to see that the network performance depends on the number of CSRs used by each vehicle, and how the data streams are allocated among the CSRs. This is the main focus of the next section.

5.3 Allocation of Multiple CSRs to a Vehicle

Allocating multiple CSRs to a vehicle leads to two key fundamental questions. Firstly, we need to ascertain a plausible value for n_{CSR}. We assume $n_{CSR} \leq 4$ for simplicity, *i.e.*, we assume that multiple CSRs are not allocated to a single data stream. Secondly, given n_{CSR}, we need to decide how the four parallel data streams should be allocated among the n_{CSR} CSRs. In this section, we find solutions to these two questions based on the average delay, and present an algorithm for multiple CSR allocation for a vehicle.

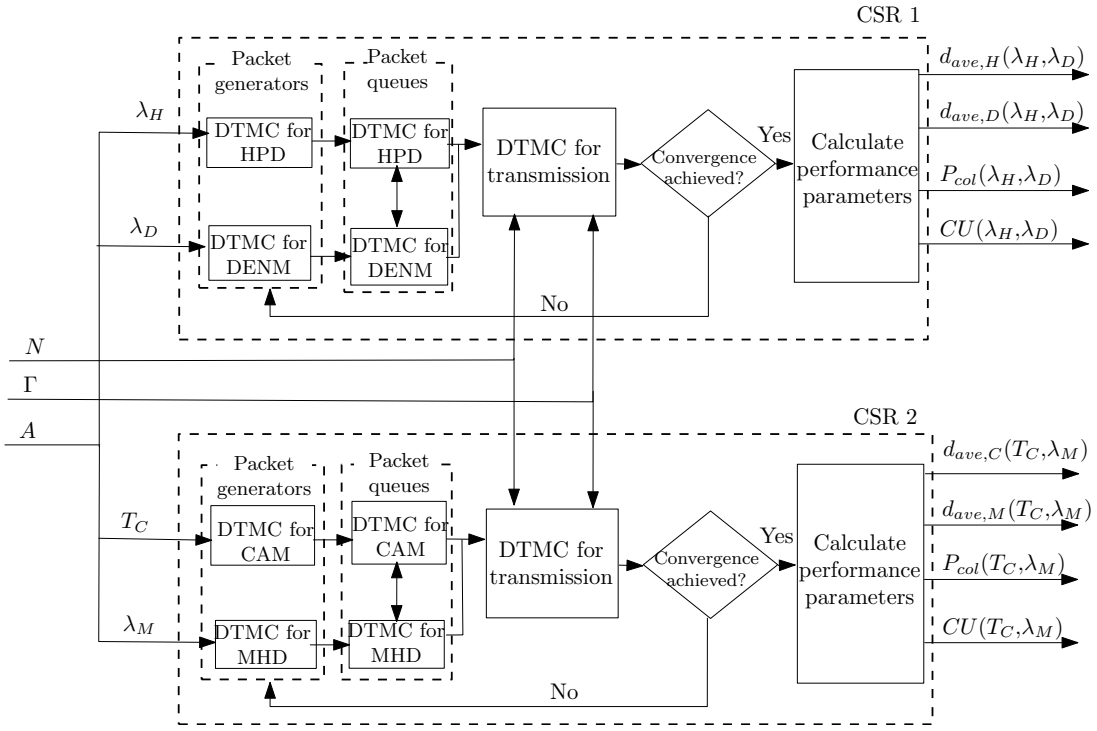

Figure 5.2: A diagram illustrating the overall model for an example scenario where $n_{CSR} = 2$.

5.3.1 Determining the Number of CSRs

It is rather intuitive that n_{CSR} is inversely proportional to N. Also, N has a direct impact on the length of the selection window Γ, which is defined as the maximum latency in ms [30], and should be set at either 20 ms, 50 ms or 100 ms according to the standard [86]. Increasing Γ increases the time gap between two successive transmissions, which in turn leads to more radio resources for the network. Thus, CSR_{tot} is proportional to Γ, where CSR_{tot} denotes the total number of available CSRs in the selection window. The standard allows allocating 80% of these CSRs to the users. Thus, $N_{\max} = 0.8CSR_{tot}/n_{CSR}$, where $N_{\max}$ is the maximum number of users that can be handled simultaneously. With larger Γ values, the system can support more users, but with a trade-off of a higher delay. For a given N, we need to obtain n_{CSR}, and then appropriately set Γ values for each of these CSRs.

To this end, we resort to allocating the same Γ value across the multiple CSRs allocated to a vehicle. This allocation can be justified as follows. Although different Γ values are allocated across the multiple CSRs, the number of simultaneous users the overall system can support is constrained by the shortest Γ value currently being used in the system. For example, consider a scenario where each

vehicle uses 2 CSRs, and we allocate Γ =20 ms ($N_{\max} = 400$) for the first CSR and Γ =50 ms ($N_{\max} = 1000$) for the second. It is not hard to see that the overall system can only support 400 users. Thus, allocating different Γ values across multiple CSRs is counter productive, and only leads to higher delay values at the MAC layer.

The relationship between n_{CSR} and $N_{\max}$ for the three values of Γ is tabulated in Table 5.1. We prefer shorter Γ values to reduce the average delay as shown in Chapter 4, and higher values for n_{CSR} to exploit higher degrees of freedom (resources) for the allocation of the parallel data streams. Figure 5.3 illustrates the selection of n_{CSR} and Γ, when N increases from 1 to 2000. The methodology associated with allocating multiple CSRs is presented using the solid red arrows, and the dashed black arrows show the equivalent transitions when the vehicle uses a single CSR as per the standard. The values inside the rectangles of the pyramidal shapes depict the value of Γ, and the values inside the green colored rectangles depict the maximum supported value of N, for each multiple CSR configuration.

Table 5.1: The relationship between n_{CSR} and $N_{\max}$ for different values of Γ.

n_{CSR}	$N_{\max}$		
	Γ=20 ms	**Γ=50 ms**	**Γ=100 ms**
1	400	1000	2000
2	200	500	1000
3	134	334	667
4	100	250	500

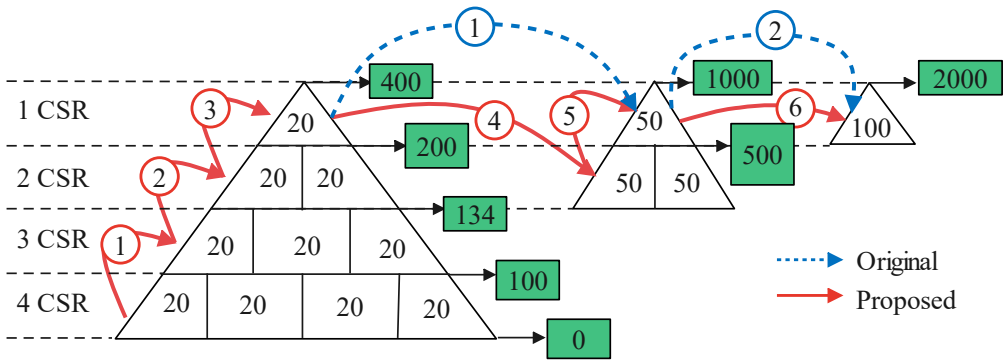

Figure 5.3: The process of selecting n_{CSR} and Γ with N.

5.3.2 Allocating the Multi-priority Data Streams Among the CSRs

Having established n_{CSR} and an appropriate value for Γ for a given N, we now face the problem of allocating the multi-priority data streams among the CSRs. We present the grouping options using Table 5.2. Let n_G denote the index of the grouping option. If $n_{CSR} = 1$, we simply allocate all data streams to the single CSR, as per the current standard, and we call this grouping option $n_G = 1$. If there are 4 CSRs, the grouping is again trivial, as we can allocate a separate CSR for each data stream. Thus, we get $n_G = 15$. The number of groups for the 2 and 3 CSR scenarios is based on the Stirling number of the second kind, thus there are 7 and 6 grouping options for each scenario, respectively.

Table 5.2: Grouping options with associated generation parameters.

n_{csr}	n_G	**Generation Parameters for CSRs**			
1 CSR		**CSR1**			
	1	λ_H, λ_D, λ_M, T_C			
2 CSRs		**CSR 1**		**CSR 2**	
	2	T_C		λ_H, λ_D, λ_M	
	3	λ_H		λ_D, T_C, λ_M	
	4	λ_D		λ_H, T_C, λ_M	
	5	λ_M		λ_H, T_C, λ_D	
	6	λ_H, T_C		λ_D, λ_M	
	7	λ_H, λ_M		λ_D, T_C	
	8	λ_H, λ_D		T_C, λ_M	
3 CSRs		**CSR 1**	**CSR 2**	**CSR 3**	
	9	T_C	λ_H	λ_D, λ_M	
	10	λ_H	λ_D	T_C, λ_M	
	11	T_C	λ_M	λ_H, λ_D	
	12	λ_D	T_C	λ_H, λ_M	
	13	λ_D	λ_M	λ_H, T_C	
	14	λ_H	λ_M	λ_D, T_C	
4 CSRs		**CSR 1**	**CSR 2**	**CSR 3**	**CSR 4**
	15	λ_H	λ_D	T_C	λ_M

We select the best grouping option $n_G^\star$ for a given n_{CSR} with respect to the average delay. Let $\mathcal{D}_{n_G,l}$ be the average delay of the l-th data stream for grouping option n_G. These delay values can be calculated using the DTMC models by appropriately setting the parameter combinations tabulated in Table 5.2 for A, as explained in reference to Figure 5.2. For example, the resulting average delay values for grouping option $n_G = 2$ are $\mathcal{D}_{2,C} = d_{avg,C}(T_C)$ and $\mathcal{D}_{2,m} = d_{avg,m}(\lambda_H, \lambda_D, \lambda_M)$ for $m \in \mathcal{I} \setminus \{C\}$. The sum average delay for grouping

option n_G is written as

$$\Delta\mathcal{D}_{n_G} = \sum_{l\in\mathcal{I}} w_l \mathcal{D}_{n_G,l},$$

where w_l, for $l \in \mathcal{I}$, denotes a weight for each data stream of interest. We set $w_H > w_D > w_C > w_M$ such that the priority management in the standard [32] is incorporated in our selection, and we select the sum average delay minimizing grouping option as the best one for a given n_{CSR}. Our approach of allocating multiple CSRs to a vehicle is formally presented through Algorithm 1.

Algorithm 1 Multiple CSR Allocation for C-V2X Mode 4.

procedure n_{CSR} & Γ ALLOCATION (N,λ_H,λ_D,λ_M,T_C)
  $\Gamma = 0$, $n_{CSR} = 0$ ▷ Initialization
    if $0 < N \leq 100 \rightarrow n_{CSR} = 4$, $\Gamma = 20$ ms
  else if $100 < N \leq 134 \rightarrow n_{CSR} = 3$, $\Gamma = 20$ ms
  else if $134 < N \leq 200 \rightarrow n_{CSR} = 2$, $\Gamma = 20$ ms
  else if $200 < N \leq 400 \rightarrow n_{CSR} = 1$, $\Gamma = 20$ ms
  else if $400 < N \leq 500 \rightarrow n_{CSR} = 2$, $\Gamma = 50$ ms
  else if $500 < N \leq 1000 \rightarrow n_{CSR} = 1$, $\Gamma = 50$ ms
  end if
  BestGroup(n_{CSR},Γ,λ_H,λ_D,λ_M,T_C)
end procedure
    function BestGroup(n_{CSR},Γ,λ_H,λ_D,λ_M,T_C)
     $best\_group = 0$ ▷ Initialization
        if $(n_{CSR} = 1) \rightarrow n_G^\star = 1$
     else if $(n_{CSR} = 2) \rightarrow n_G^\star = \underset{k\in\{2,\ldots,8\}}{\arg\min}\ \Delta\mathcal{D}_k$
     else if $(n_{CSR} = 3) \rightarrow n_G^\star = \underset{k\in\{9,\ldots,14\}}{\arg\min}\ \Delta\mathcal{D}_k$
     else if $(n_{CSR} = 4) \rightarrow n_G^\star = 15$
     end if
     Return $n_G^\star$
    end function

5.4 Numerical Results and Discussion

This section presents numerical results that highlight the performance of using multiple CSRs by the vehicles according to Algorithm 1. The reference packet formats of HPD, DENM, CAM, and MHD are set according to [84,85]. HPD and DENM packets are retransmitted at fixed intervals for added reliability [78] as per the standard, and for the results, we have set the number of repetitions to 8 and 5 times, respectively. The candidate values for λ_m, where $m \in \mathcal{I} \setminus \{C\}$, are set by being consistent with the example use case scenarios in [67] and T_C is set between 100 ms and 1 s according to standard [84]. We set $w_H = 0.4$, $w_D = 0.3$,

$w_C = 0.2$, and $w_M = 0.1$ to extend the priority management in the standard [32] into the grouping methodology.

Table 5.3: The average delay reduction percentages with N for CAM and MHD packets.

N	n_{CSR}	Γ **(ms)**	**The average delay reduction (%)**											
			$\lambda_H = \lambda_D = 0.1$, $\lambda_M = 1$ **packets/s**						$\lambda_H = \lambda_D = 1$, $\lambda_M = 10$ **packets/s**					
			$T_C = 100$ **ms**			$T_C = 500$ **ms**			$T_C = 100$ **ms**			$T_C = 500$ **ms**		
			$n_G^\star$	**CAM**	**MHD**	$n_G^\star$	**CAM**	**MHD**	$n_G^\star$	**CAM**	**MHD**	$n_G^\star$	**CAM**	**MHD**
$[0.100)$	4	20	15	9.8	14.2	15	0.1	0.6	15	11.5	26.2	15	0.2	16.3
$[100, 134)$	3	20	11	9.8	14.2	14	0.04	0.6	11	11.5	26,2	14	0.13	16.3
$[134, 200)$	2	20	2	9.8	11.0	5	0.01	0.6	2	11.5	18.1	5	0.05	16.3
$[200, 400)$	1	20	1	-	-	1	-	-	1	-	-	1	-	-
$[400, 500)$	2	50	2	54.7	50.4	5	0.03	3.2	2	77.4	80.7	5	0.3	73.1

5.4.1 Average Delay

Firstly, we present the results on the average delay. Fig 5.4 illustrates the average delay behavior of CAM and MHD packets with N at $\lambda_H = \lambda_D = 1$, $\lambda_M = 10$ packets/s and $T_C = 100$ ms. As shown in this figure, the average delay is mainly sensitive to Γ, exhibiting a step-wise increase when Γ switches from a shorter to a longer value, and constant with respect to N for fixed Γ. It was noticed that delay gains for HPD and DENM were negligibly small due to their higher priority levels, thus omitted in the results. The higher priority packets are served first regardless of the number of CSRs, and hence, the gains are insignificant. It can be seen that the average delay values can be maintained below 100 ms thanks to the utilization of multiple CSRs. Further, results on the average delay reduction percentages for CAM and MHD data streams relative to using a single CSR as per the standard, are tabulated in Table 5.3.

Firstly, while focusing on less critical scenarios such as roadwork warnings and safety function out of normal condition warnings, where the packet generation rates are considerably lower ($\lambda_D = 0.1$ packets/s), we can observe clear gains of utilizing multiple CSRs at each vehicle. The maximum average delay reduction percentage for CAM is 54.7%, which is around 30 ms, and for MHD, it is 50.4%, which is around 48.9 ms. We can expect the gains for MHD to increase further at higher λ_M values. For example, if $\lambda_M = 10$, the gain is 69.2% which is 236 ms. While focusing on more critical scenarios, such as emergency electronic brake lights and warnings from emergency vehicles that have higher packet generation rates ($\lambda_D = 1$), we can observe very high gains for both CAM and MHD, *i.e.,* a maximum delay reduction percentage of 77.4% (85 ms) and 80.7% (334 ms), respectively, which can also be observed in the range $N \in [400, 500]$ in Figure 5.4. Thus, the multiple CSR configurations can contribute considerably to alleviate the issue of stale packets in low priority queues. In general, the results show that the proposed method works favorably for both less critical and critical scenarios when considering the average delay. Furthermore, it is useful when more frequent location updates are required, which is achieved using CAM. This can be seen by comparing the gains for $T_C = 100$ ms with $T_C = 500$ ms. Thus, the multiple CSR configuration will be ideal for applications that require high CAM rates, which is in the magnitude of 10 Hz according to the standard [67].

Moreover, based on the $n_G^\star$ values, we can provide the following insights on allocating the multiple CSRs among the data streams. For 2 CSR configurations, it can be observed that allocating the periodic and event-triggered traffic for

separate CSRs performs better when the CAM rate is high. On the other hand, better delay-wise performance can be obtained by allocating a separate CSR for MHD when the CAM rate is low. This eliminates the necessity of MHD packets waiting till all higher priority queues are empty. For 3 CSR configurations, better delay-wise performance can be obtained by allocating a CSR each for CAM and MHD streams, and the other CSR for HPD and DENM streams, given that the CAM rate is high. As the system considers both HPD and DENM packets to have relatively higher priority, and hence transmits with minimum delay, allocating a CSR each for these two data streams does not show an advantage in this scenario. However, at lower CAM rates, we allocate a CSR each for MHD, HPD and DENM streams, and CAM can be grouped with the data stream having the lowest generation rate. In our results, we observe that the grouping was with DENM as it has a lower effective rate compared to HPD due to the lower number of packet repetitions.

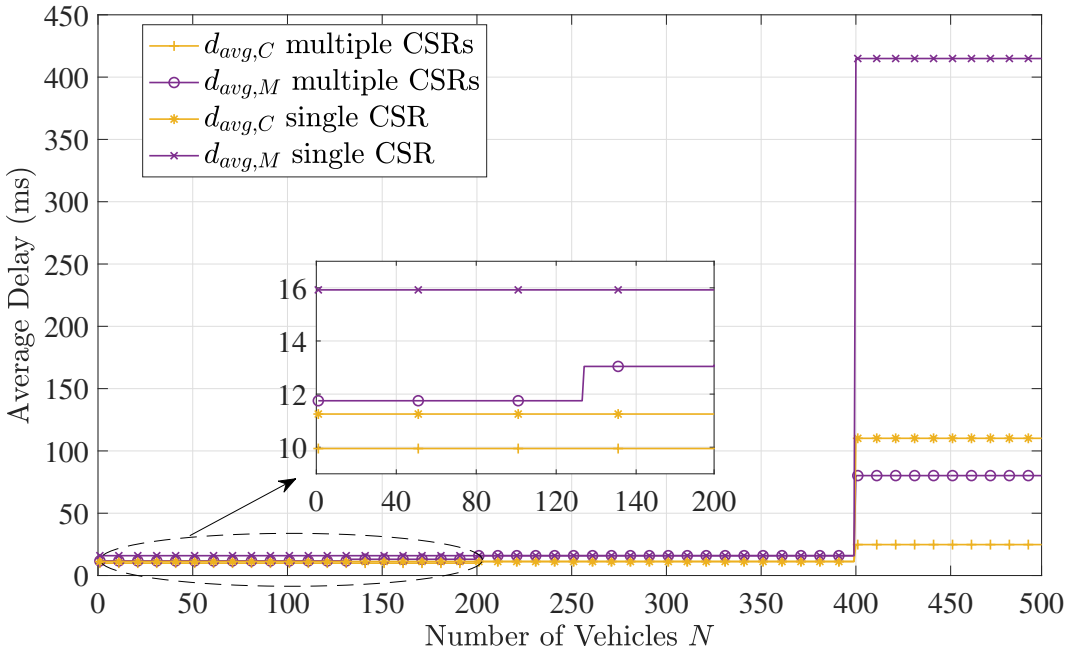

Figure 5.4: The behavior of average delay vs N at $\lambda_H = \lambda_D = 1$, $\lambda_M = 10$ packets/s, and $T_C = 100$ ms.

5.4.2 Collision Probability and Channel Utilization

Although favorable in terms of delay, using multiple CSRs may lead to a trade-off in terms of higher packet collisions. The variation of per CSR collision probability for the single and multiple CSR configurations are illustrated in Figure 5.5. The

collision probability increases exponentially with N. We can also observe that Γ has a significant impact on the collision probability as the collision probability reduces significantly when the value of Γ increases. This is thanks to the availability of more radio resources at higher Γ values as we experienced in Chapter 4.

When comparing the collision probabilities of the two configurations, it can be seen that utilizing multiple CSRs lead to higher collision probability values in $0 < N \leq 200$ and $400 < N \leq 500$. This is due to the higher number of overlaps in the selection windows when multiple CSRs are used as explained in [101]. Therefore, there is a clear tradeoff of using multiple CSRs. However, it can be seen from Figure 5.5 that the maximum increase in collision probability is approximately 0.6% (at $N = 99$)when compared to using a single CSR, which is rather insignificant compared to the gains achieved on delay and priority management.

We already saw that the average delay increases with Γ, and in Section 5.3 we showed that each Γ has its respective N_{max}. We can increase the N_{max} threshold levels further if the standard allows allocating a higher percentage of available CSRs to the users, *i.e.*, increasing the 80% parameter in the SPS algorithm stated in Section 5.3. In that case, allocating multiple CSRs may deem even more favorable is terms of average delay. However, we can observe from Figure 5.5 that this change leads to an exponential increase in the collision probability. Therefore, fine-tuning N_{max} needs to be done only after carefully studying the QoS requirements of the applications. The behavior of channel utilization with N is shown in Figure 5.6. The figure clearly shows how the channel utilization has been exploited in the ranges of $0 < N \leq 200$ and $400 < N \leq 500$ to achieve the initial objectives.

We end the discussion by providing some insights on some implications of the proposed method. Firstly, let us focus on the SPS algorithm. In the SPS algorithm according the current standard, each vehicle is capable of tracking the CSRs used by itself and the neighboring vehicles within the sensing window. These identified CSRs are excluded when selecting a CSR for the subsequent transmission. Using multiple CSRs at each vehicle will not bring about major changes to how the SPS algorithm tracks CSRs used by neighboring vehicles. However, the SPS algorithm needs to be slightly mortified to identify and exclude the CSRs used within the target vehicle itself, to minimize the internal collisions. The authors note that the proposed method may also cause changes in the hardware setup as parallel transmission is required, but with the developments in multi-antenna technologies, handling the hardware implications seems

practically feasible. Extensive details on hardware implications are beyond the scope of this paper.

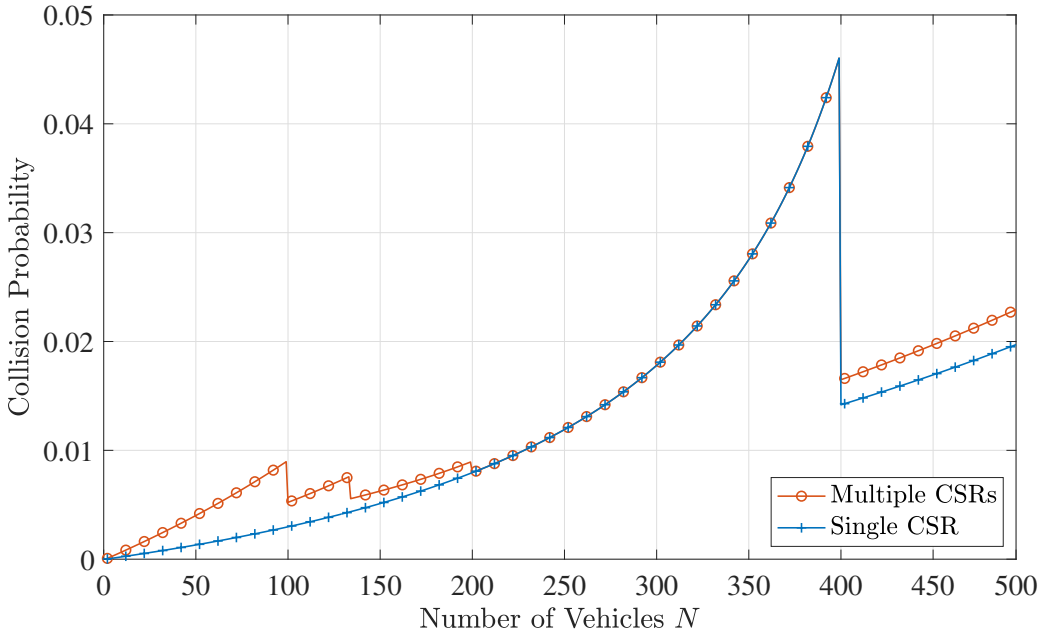

Figure 5.5: The behavior of collision probability vs N at $\lambda_H = \lambda_D = 1$, $\lambda_M = 10$ packets/s, and $T_C = 100$ ms.

5.5 Conclusions

This chapter has focused on a vehicular network that utilizes C-V2X Mode 4 for communication, and supports multi-priority data streams to fulfill varying QoS constraints of ITS use cases. It has proposed increasing the channel utilization of the network through the allocation of multiple CSRs at each vehicle, and has studied its achievable performance gains at the MAC layer. The proposed method has led to two fundamental questions, which are, how many CSRs should be allocated to each vehicle, and how the multi-priority data streams should be allocated among them. The number of CSRs at each vehicle has been ascertained as a function of total number of neighboring vehicles for the target vehicle, and a procedure has been introduced for allocating the multi-priority data streams among them based on the average delay in the network. The results have shown that using multiple CSRs at each vehicle can lead to significant gains in the network in terms of average delay. In particular, the average delay of lower priority data streams can be improved significantly by allocating them separate CSRs, which ameliorates the risk of stale packets. As a trade-off, an increase

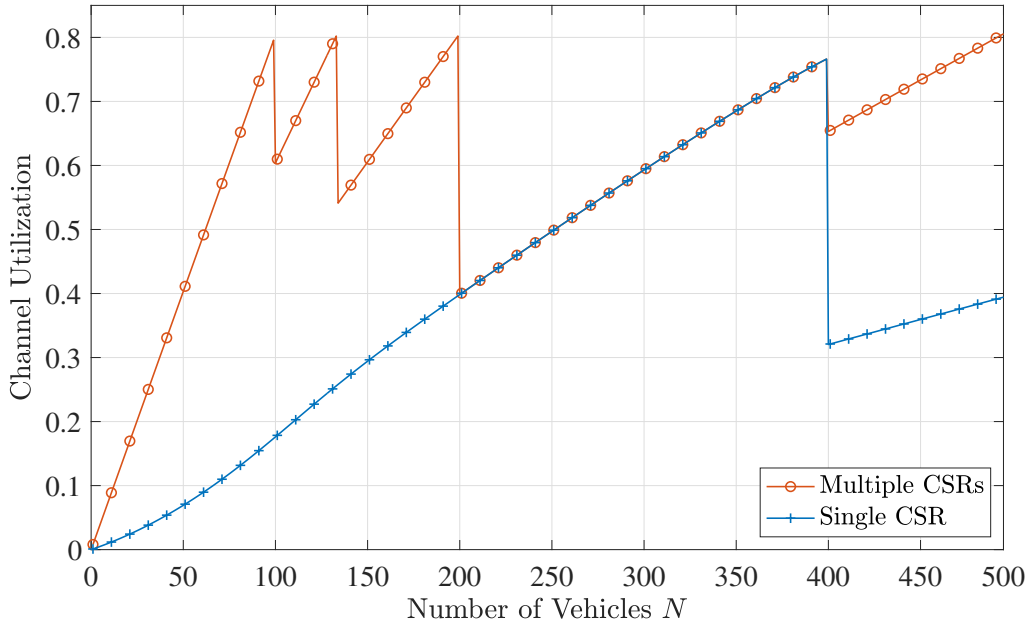

Figure 5.6: The behavior of channel utilization vs N at $\lambda_H = \lambda_D = 1$, $\lambda_M = 10$ packets/s, and $T_C = 100$ ms.

in the collision probability can be observed, but the performance loss is almost insignificant compared to the delay gains.

Chapter 6

CONCLUSIONS AND FUTURE WORK

6.1 Conclusions

Unique characteristics of vehicular networks have introduced new implications, and therefore, necessitate the enhancement or provision of new techniques to ensure fast, secure, and reliable vehicular communications. The connected vehicle concept has become a mainstream reality, where vehicles equipped with communication modules are networked with their immediate surroundings. Connected vehicles have become the third fastest-growing type of connected devices after smartphones and tablets. Vehicular applications and communications technologies have collectively referred to as V2X, broadly classified into four different types: V2V, V2I, V2N, and V2P. This thesis has studied two V2X communication technologies named IEEE 802.11p and C-V2X Mode 4, showing similar characteristics such as distributed coordination. We have compared their MAC layer performance with different application requirements and have proposed an enhancement for the MAC layer performance of C-V2X Mode 4.

Firstly, we have studied the MAC layer performance of C-V2X Mode 4 and IEEE 802.11p utilizing DTMCs, incorporating the generator and queue models for CAM and DENM. We have utilized performance metrics such as the average delay, collision probability, and channel utilization for the performance comparison. The results have shown that the average delay of C-V2X Mode 4 is comparatively higher than IEEE 802.11p. On the other hand, the collision probability of a vehicle communicating using C-V2X Mode 4 is lower than its counterpart. The results have also shown that the average delay of C-V2X has a locally optimal combination of CAM and DENM packet arrival rates, which can be utilized to reduce delays in C-V2X further. Moreover, the DCC algorithm's TRC technique can regulate the collision probability and the channel utilization of a vehicle communicating using IEEE 802.11p.

Secondly, we have focused on the MAC layer performance of the two V2X com-

munication enabling technologies in the presence of multi priority data streams such as HPD, DENM, CAM, and MHD. We have modified the developed DTMC for the MAC layer operation to support the multi-priority data streams. Especially, the EDCA mechanism model in IEEE 802.11p with different priority ACs. We have extended CAM and DENM packet generators and queue models to support all four types of packets by considering their characteristics. The steady-state probabilities of the models have been utilized to derive expressions for key performance indicators at the MAC layer, including the average delay, collision probability, throughput, and the channel utilization. The results have firstly highlighted the importance of considering all four parallel data streams when studying the MAC layer performance of the two technologies. Priority management has been implemented successfully in both technologies. However, it can be seen that IEEE 802.11p treats multi-priority data streams more fairly compared to its counterpart, thanks to its inbuilt EDCA mechanism. IEEE 802.11p is also superior in average delay, but C-V2X Mode 4 exhibits better performance in terms of collision resolution, leading to higher throughput values. Further insights have been presented on the possible improvements of both technologies.

From the study of the MAC layer operation of C-V2X Mode 4 with multi-priority data streams, we have observed that low priority data streams experience higher average delay, causing a risk for stale packets in low priority queues. We have proposed allocating multiple CSRs for each vehicle to solve this problem at the expense of increased channel utilization in the system. The proposed method has led to two fundamental questions, which are, how many CSRs should be allocated to each vehicle, and how the multi-priority data streams should be allocated among them. We have proposed an algorithm to be implemented in the vehicles for CSR allocation and distributing the multiple data streams among the CSRs. The results have shown that using multiple CSRs at each vehicle can lead to significant gains in the network in terms of average delay. In particular, the average delay of lower priority data streams can be improved significantly by allocating them separate CSRs, which reduces the risk of stale packets. As a trade-off, an increase in the collision probability can be observed, but the performance loss is almost insignificant compared to the delay gains.

6.2 Future Work

Before concluding this thesis, we will briefly present some ideas which will motivate future studies on this topic.

6.2.1 Modeling the IEEE 802.11bd MAC Layer Performance by Using DTMCs

During the evolution of IEEE 802.11p, priority was given to developing a vehicular communication standard that assisted vehicular safety, proper traffic management, and other value-added applications, such as vehicular diagnostics and parking. The requirements specified for 802.11p were to support relative speeds up to 200 km/h, the latency of around 100 m, and a transmission range of up to 1000 m.

Assuming that 802.11p was developed about two decades ago, advanced PHY and MAC techniques introduced in 802.11n/ac/ax can be influenced to enhance 802.11p. With this goal, the IEEE 802.11 next-generation V2X study group was created in March 2018. After an initial feasibility study, the IEEE 802.11bd task group was formed in January 2019. The primary design goals of 802.11bd contain supporting the following [104].

- Achieving twice the MAC throughput of 802.11p with relative velocities up to 500 km/h.
- Achieving twice the communication range of 802.11p.
- Vehicle positioning in affiliation with V2X communications.
- Backward compatibility features with IEEE 802.11p.

A similar modeling procedure presented in this thesis can be carried out in the future for IEEE 802.11bd to quantify the performance enhancement from the evolved standard.

6.2.2 Modeling the NR-V2X MAC Layer Performance by Using DTMCs

The NR V2X study Item [105] implies that the design goals of NR V2X are not to replace C-V2X, but to supplement C-V2X in supporting particular use cases that C-V2X cannot support. Since C-V2X is already standardized and commercial deployments are underway, C-V2X and NR V2X might likely coexist in the same geographical area, where newer vehicles will have C-V2X and NR V2X abilities. Under such events, use cases that can be supported reliably by using C-V2X use C-V2X procedures, while the remaining use cases use NR V2X procedures [105]. However, to guarantee that NR V2X can deliver unified support for every V2X application in the future, NR V2X must be competent in supporting not only

advanced V2X applications, but also basic safety applications that are backed by current C-V2X.

NR V2X is designed to support V2X applications with differing degrees of latency, reliability, and throughput conditions. Some require transmitting periodic messages from these use cases, while many NR V2X use cases are based on reliable delivery of event-driven messages. Furthermore, some scenarios require utilizing broadcast packets, while others, such as vehicle platooning, require transmitting packets only to a specific subset of vehicles to increase efficiency. In some scenarios, 3GPP notices benefits in transmitting packets to only a single vehicle [106]. Therefore, two new communication types, unicast and groupcast, will be introduced in NR V2X to support such scenarios. Similarly, in IEEE 802.11bd, NR V2X also considers the use of mmWave bands for V2X applications, particularly for applications that require a short-range and significant throughput.
The NR V2X Study Item outlines its following objectives.

- Enhanced sidelink and Uu design: Re-design sidelink and Uu procedures in order to support advanced V2X applications.
- Uu Identify enhancements for configuration of sidelink resources using the NR Uu interface.
- Study mechanisms to identify the best interface (among LTE sidelink, NR sidelink, LTE Uu and NR Uu) for given V2X message transmission.
- Study solutions that meet the QoS requirements of different radio interfaces.
- Feasibility study and technical solutions for the coexistence of C-V2X and NR V2X within a single device, also referred to as in-device coexistence.

A similar modeling procedure presented in this thesis can be carried out in the future for NR-V2X to quantify the performance enhancement from the evolved standard.

6.2.3 Enhance the DTMC model by taking in to account the real sensing mechanism.

In the DTMC model, the real sensing mechanism is not considered since we need to consider received power. Therefore, the impact of relative distance, exposed terminals, and hidden terminals are omitted in the current models, and only MAC layer performance is modeled. However, suppose we integrate the physical layer performance into this DTMC model. In that case, we can investigate the effect

of the real sensing mechanism and catch the impact of relative distance, exposed, and hidden terminals into the composite model.

References

[1] ETSI, "Intelligent transport systems (ITS); Access layer specification for intelligent transport system operating in the 5 GHz frequency band," European Telecommunications Standards Institute (ETSI), European Standard telecommunications series (EN) 302 663, Jan. 2020, version 1.3.1.

[2] L. Lusvarghi and M. L. Merani, "On the coexistence of aperiodic and periodic traffic in cellular vehicle-to-everything," *IEEE Access*, vol. 8, pp. 207 076–207 088, Nov. 2020.

[3] A. Bazzi, A. O. Berthet, C. Campolo, B. M. Masini, A. Molinaro, and A. Zanella, "On the design of sidelink for cellular V2X: A literature review and outlook for future," *IEEE Access*, vol. 9, pp. 97 953–97 980, Jul. 2021.

[4] M. A. Khan, S. Ghosh, S. A. Busari, K. M. S. Huq, T. Dagiuklas, S. Mumtaz, M. Iqbal, and J. Rodriguez, "Robust, resilient and reliable architecture for V2X communications," *IEEE Transactions on Intelligent Transportation Systems*, vol. 22, no. 7, pp. 4414–4430, Jun. 2021.

[5] M. Muhammad and G. A. Safdar, "Survey on existing authentication issues for cellular-assisted V2X communication," *Vehicular Communications*, vol. 12, pp. 50–65, Apr. 2018.

[6] M. Hasan, S. Mohan, T. Shimizu, and H. Lu, "Securing vehicle-to-everything (V2X) communication platforms," *IEEE Transactions on Intelligent Vehicles*, vol. 5, no. 4, pp. 693–713, Dec. 2020.

[7] A. Costandoiu and M. Leba, "Convergence of V2X communication systems and next generation networks," *IOP Conference Series: Materials Science and Engineering*, vol. 477, p. 012052, Feb. 2019.

[8] V. Maglogiannis, D. Naudts, S. Hadiwardoyo, D. van den Akker, J. Marquez-Barja, and I. Moerman, "Experimental V2X evaluation for C-V2X and ITS-G5 technologies in a real-life highway environment," *IEEE Transactions on Network and Service Management*, pp. 1–1, Nov. 2021.

[9] J.-K. Bae, M.-C. Park, E.-J. Yang, and D.-W. Seo, "Implementation and performance evaluation for DSRC-based vehicular communication system," *IEEE Access*, vol. 9, pp. 6878–6887, Dec. 2021.

[10] Z. H. Mir, J. Toutouh, F. Filali, and Y.-B. Ko, "Enabling DSRC and c-v2x integrated hybrid vehicular networks: Architecture and protocol," *IEEE Access*, vol. 8, pp. 180 909–180 927, Oct. 2020.

[11] G. Bianchi, "Performance analysis of the IEEE 802.11 distributed coordination function," *IEEE Journal on Selected Areas in Communications*, vol. 18, no. 3, pp. 535–547, Mar. 2000.

[12] S. Eichler, "Performance evaluation of the IEEE 802.11p WAVE communication standard," in *Proc. IEEE Vehicular Technology Conference,* Baltimore, MD, USA, Oct. 2007, pp. 2199–2203.

[13] A. Jafari, S. Al-Khayatt, and A. Dogman, "Performance evaluation of IEEE 802.11p for vehicular communication networks," in *Proc. International Symposium on Communication Systems, Networks Digital Signal Processing,* Poznan, Poland, Jul. 2012, pp. 1–5.

[14] K. Bilstrup, E. Uhlemann, E. G. Strom, and U. Bilstrup, "Evaluation of the IEEE 802.11p MAC method for vehicle-to-vehicle communication," in *Proc. IEEE Vehicular Technology Conference,* Calgary, AB, Canada, Sep. 2008, pp. 1–5.

[15] S. Cao and V. C. Lee, "An accurate and complete performance modeling of the IEEE 802.11p MAC sublayer for VANET," *Computer Communications*, vol. 149, pp. 107–120, Jan. 2020.

[16] A. K. Gizzini, M. Chafii, A. Nimr, and G. Fettweis, "Deep learning based channel estimation schemes for IEEE 802.11p standard," *IEEE Access*, vol. 8, pp. 113 751–113 765, Jun. 2020.

[17] A. A. Almohammedi and V. Shepelev, "Saturation throughput analysis of steganography in the IEEE 802.11p protocol in the presence of non-ideal transmission channel," *IEEE Access*, vol. 9, pp. 14 459–14 469, Jan. 2021.

[18] IEEE, "IEEE standard for information technology– local and metropolitan area networks– specific requirements– part 11: Wireless LAN medium access control (MAC) and physical layer (PHY) specifications amendment 6: Wireless access in vehicular environments," *IEEE Std 802.11p-2010*, pp. 1–51, Jul. 2010.

[19] ——, "IEEE standard for information technology–telecommunications and information exchange between systems local and metropolitan area networks–specific requirements part 11: Wireless LAN medium access control (MAC) and physical layer (PHY) specifications," *IEEE Std 802.11-2012*, pp. 1–2793, Mar. 2012.

[20] ——, "IEEE standard for information technology—telecommunications and information exchange between systems local and metropolitan area networks—specific requirements - part 11: Wireless LAN medium access control (MAC) and physical layer (PHY) specifications," *IEEE Std 802.11-2016*, pp. 1–3534, Dec. 2016.

[21] S. Chen, J. Hu, Y. Shi, L. Zhao, and W. Li, "A vision of C-V2X: Technologies, field testing, and challenges with chinese development," *IEEE Internet of Things Journal*, vol. 7, no. 5, pp. 3872–3881, Feb. 2020.

[22] F. Eckermann, M. Kahlert, and C. Wietfeld, "Performance analysis of C-V2X Mode 4 communication introducing an open-source C-V2X simulator," in *Proc. IEEE Vehicular Technology Conference,* Honolulu, USA, Nov. 2019, pp. 1–5.

[23] A. Nabil, K. Kaur, C. Dietrich, and V. Marojevic, "Performance analysis of sensing-based semi-persistent scheduling in C-V2X networks," in *Proc. IEEE Vehicular Technology Conference,* Chicago, IL, USA, Aug. 2018, pp. 1–5.

[24] K. Z. Ghafoor, M. Guizani, L. Kong, H. S. Maghdid, and K. F. Jasim, "Enabling efficient coexistence of DSRC and C-V2X in vehicular networks," *IEEE Wireless Communications*, vol. 27, no. 2, pp. 134–140, Apr. 2020.

[25] M. Emara, M. C. Filippou, and D. Sabella, "MEC-assisted end-to-end latency evaluations for C-V2X communications," in *Proc. European Conference on Networks and Communications,* Ljubljana, Slovenia, Jun. 2018, pp. 1–9.

[26] V. V. Chetlur and H. S. Dhillon, "Coverage and rate analysis of downlink cellular vehicle-to-everything (C-V2X) communication," *IEEE Transactions on Wireless Communications*, vol. 19, no. 3, pp. 1738–1753, Mar. 2020.

[27] W. Qi, B. Landfeldt, Q. Song, L. Guo, and A. Jamalipour, "Traffic differentiated clustering routing in DSRC and C-V2X hybrid vehicular networks," *IEEE Transactions on Vehicular Technology*, vol. 69, no. 7, pp. 7723–7734, Jul. 2020.

[28] Q. Chen, H. Jiang, and G. Yu, "Service oriented resource management in spatial reuse-based C-V2X networks," *IEEE Wireless Communications Letters*, vol. 9, no. 1, pp. 91–94, Jan. 2020.

[29] F. A. Schiegg, N. Brahmi, and I. Llatser, "Analytical performance evaluation of the collective perception service in C-V2X Mode 4 networks," in *Proc. IEEE Intelligent Transportation Systems Conference,* Auckland, New Zealand, Oct. 2019, pp. 181–188.

[30] 3GPP, "Evolved universal terrestrial radio access (E-UTRA); Physical layer procedures," 3rd Generation Partnership Project (3GPP), Technical Specification (TS) 36.213, Apr. 2017, version 14.2.0.

[31] ——, "Evolved universal terrestrial radio access (E-UTRA); Medium access control (MAC) protocol specification," 3rd Generation Partnership Project (3GPP), Technical Specification (TS) 36.321, Jul. 2017, version 14.3.0.

[32] ETSI, "Intelligent transport systems (ITS); Vehicular communications; geonetworking; part 4: Geographical addressing and forwarding for point-to-point and point-to-multipoint communications; sub-part 2: Media-dependent functionalities for ITS-G5," European Telecommunications Standards Institute (ETSI), Technical Specification (TS) 102 636-4-2, Oct. 2013, version 1.1.1.

[33] Z. Li, M. A. Uusitalo, H. Shariatmadari, and B. Singh, "5G URLLC: Design challenges and system concepts," in *Proc. International Symposium on Wireless Communication Systems,* Lisbon, Portuga, Aug. 2018, pp. 1–6.

[34] P. Popovski, K. F. Trillingsgaard, O. Simeone, and G. Durisi, "5G wireless network slicing for eMBB, URLLC, and mMTC: A communication-theoretic view," *IEEE Access*, vol. 6, pp. 55 765–55 779, Sep. 2018.

[35] A. Anand, G. de Veciana, and S. Shakkottai, "Joint scheduling of URLLC and eMBB traffic in 5G wireless networks," *IEEE/ACM Transactions on Networking*, vol. 28, no. 2, pp. 477–490, Feb. 2020.

[36] M. Alsenwi, N. H. Tran, M. Bennis, A. Kumar Bairagi, and C. S. Hong, "eMBB-URLLC resource slicing: A risk-sensitive approach," *IEEE Communications Letters*, vol. 23, no. 4, pp. 740–743, Feb. 2019.

[37] P. Popovski, C. Stefanovic, J. J. Nielsen, E. de Carvalho, M. Angjelichinoski, K. F. Trillingsgaard, and A.-S. Bana, "Wireless access in ultra-reliable low-latency communication (URLLC)," *IEEE Transactions on Communications*, vol. 67, no. 8, pp. 5783–5801, May 2019.

[38] A. Anand and G. de Veciana, "Resource allocation and HARQ optimization for URLLC traffic in 5G wireless networks," *IEEE Journal on Selected Areas in Communications*, vol. 36, no. 11, pp. 2411–2421, Oct. 2018.

[39] B. Chang, L. Zhang, L. Li, G. Zhao, and Z. Chen, "Optimizing resource allocation in URLLC for real-time wireless control systems," *IEEE Transactions on Vehicular Technology*, vol. 68, no. 9, pp. 8916–8927, Jul. 2019.

[40] A. Azari, M. Ozger, and C. Cavdar, "Risk-aware resource allocation for URLLC: Challenges and strategies with machine learning," *IEEE Communications Magazine*, vol. 57, no. 3, pp. 42–48, Mar. 2019.

[41] T. N. Weerasinghe, I. A. M. Balapuwaduge, and F. Y. Li, "Preamble reservation based access for grouped mMTC devices with URLLC requirements," in *Proc. IEEE International Conference on Communications,* Shanghai, China, May 2019, pp. 1–6.

[42] F. Ganhão, L. Bernardo, R. Dinis, R. Oliveira, and P. Pinto, "Uplink performance evaluation of packet combining ARQ for MPR prefix-assisted DS-CDMA," *IEEE Transactions on Communications*, vol. 63, no. 7, pp. 2685–2697, Jul. 2015.

[43] I. Inan, F. Keceli, and E. Ayanoglu, "Analysis of the 802.11e enhanced distributed channel access function," *IEEE Transactions on Communications*, vol. 57, no. 6, pp. 1753–1764, Jun. 2009.

[44] L. Guntupalli and F. Y. Li, "DTMC modeling for performance evaluation of DW-MAC in wireless sensor networks," in *Proc. IEEE Wireless Communications and Networking Conference,* Doha, Qatar, Apr. 2016, pp. 1–6.

[45] L. Guntupalli, F. Y. Li, and J. Martinez-Bauset, "Event-triggered sleeping for synchronous DC MAC IN WSNs: Mechanism and DTMC modeling," in *Proc. IEEE Global Communications Conference,* Washington, DC, USA, Dec. 2016, pp. 1–6.

[46] L. Guntupalli, J. Martinez-Bauset, and F. Y. Li, "Cooperative or non-cooperative transmission in synchronous DC WSNs: A DTMC-based approach," in *Proc. IEEE International Conference on Communications,* Paris, France, May 2017, pp. 1–6.

[47] G. P. Wijesiri and F. Y. Li, "Frame based equipment medium access in LTE-U: Mechanism enhancements and DTMC modeling," in *Proc. IEEE Global Communications Conference,* Singapore, Dec. 2017, pp. 1–6.

[48] I. A. M. Balapuwaduge and F. Y. Li, "Hidden markov model based machine learning for mMTC device cell association in 5G networks," in *Proc. IEEE International Conference on Communications,* Shanghai, China, May 2019, pp. 1–6.

[49] S. S. Gokhale and K. S. Trivedi, "Analytical models for architecture-based software reliability prediction: A unification framework," *IEEE Transactions on Reliability*, vol. 55, no. 4, pp. 578–590, Nov. 2006.

[50] L. Guntupalli, M. Gidlund, and F. Y. Li, "An on-demand energy requesting scheme for wireless energy harvesting powered IoT networks," *IEEE Internet of Things Journal*, vol. 5, no. 4, pp. 2868–2879, Jun. 2018.

[51] Z. Tao and S. Panwar, "Throughput and delay analysis for the IEEE 802.11e enhanced distributed channel access," *IEEE Transactions on Communications*, vol. 54, no. 4, pp. 596–603, Apr. 2006.

[52] H. Wu, X. Wang, Q. Zhang, and X. Shen, "IEEE 802.11e enhanced distributed channel access (EDCA) throughput analysis," in *Proc. IEEE International Conference on Communications,* Istanbul, Turkey, vol. 1, Jun. 2006, pp. 223–228.

[53] Y. Ge, J. C. Hou, and S. Choi, "An analytic study of tuning systems parameters in IEEE 802.11e enhanced distributed channel access," *Computer Networks*, vol. 51, no. 8, pp. 1955–1980, Jun. 2007.

[54] C.-l. Huang and W. Liao, "Throughput and delay performance of IEEE 802.11e enhanced distributed channel access (EDCA) under saturation condition," *IEEE Transactions on Wireless Communications*, vol. 6, no. 1, pp. 136–145, Feb. 2007.

[55] I. Inan, F. Keceli, and E. Ayanoglu, "Saturation throughput analysis of the 802.11e enhanced distributed channel access function," in *Proc. IEEE International Conference on Communications,* Glasgow, UK, Jun. 2007, pp. 409–414.

[56] ——, "Modeling the 802.11e enhanced distributed channel access function," in *Proc. IEEE Global Telecommunications Conference,* Washington, DC, USA, Nov. 2007, pp. 2546–2551.

[57] G. Naik, B. Choudhury, and J. Park, "IEEE 802.11bd 5G NR V2X: Evolution of radio access technologies for V2X communications," *IEEE Access*, vol. 7, pp. 70 169–70 184, May 2019.

[58] A. Bazzi, G. Cecchini, M. Menarini, B. M. Masini, and A. Zanella, "Survey and perspectives of vehicular Wi-Fi versus sidelink cellular-V2X in the 5G era," *Future Internet*, vol. 11, no. 6, p. 122, May 2019.

[59] J. R. Gallardo, D. Makrakis, and H. T. Mouftah, "Performance analysis of the EDCA medium access mechanism over the control channel of an IEEE 802.11p WAVE vehicular network," in *Proc. IEEE International Conference on Communications,* Dresden, Germany, Jun. 2009, pp. 1–6.

[60] J. Zheng and Q. Wu, "Performance modeling and analysis of the IEEE 802.11p EDCA mechanism for VANET," *IEEE Transactions on Vehicular Technology*, vol. 65, no. 4, pp. 2673–2687, Apr. 2016.

[61] ETSI, "Intelligent transport systems (ITS); Vehicular communications; Geonetworking; part 3: Network architecture," European Telecommunications Standards Institute (ETSI), Technical Specification (TS) 102 636-3, Mar. 2010, version 1.1.1.

[62] C. Belagal Math, H. Li, S. Heemstra de Groot, and I. G. Niemegeers, "V2X application-reliability analysis of data-rate and message-rate congestion control algorithms," *IEEE Communications Letters*, vol. 21, no. 6, pp. 1285–1288, Jun. 2017.

[63] I. Ismath, T. Samarasinghe, D. Dias, M. Wimalarathna, W. Rasanga, N. Jayaweera, and Y. Nugera, "Emergency vehicle traversal using DSRC/WAVE based vehicular communication," in *Proc. IEEE Intelligent Vehicles Symposium,* Paris, France, Jun. 2019, pp. 1981–1986.

[64] S. Pallewatta, P. S. Lakmali, S. Wijewardana, P. Ranathunga, T. Samarasinghe, and D. Dias, "802.11p: Insights from the MAC and physical layers for a cooperate car following application," in *Intelligent Transport Systems – From Research and Development to the Market Uptake*, T. Kováčiková, Ľ. Buzna, G. Pourhashem, G. Lugano, Y. Cornet, and N. Lugano, Eds. Cham: Springer International Publishing, Jul. 2018, pp. 226–236.

[65] S. S. Husain, A. Kunz, A. Prasad, E. Pateromichelakis, and K. Samdanis, "Ultra-high reliable 5G V2X communications," *IEEE Communications Standards Magazine*, vol. 3, no. 2, pp. 46–52, Sep. 2019.

[66] K. Ganesan, J. Lohr, P. B. Mallick, A. Kunz, and R. Kuchibhotla, "NR sidelink design overview for advanced V2X service," *IEEE Internet of Things Magazine*, vol. 3, no. 1, pp. 26–30, Apr. 2020.

[67] ETSI, "Intelligent transport systems (ITS); vehicular communications; Basic Set of Applications; Definitions," European Telecommunications Standards Institute (ETSI), Technical Report (TR) 102 638, Jun. 2009, version 1.1.1.

[68] R. Molina-Masegosa and J. Gozalvez, "LTE-V for sidelink 5G V2X vehicular communications: A new 5G technology for short-range vehicle-to-everything communications," *IEEE Vehicular Technology Magazine*, vol. 12, no. 4, pp. 30–39, Dec. 2017.

[69] J. Norris, *Markov Chains.* Cambridge University Press, 1998.

[70] Durham University. (2016). Probability II: MATH 2647. [Online]. Available: https://maths.durham.ac.uk/stats/courses/ProbMC2H

[71] Z. Tong, H. Lu, M. Haenggi, and C. Poellabauer, "A stochastic geometry approach to the modeling of DSRC for vehicular safety communication," *IEEE Transactions on Intelligent Transportation Systems*, vol. 17, no. 5, p. 1448–1458, Feb. 2016.

[72] J. Tian and L. Xu, "An analysis model of IEEE 802.11p with difference services," *Journal of Physics*, vol. 910, no. 1, p. 012068, Oct. 2017.

[73] Y. Y. Nasrallah, I. Al-Anbagi, and H. T. Mouftah, "A realistic analytical model of IEEE 802.11p for wireless access in vehicular networks," in *Proc. International Conference on Connected Vehicles and Expo,* Vienna, Austria, Nov. 2014, pp. 1029–1034.

[74] R. Molina-Masegosa, J. Gozalvez, and M. Sepulcre, "Configuration of the C-V2X Mode 4 sidelink PC5 interface for vehicular communication," in *Proc. International Conference on Mobile Ad-Hoc and Sensor Networks,* Shenyang, China, Dec. 2018, pp. 43–48.

[75] M. Gonzalez-Martín, M. Sepulcre, R. Molina-Masegosa, and J. Gozalvez, "Analytical models of the performance of C-V2X Mode 4 vehicular communications," *IEEE Transactions on Vehicular Technology*, vol. 68, no. 2, pp. 1155–1166, Feb. 2019.

[76] R. Molina-Masegosa, J. Gozalvez, and M. Sepulcre, "Comparison of IEEE 802.11p and LTE-V2X: An evaluation with periodic and aperiodic messages of constant and variable size," *IEEE Access*, vol. 8, pp. 121 526–121 548, 2020.

[77] A. Bazzi, C. Campolo, A. Molinaro, A. O. Berthet, B. M. Masini, and A. Zanella, "On wireless blind spots in the C-V2X sidelink," *IEEE Transactions on Vehicular Technology*, vol. 69, no. 8, pp. 9239–9243, Aug. 2020.

[78] F. Romeo, C. Campolo, A. Molinaro, and A. O. Berthet, "DENM repetitions to enhance reliability of the autonomous mode in NR V2X sidelink," in *Proc. IEEE Vehicular Technology Conference,* Antwerp, Belgium, May 2020, pp. 1–5.

[79] A. F. M. Shahen Shah, H. Ilhan, and U. Tureli, "Modeling and performance analysis of the IEEE 802.11p MAC for VANETs," in *Proc. International Conference on Telecommunications and Signal Processing,* Budapest, Hungary, Jul. 2019, pp. 393–396.

[80] F. Kaabi, P. Cataldi, F. Filali, and C. Bonnet, "Performance analysis of IEEE 802.11p control channel," in *Proc. International Conference on Mobile Ad-hoc and Sensor Networks,* Hangzhou, China, Dec. 2010, pp. 211–214.

[81] C. Han, M. Dianati, R. Tafazolli, R. Kernchen, and X. Shen, "Analytical study of the IEEE 802.11p MAC sublayer in vehicular networks," *IEEE Transactions on Intelligent Transportation Systems*, vol. 13, no. 2, pp. 873–886, Jun. 2012.

[82] L. F. Abanto-Leon, A. Koppelaar, and S. H. de Groot, "Enhanced C-V2X Mode 4 subchannel selection," in *Proc. IEEE Vehicular Technology Conference,* Chicago, USA, Aug. 2018, pp. 1–5.

[83] A. Haider and S.-H. Hwang, "Adaptive transmit power control algorithm for sensing-based semi-persistent scheduling in C-V2X Mode 4 communication," *Electronics*, vol. 8, no. 8, Jul. 2019.

[84] ETSI, "Intelligent transport systems (ITS); vehicular communications; basic set of applications; part 2: Specification of cooperative awareness basic

service," European Telecommunications Standards Institute (ETSI), Technical Specification (TS) 102 637-2, Mar. 2011, version 1.2.1.

[85] ——, "Intelligent transport systems (ITS); vehicular communications; basic set of applications; part 3: Specification of decentralized environmental notification basic service," European Telecommunications Standards Institute (ETSI), Technical Specification (TS) 102 637-3, Sep. 2010, version 1.1.1.

[86] 3GPP, "Evolved universal terrestrial radio access (E-UTRA) and evolved universal terrestrial radio access network (E-UTRAN); Overall description; stage 2," 3rd Generation Partnership Project (3GPP), Technical Specification (TS) 36.300, Dec. 2016, version 14.1.0.

[87] M. Wang et al., "Comparison of LTE and DSRC-based connectivity for intelligent transportation systems," in *Proc. IEEE Vehicular Technology Conference,* Sydney, Australia, Jun. 2017, pp. 1–5.

[88] T. V. Nguyen et al., "A comparison of cellular vehicle-to-everything and dedicated short range communication," in *Proc. IEEE Vehicular Networking Conference,* Torino, Italy, Nov. 2017, pp. 101–108.

[89] A. Bazzi, B. M. Masini, A. Zanella, and I. Thibault, "On the performance of IEEE 802.11p and LTE-V2V for the cooperative awareness of connected vehicles," *IEEE Transactions on Vehicular Technology*, vol. 66, no. 11, pp. 10 419–10 432, Nov. 2017.

[90] V. Vukadinovic et al., "3GPP C-V2X and IEEE 802.11p for vehicle-to-vehicle communications in highway platooning scenarios," *Ad Hoc Networks*, vol. 74, pp. 17–29, May 2018.

[91] J. Thota, N. F. Abdullah, A. Doufexi, and S. Armour, "Performance of car to car safety broadcast using cellular V2V and IEEE 802.11p," in *Proc. IEEE Vehicular Technology Conference,* Porto, Potugal, Jun. 2018, pp. 1–5.

[92] W. Anwar, K. Kulkarni, T. R. Augustin, N. Franchi, and G. Fettweis, "PHY abstraction techniques for IEEE 802.11p and LTE-V2V: Applications and analysis," in *Proc. IEEE Globecom Workshops,* Abu Dhabi, UAE, Dec. 2018, pp. 1–7.

[93] G. Cecchini, A. Bazzi, B. M. Masini, and A. Zanella, "Performance comparison between IEEE 802.11p and LTE-V2V in-coverage and out-of-coverage for cooperative awareness," in *Proc. IEEE Vehicular Networking Conference,* Torino, Italy, Nov. 2017, pp. 109–114.

[94] S. Kuehlmorgen, P. Schmager, A. Festag, and G. Fettweis, "Simulation-based evaluation of ETSI ITS-G5 and Cellular-VCS in a real-world road traffic scenario," in *Proc. IEEE Vehicular Technology Conference,* Chicago, USA, Aug. 2018, pp. 1–6.

[95] Y. Jeon, S. Kuk, and H. Kim, "Reducing message collisions in sensing-based semi-persistent scheduling (SPS) by using reselection lookaheads in cellular V2X," *Sensors*, vol. 18, no. 12, p. 4388, Dec. 2018.

[96] G. P. Wijesiri, J. Haapola, and T. Samarasinghe, "A Markov perspective on C-V2X Mode 4," in *Proc. IEEE Vehicular Technology Conference,* Hawaii, USA, Sep. 2019, pp. 1–6.

[97] C. D. Manning, P. Raghavan, and H. Schutze, *Introduction to Information Retrieval*. Cambridge University Press, 2008.

[98] N. Bouchemal, R. Naja, and S. Tohme, "Traffic modeling and performance evaluation in vehicle to infrastructure 802.11p network," *Ad Hoc Networks*, pp. 82–99, Jan. 2014.

[99] J. Santa, F. Pereñíguez, A. Moragón, and A. F. Skarmeta, "Vehicle-to-infrastructure messaging proposal based on CAM/DENM specifications," in *Proc. IFIP Wireless Days,* Valencia, Spain, Nov. 2013, pp. 1–7.

[100] D. Martín-Sacristán et al., "Evaluation of LTE-advanced connectivity options for the provisioning of V2X services," in *Proc. IEEE Wireless Communications and Networking Conference,* Barcelona, Spain, Apr. 2018, pp. 1–6.

[101] G. P. Wijesiri, J. Haapola, and T. Samarasinghe, "A discrete-time Markov chain based comparison of the MAC layer performance of C-V2X Mode 4 and IEEE 802.11p," *IEEE Transactions on Communications*, vol. 69, no. 4, pp. 2505–2517, Apr. 2021.

[102] G. P. Wijesiri, J. Haapola, and T. Samarasinghe, "The effect of multiple access categories on the MAC layer performance of IEEE 802.11p," in *Proc. IEEE Global Communication Conference,* Taipei, Taiwan, Dec. 2020.

[103] A. Alsuhaim, "NS3 example project," Nov. 2020. [Online]. Available: https://github.com/addola/NS3-HelperScripts/tree/master/examples/WaveTest.

[104] H. Z. B. Sun, "IEEE 802.11-18/0861r9: 802.11 NGV proposed PAR," *presented at the IEEE 802.11 NGV Meeting*, Nov. 2019.

[105] Vodafone, "RP-181480: New SID: Study on NR V2X," in *Proc. 3GPP Plenary Meeting,* San Diego, CA, USA, vol. 80, Jun. 2018, p. 1–10.

[106] 3GPP, "Study on enhancement of 3GPP support for 5G V2X services," 3rd Generation Partnership Project, Technical Report (TR) 22.886, Dec. 2018, version 16.2.0.